Designing Thermal modulators for portable GC × GC systems

by

Dibyadeep Paul

A dissertation submitted in partial fulfillment
of the requirements for the degree of
Doctor of Philosophy
(Mechanical Engineering)
in The University of Michigan
2015

Doctoral Committee:

Professor Katsuo Kurabayashi, Chair
Professor Xudong Fan
Professor Yogesh B. Gianchandani
Associate Professor Pramod Sangi Reddy

To my family.

Table of Contents

List of Figures

List of Tables

Abstract

Microelectromechanical systems (MEMS) have been used for a wide variety of applications. Such devices have the advantage of scale and can be manufactured in bulk. One of the active areas of MEMS research is the development of micro-scale gas chromatography (μGC). This is because, numerous industries such as petrochemicals, forensics, space exploration etc need a portable and real-time method to analyze and detect trace amounts of Volatile organic compounds(VOCs) from a complex mixture of chemicals. Particularly two-dimensional gas chromatography has the potential to perform such portable, real-time analysis of complex gas mixtures.

Our previous work has demonstrated the development of the first microscale thermal modulator for use in two-dimensional gas chromatography. However, our demonstration was limited to very simple mixtures. Rapid, comprehensive two-dimensional gas chromatographic (GC×GC) separations by use of a microfabricated mid-point thermal modulator (μTM) are demonstrated and the effects of various μTM design and operating parameters on performance are characterized here. A 9 compound structured chromatogram and a 21-component separation was achieved in < 3 min. The potential for creating portable μGC×μGC systems is discussed.

Next we demonstrate GC × GC with all microfabricated components. The first dimension consists of two series coupled μcolumn chips with etched channels, wall-coated

with a PDMS stationary phase. The second dimension consists of a μcolumn chip with wall-coated with either a trigonal tricationic room-temperature ionic liquid (RTIL) or a commercial poly(trifluoropropylmethyl siloxane) (OV-215) stationary phase. Conventional injection methods and flame ionization detection were used. Temperature-ramped separations of a simple alkane mixture using the RTIL-coated ^{2}D μcolumn produced reasonably good peak shapes and modulation numbers. Substituting OV-215 as the ^{2}D μcolumn stationary phase markedly improved the performance, and a structured 22-min chromatogram of a 36-component mixture was generated with modulated peak *fwhm* values ranging from 90 to 643 ms and modulation numbers of 1-6.

Current conventional thermal modulators can achieve FWHH of modulated peaks of ~ 10 ms, which is necessary to obtain optimum peak capacity in GC × GC. This is achieved by using tremendous amounts of cryogenic consumables or high amounts of power. However, since we are limited in the amount of cooling power we can use, we need to understand the fundamental physics governing the thermal modulation, and optimize our modulators. Hence we developed a theoretical model of single-stage thermal modulation processes based on fundamental physics of gas chromatography (GC) with the aim to elucidate factors leading to improvements in GC×GC analyses. Model predictions were compared with experimental data obtained using our microfabricated thermal modulator (μTM) operating as a single-stage thermal modulator and excellent match is obtained.

To make a more realistic model, we demonstrate the physics behind the operation of a two-stage modulator. We show that parameters such as the time constant of modulation can be used to reduce the FWHH, breakthrough and hence improve the peak capacity of the GC

× GC significantly. Going forward, this theory can be used to optimize the performance of the thermal modulator and coupled with thermal simulations to design the next generation of thermal modulators.

Chapter 1. Introduction: Literature Review

1.1. Research Introduction and Background

Gas chromatography is one of the oldest analytical techniques available and is widely used in various industries such as forensics, environmental pollution, chemical weapons detection etc. [1, 2] Conventional gas chromatography is also known as one dimensional gas chromatography (1D GC). In 1D GC, volatile organic compounds (VOCs) are sampled from the environment using a pump and a sharp band is injected into a long narrow-bore capillary column using a injector such as a 6-port value. While various column configurations can be found in literature, the typical column in a bench scale GC system is usually 30 m long with a bore diameter of 180 μm, and has a 0.2 μm coating of polydimethylsiloxane (PDMS) on the inside of the capillary. As the band flows through the column it gets separated out into multiple bands consisting of individual analytes present in the original VOC mixture. This happens because each analyte interacts with the stationary phase and is partially retained within the stationary phase. The degree of retention of any analyte in the stationary phase is inversely proportional to the boiling point of the compound. Hence, analytes with low boiling points elute first followed by higher boiling point counter-parts. A Flame-ionization-detector (FID) is used to analyze the flux of the species eluting out of the capillary column. However, one of the major problems with one dimensional gas chromatography is that if the mixture is

very complex and consists of thousands of species, separation of the species is very time consuming taking somewhere from hours to days.

Figure 1.1A typical Gas chromatography system

An additional need for numerous industries is the ability to not only separate and identify individual components of a VOC mixture but do so rapidly, and on site [3]. While miniaturized versions of convention gas chromatography exist in literature, due to limitations in column length, they are not able to separate the complexity of gas mixtures present in real-life scenarios. The addition of a second dimension in comprehensive two dimension gas chromatography adds higher selectivity, and has the potential to separate much more complex mixtures in a real-time and portable fashion [4].

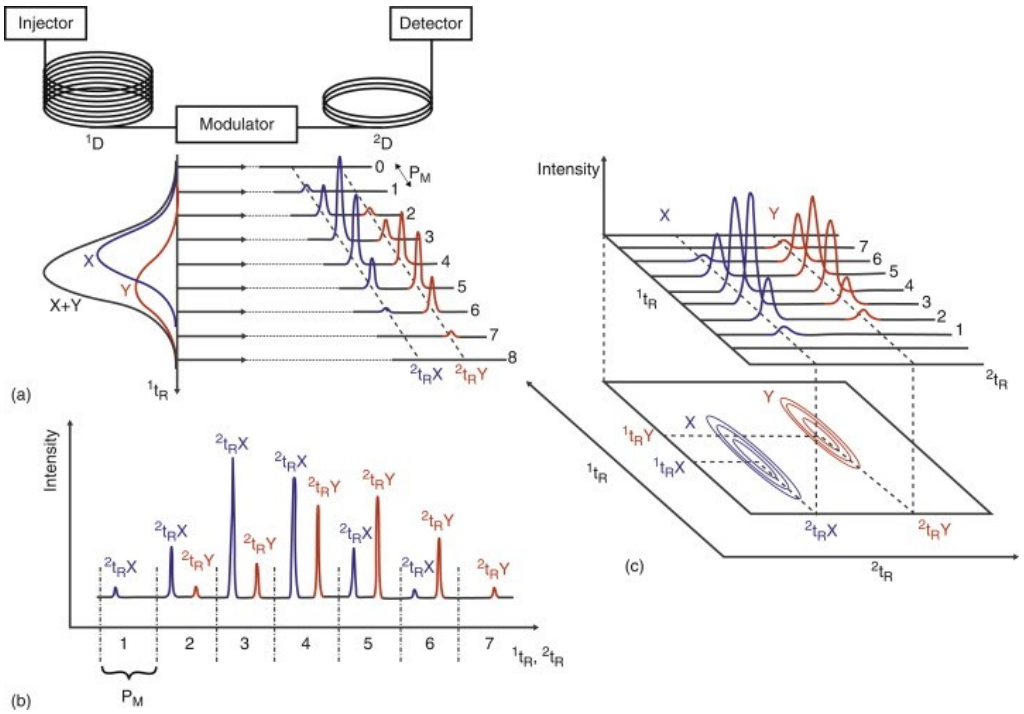

Figure 1.2Scheme of the column coupling in the GC×GC setup and of how data are handled (not to scale) [4]. (A) The modulator allows rapid sampling of the analytes eluting out of 1D and reinjection in 2D. The modulation process is illustrated for two overlapping compounds (X and Y) coming out of 1D at a defined first-dimension retention time (1tR). As the modulation process occurs during a defined PM, narrow bands of sampled analytes are entering 2D and appear to have different second-dimension retention times (2tRX and 2tRY). (B) Raw data signal as recorded by the detector through the entire separation process. (C) Construction of the two-dimensional contour plot from the collected high-speed secondary chromatograms of (B), in which similar signal intensities are connected by contour lines.

Comprehensive two-dimensional gas chromatography consists of two columns serially connected with a coupler known as the modulator [5]. The two columns are usually of different inner diameters and lengths, with the first column having much longer length and higher inner diameter compared to the second column. This is because the species need to flow rapidly through the second dimension to prevent wrap around. While many different combinations have been tried, typically a 30 m long, 180 micron i.d. PDMS coated 1st dimension column, and a 1 m long, 100 micron i.d. PEG coated 2nd dimension column is

used for the 2nd dimension column [6]. The sample is extracted from the environment and injected into the 1st dimension column. The separation in the 1st dimension is similar to that in conventional gas chromatography. As the species arrives at the modulator, it takes small chunks of the incoming species, compresses it into sharp bands and injects it into the second dimension. This process uncouples the separation that happens in the first and second dimension. In the absence of the modulator, the separation that happened in the first dimension would recombine, and as a result it would be impossible to identify the 1st and 2nd dimension retention times.

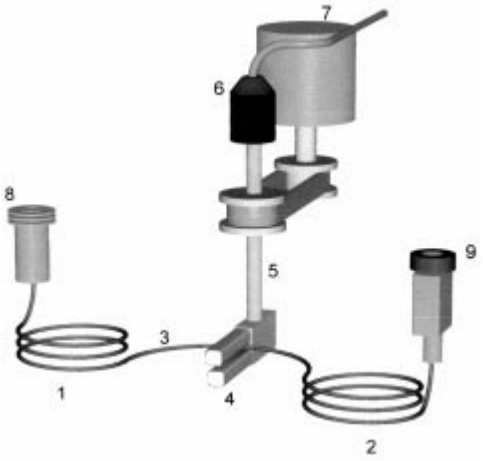

Figure 1.3a. Solid model schematic of a rotating heater thermal modulation system configured for GC6GC. The diameters of capillary columns exaggerated for clarity. 1. First-dimension capillary column; 2. Second-dimension capillary column; 3. Modulator tube; 4. Rotating heater ("sweeper"); 5. Machineable ceramic shaft; 6. Rotating electrical feed-through with electrical cable; 7. Stepper motor; 8. Injector; 9. Detector.

Initial portable gas chromatography systems used capillary columns which were tightly encapsulated into a confined space. However there is an inherent limitation to miniaturization in this top down fabrication and assembly process. A better way to fabricate such columns is using MEMS fabrication processes, which can etch channels into a very small space while retaining the length necessary. Further, these MEMS columns can be temperature regulated by on chip heaters and sensors, where as conventional columns might need more sophisticated and cumbersome techniques. As the scale reduces, the thermal mass of the device decreases, resulting in lower power required to heat the devices as well as a lower thermal time constants. The combination of these factors makes micro-fabricated columns very attractive. However, one of the challenges in using micro-fabricated columns in gas chromatography is the coating of these columns. Due to the tight bends, the stationary

phase coating process leads to non-uniform coating thickness at the bends as well as along the column surface [7, 8]. However, our colleague in the Chemistry department has been able to develop a coating process to alleviate most of these issues [9]. Further, we have developed capability to coat PEG on the columns as well.

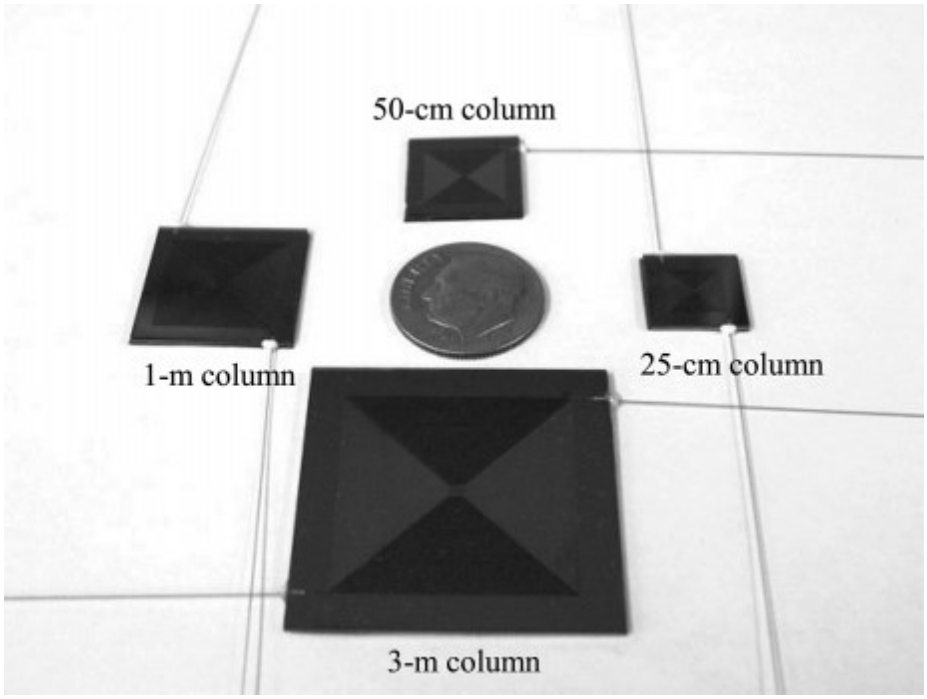

Figure 1.4Photograph of silicon on glass microfabricated columns. [7, 8]

There are primarily two types of modulators that exist in literature: flow-switching modulators that operate as high-frequency diversion valves and thermal modulators that sample the first dimension more completely [10]. Valve based thermal modulators operate by diverting between 20 and 90% of the effluent into the second dimension. They can operate at much higher frequency compared to thermal modulators, however since only a fraction of the effluent is analyzed in the second dimension; it's not a comprehensive separation. Among thermal modulators there are essentially three types: cryogenically cooled thermal

modulators, jet-pulsed thermal modulators and heat-based thermal modulators [11, 12, 13]. In heat based modulators, the sample is trapped in the thick stationary-phase of the modulator tube [14]. A heat pulse is applied to the section of the column which elutes the species into the second dimension. In cryogenic thermal modulators, a jet of liquid nitrogen traps the species in a short section of the column. When the jet is removed, the temperature of the column equilibrates with that of the oven, thus releasing a sharp pulse into the second dimension [13]. In a jet pulsed thermal modulator, jets of hot and cold fluid flow over a section of the capillary tube sequentially, to trap and elute the species into the second dimension [15]. One of the major problems with all these modulators is that they are difficult to scale down to miniaturized versions.

Current generation of thermal modulators are usually two-stage thermal modulators. Heat is applied to the two stages at a certain phase lag known as Offset (O_s). Both stages are cooled continuously using various methodologies as highlighted above. At the start of the modulation cycle, the heater is turned on for a short duration. This sharp increase in temperature desorbs any species adsorbed in the stationary phase of the first stage into the second stage. Since the second stage is at the minimum trapping temperature, the desorbed species gets adsorbed in the second stage. Further, species keep moving into the thermal modulator during the heating phase of the first stage, as well as during the cooling phase of the first stage. This is because, when the heater is turned off on the first stage, the temperature drop is not instantaneous; as a result not all the species flowing into the first stage is adsorbed into the first stage. The second stage heater is then turned on for a short duration, which elutes any adsorbed species into the ^{2}D. The presence of this second stage

thus helps prevent any leakage of species and subsequent band-broadening that would have happened in its absence [16, 10]. A further benefit of the two stage modulation is the peak sharpening, due to the sequential trapping and focusing of species as it moves through the modulator.

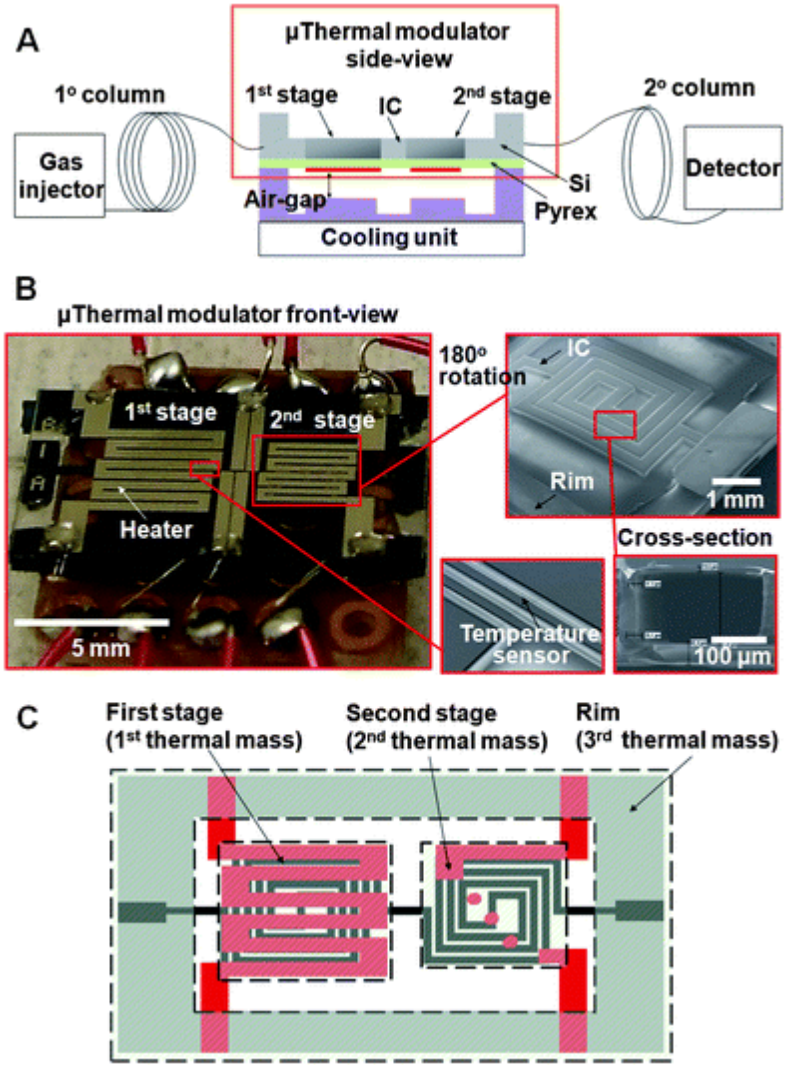

Figure 1.5Miniaturized thermal modulator (μTM). (A) Schematic of GC×GC system incorporating the μTM. Key components of the μTM are two-stage silicon-microchannels, a Pyrex membrane, and interconnection channels (ICs). A Si-spacer maintains the air-gap between the μTM and the cooling unit. The cooling unit has a thermoelectric cooler and a fan

cooler. The thermoelectric cooler keeps the temperature of the μTM approximately at −55 °C when there is no heating in the μTM stages. We vary the size of the Pyrex membrane, the air gap, and the IC to explore the optimal device performance. (B) Photographs of μTM. Each stage has serpentine microchannels (250 μm-width and 140 μm-depth) on its back side, on-chip microheaters and temperature sensors on its front side. The microchannel lengths on the first and second stages are 4.2 cm and 2.8 cm, respectively. A rim structure is used to reinforce the mechanical strength of the μTM. (C) Control volumes for the lumped thermal model. Each thermal mass includes the Si layer and the corresponding Pyrex membrane area. [17]

Our thermal modulator is built based on similar principles as conventional two stage thermal modulators. It consists of two stages, which are cooled by thermoelectric coolers, and are heated sequentially by heaters patterned on the surface of the stages. The design of the thermal modulator is based on previous studies by Libardoni et al. using an air cooled two-stage thermal modulator [12]. Lumped model and finite element method simulations are used to design various elements such as the placement of the TEC with respect to the μTM chip, distance between the stages of the modulator etc. The thermal modulator is fabricated using MEMS fabrication techniques with a combination of various surface and bulk micromachining techniques. The channels are etched using a deep-reactive-ion-etching (DRIE) technique using photoresist and thermal oxide as a mask. We use boron doping to form a very uniform channel wall thickness. Using anodic bonding, the channels are capped with a 100 μm Pyrex glass wafer. Four Ti/Pt resistive heaters and temperature sensors are patterned on the surface using negative photolithography and metal evaporation. Finally, a combination of DRIE and EDP etching is used etch away the excess silicon, and leave a uniform channel wall thickness. The wafer is then diced to form the individual μTM chips.

The μTM chip is then annealed to reduce electrical noise, by prolonged high temperature baking in a GC oven. Next, the chip is coated internally with PDMS to a thickness of ~0.3 μm, using static coating methods. It is then attached to a PCB board and wire-bonded. Spacers are aligned on to the backside of the chip, and mounted on top of the TEC, using a vertical height gage. To cross-link the stationary phase, the onboard heaters are switched on and held at ~ 200 ^{o}C for 2 hrs. The first and second dimension capillaries are then connected to the thermal modulator, to perform the experiments [17, 18, 19].

1.2. Research Motivation

The need for portable real-time comprehensive two-dimensional gas chromatography was stated earlier. To achieve such a system, we have already shown the performance of the system with very simple test samples. However, we need to show the use of our thermal modulator with more complex mixtures found in real-life mixtures. To demonstrate the performance of our system for real life situations, we first perform experiments to determine the optimum operating conditions for our thermal modulator. Based on these operating conditions, we demonstrate the separation of a complex VOC mixture within a very short time interval. Since introduction of multiple new subsystems, increases the complexity of the system, and the unknowns, our first demonstration uses conventional capillary column. However, we realize the need to use micro-fabricated capillary columns because they occupy smaller real-estate on the system, are less power thirsty and can be heated using on-board heaters and sensors. Another limitation for the use of GC x GC for real-mixtures is that, a number of real-life VOCs have very high boiling points. To trap and elute these components

quickly, the eluent temperature of the TM needs to be approximately 50 degrees higher than that of the boiling point of the compound. Typically PDMS is the used as the stationary phase of the TM. However, PDMS is unstable at such high temperatures are required for high boiling point compounds. New stationary phases need to be tested in GC x GC systems and their performance demonstrated.

Further, our previous experiments have demonstrated that the FWHH of the injection peak of our thermal modulator is approximately 100 ms or larger. Current state of the art bench-top thermal modulators can achieve FWHH which is 10 ms or smaller. A number of theoretical studies have shown that if the FWHH of the modulated peak is not that small, GC x GC is unable to lead to a significant improvement in peak separation capability compared to 1D GC. However, till date no model for thermal modulation has been developed. This is partly because most issues associated with thermal modulation can be overcome by reducing the trapping temperature in benchtop thermal modulators. While this is possible in bench-top systems, portable systems have much stricter power and consumable requirements. To understand the influence of various parameters on the FWHH of the modulated peak, we have developed a fundamental physics based model for our TM. Due to the presence of multiple parameters which could potentially influence the operation of the thermal modulator, we work on develop design rules which will help us design the second generation of thermal modulators.

1.3. Thesis Outline

The work accomplished in order to complete the research objectives is organized into five sections. These are outlined below:

Chapter II – Review of Related Studies: This chapter provides an overview of the some related studies in relation to portable gas chromatography and portable two-dimensional gas chromatography. Further, we look into various bench scale modulators that have been demonstrated in the past, and review the literature for modeling gas chromatography systems.

Chapter III - Comprehensive Two-Dimensional Gas Chromatographic Separations with a Micro-fabricated Thermal Modulator: Our previous studies demonstrated the design and operation of our thermal modulator using very simple text mixtures. In this study we demonstrate the use of our thermal modulator to perform comprehensive two-dimensional gas chromatography of a real-life mixture. We discuss the process of optimizing the thermal modulator operation, the tests involved in demonstrating GC x GC of the text mixture and show that a structured chromatogram is obtained in our separation.

Chapter IV - μGC × μGC: Comprehensive Two-Dimensional Gas Chromatographic Separations with Microfabricated Components: Conventional capillary columns were used in demonstrating GC x GC using our micro-scale thermal modulator in the previous chapter. To miniaturize the system and make it truly portable we use micro-fabricated columns coated with stationary phases as the columns for gas chromatography. Further, we show the viability of two different stationary phases which are stable at high temperatures in the second

dimension. This allows us to demonstrate portable temperature ramped GC x GC of two complex mixtures within a very short period of time.

Chapter V - First-principle modeling and characterization of thermal modulation in comprehensive GC×GC using a micro-fabricated device: To improve the performance of our thermal modulator, we need to understand the influence of various design parameters on the operation of our device. Towards that goal, we develop a fundamental mass transfer and chemical kinetics based model which also considers the presence of potential coldspots in the design. We design experiments which validate our model within 10% error, and propose some modifications which can drastically improve the performance of our device

Chapter VI - Effect of thermal time constant of primary stage on the peak capacity and breakthrough of a micro-scale thermal modulator: The previous chapter builds a fundamental physics based model for our micro-fabricated thermal modulator operating as a single stage device. However, our thermal modulator is designed to be a two-stage device, which sequentially traps and focuses the incoming species. We develop a model for this device and demonstrate the various stage of modulation and the influence of the thermal time constant of the first stage on the operation of the device

Chapter VII – Conclusions and Future Work: The final chapter summarizes the work that is presented before and discusses the impact of the presented research. We discuss some of the results from the parametric studies that were performed, and some design modifications which can significantly improve the performance of this device.

Chapter 2. Theory

2.1. Gas Chromatography microsystems

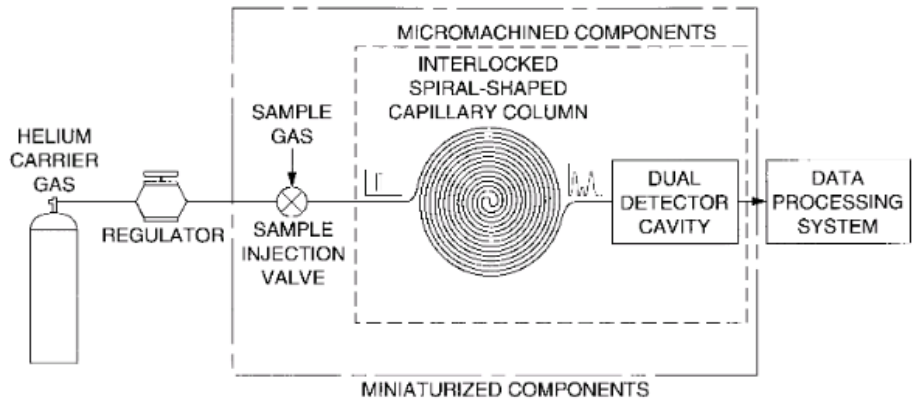

Figure 2.1Functional block diagram of the micromachined gas chromatography (GC) system

Most μGC sysems consist of multiple components: micropreconcentrators, [20, 21, 22, 23] microcolumns [24, 25, 3], micro-pumps [26], sensors [27, 28, 29] as well associated electronics to power the operation of the device. There have been multiple studies which have demonstrated a full working μGC system [30, 31, 32], however there has been only one study which has demonstrated a working $\mu GC \times \mu GC$system. In the following sections, we review a few of these microsystems [33, 34, 35, 36].

The first micro-fabricated gas analysis system was demonstrated by Terry et al [37]. In 1994, Reston and Kolesar demonstrated a miniature gas chromatography system consisting of a miniature sample injector, a rectangular shaped coated micro-fabricated

capillary column and a micro-fabricated dual detector system consisting of a CuPe-coated chemi-resistor and a thermal conductivity detector [38, 39].

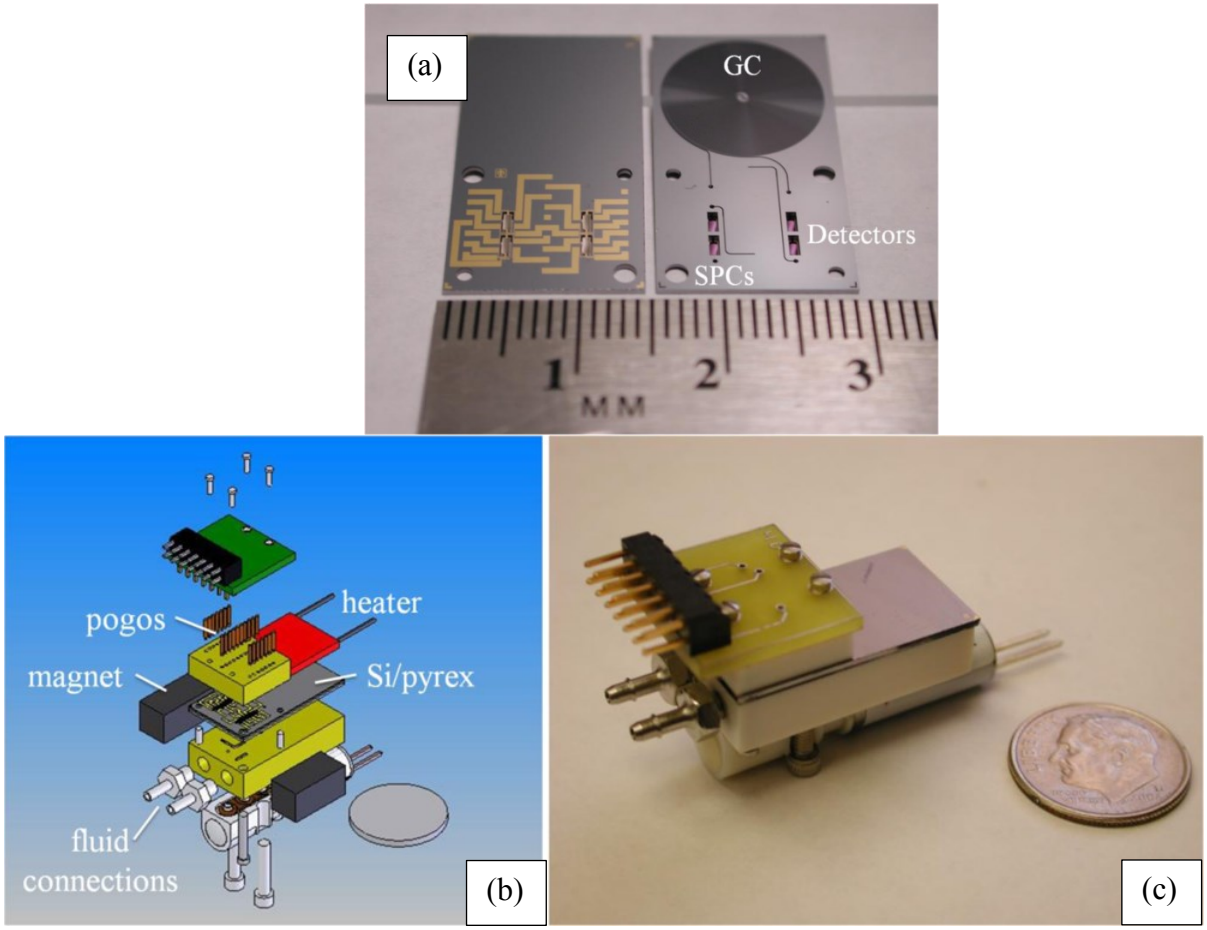

Figure 2.2 (a) Two monolithically integrated μGCs chips side-by-side. The chip on the left-hand side has the metallic traces used to electrically connect the PCand sensor shown face up. The chip on the right hand side is metal-side down to show the fluidic channels and deep reactive ion etched (DRIE) μGC channel (b) Expanded solid model showing the Si/pyrex device, electrical and fluidic connections, external valve for switching between PC and detector modes, magnets for PPR actuation, and a disk the size of a US dime to illustrate size. (c) Device and packaging. Magnets and heater are not shown. [40].

The system developed by Reston et al, also called silicon micromachined gas chromatography system (SMGCS) consisted of a 90 cm long, rectangular micro-fabricated column of dimension 300 × 10 μm, and a dual detector (based upon a chemiresistor and a

thermal conductivity detector (TCD) bead). To coat the stationary phase inside the micro-column, the authors sublimated a thick copper phthalocyanine film onto the surfaces of the etched channels of the silicon substrate. This allowed them to develop a uniform 200 nm thick coating on the channel surface. A Pyrex cover-plate was then anodically bonded at low temperature (300 ^{o}C). These two techniques combined enabled them to deposit a uniform stationary phase coating which would have been impossible otherwise. Based on this device, the authors demonstrated the isothermal separation of ammonia and nitrogen dioxide within 30 minutes.

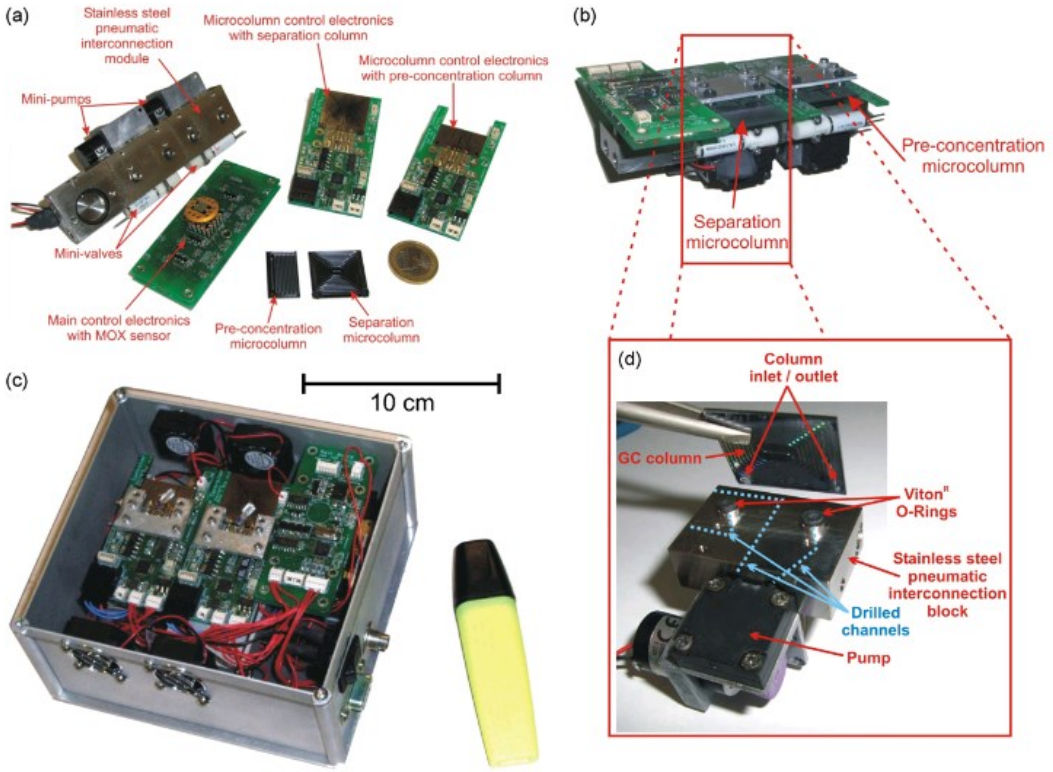

Figure 2.3Photograph of the prototypal miniGC system: single components (a), assembled miniGC (b), complete packaged prototype (c) and close-up on the pneumatic interconnections (d)

The need for robust and portable instruments for 'in-the-field' and 'on-site' detection of concentrations of chemical species such as chemical warfare agents, biohazards, petrochemicals, etc. has been the major driver for development in the field of micro-scale gas chromatography. Driven by the needs of national security, Sandia National lab has been very active in the field of portable gas chromatography through their program "Micro-analytical Systems' [35, 41, 40]. Their $\mu Chemlab$ gas analysis system consists of multiple microfabricated components: a sample pre-concentrator, a chromatography column and a surface acoustic wave detector. The pre-concentrator adsorbs species from the environment

on to a thermally isolated (and sol-gel coated) membrane. Next, a sharp voltage pulse heats the membrane using resistive heating to 200 ^{o}C within 10 ms, resulting in a very sharp and well-defined injection volume. This is possible because the film is really small thus having very small thermal mass. The chromatography columns were fabricated with reactive ion etching to a cross-sectional area of 300×300 μm and were be packed with porous materials. The columns were then coated with a thin layer of the stationary phase material. These were then used as chromatographic columns for the separation of gasses and volatile organic compounds. Detection of the separated species is performed using an array of chemically modified SAW sensors. These provide high sensitivity and unique response patterns. The entire integrated system has been shown to successfully separate and detect a wide range of chemical species at parts-per-billion concentrations.

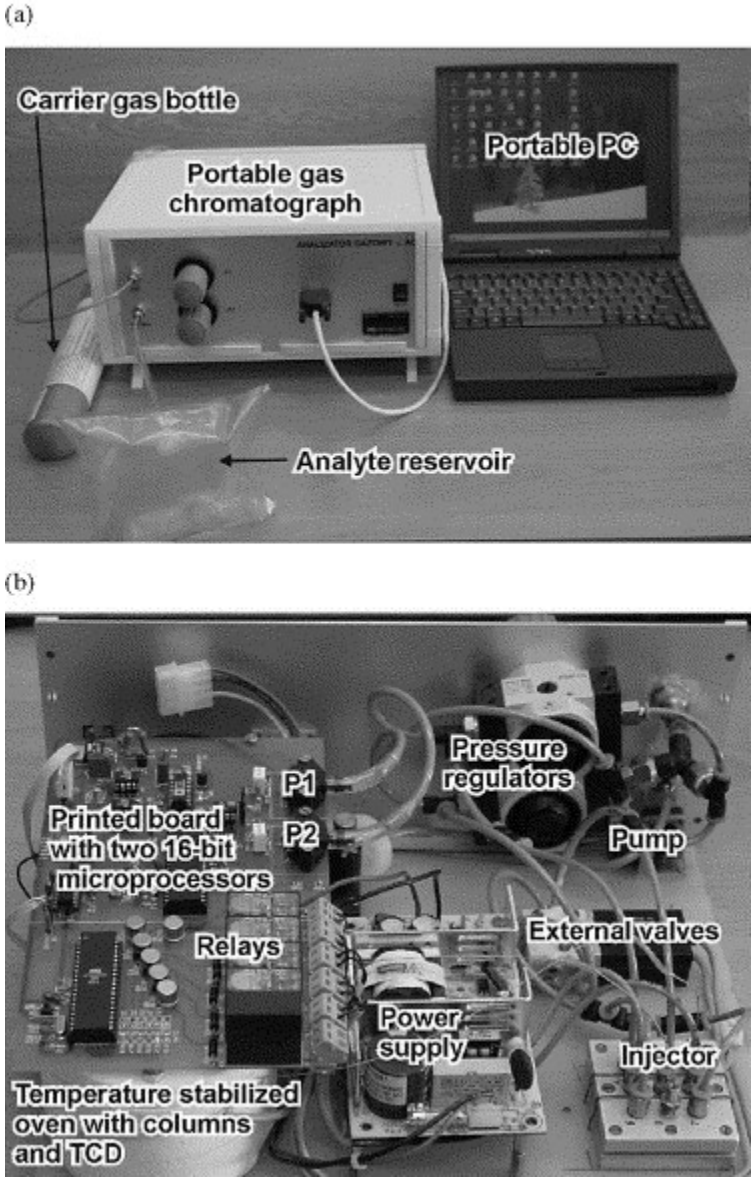

Figure 2.4. The portable gas chromatograph: (a) the device with a co-working equipment, note small He bottle, analyte reservoir, and portable PC, (b) internal view of the chromatograph. [25]

Several laboratories have been involved in the development of whole μGC system, assembled from separately fabricated subsystems for environmental analysis of trace amounts of compounds [33, 34, 25]. Dziuban et al developed the first portable GC system using a micro-machined injector and thermal conductivity detector. The micro-machined

injector compresses the vapor sample by electromagnetic valve actuations and injects it into the column. The injector is fabricated on a $3.5 \times 3.5 \times 2.5\ mm^3$ glass/silicon/glass die. To detect the concentration profile, three types of Thermal Conductivity Detectors (TCDs) are tested: 1) four thin-film Pt heaters/thermos-resistors made on thin silicon nitride CVD deposited membrane suspended over deeply etched in silicon substrate 2) in-line serial miniature spirals made out of tin Pt solid wire assembled inside a glass/silicon chip and 3) in-line parallel spirals made out of thin Pt solid wire assembled inside glass/silicon chip [25]. Recently in 2009, Zampolli et al developed an improved micro-gas chromatography system, with micro-machined gas chromatographic (GC) columns in combination with high sensitivity MOX detectors and novel pre-concentration materials. This system can perform portable, stand-alone sub-ppb level monitoring of aromatic volatile organic compounds (VOC) [34].

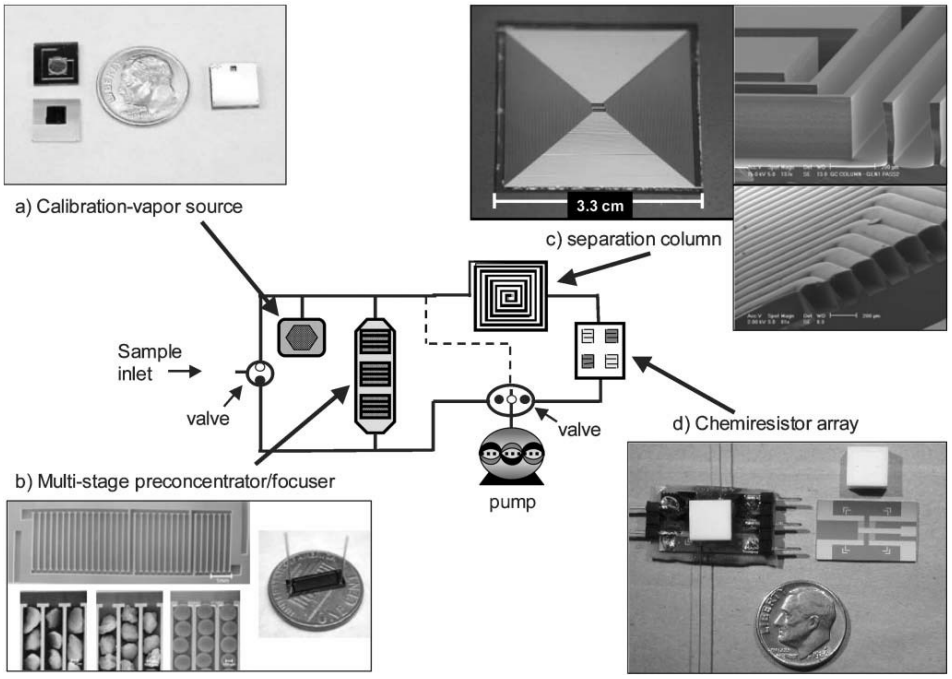

Figure 2.5Block diagram of the MEMS μGC prototype analytical system: (a) calibration-vapor source before (left) and after (right) assembly; diffusion channel and headspace aperture can be seen in the top section and macro-PS reservoir can be seen in the bottom section; (b) 3-stage adsorbent μPCF prior to loading and sealing (top left), with close-up SEM images of each section loaded with adsorbents (lower left) and assembled structure with capillary interconnects on a U. S. penny; (c) 3 m separation-column chip (left) with close up views of the channel cross-sections prior to (top right) and after (lower right) sealing; (d) detector assembly with 4-chemiresistor array chip (right), Macor lid (white square structure), and sealed detector with connecting capillaries mounted on a custom mounting fixture (left). The dashed line is a flow-splitter (see text). [33]

At University of Michigan, Ann Arbor, the Engineering Research Center for Wireless Integrated Microsystems (WIMS) has developed the first hybrid micro-fabricated gas chromatography, with all of its analytical components consisting of MEMS devices such as an on-board calibration-vapor source, a micro-fabricated pre-concentrator, a separation column and a multi-sensor array. Aging and drift were compensated by using calibrant vapor generated by diffusion from a liquid reservoir in the micro-fabricated pre-concentrator. The

micro-preconcentrator consists of three stages and traps the organic vapors using three types of carbon-based adsorbents packed in the stages of the μPCF. A sharp heat pulse desorbs the captured analytes and injects them as a sharp peak into the separation channel. The separation column consists of spiral silicon microchannels which are capped using Pyrex covers. An array of four chemiresistors is used as a detector for the μGC system.

A second generation of μGC has been in the works to develop a complete field-deployable μGC system at the WIMS center [33, 42]. This system has been shown to have improved design and performance of different components of the μGC system mentioned before. This system can detect target analytes at sub-ppb concentrations in the presence of a complex VOC mixture. The new hybrid μGC still requires external power supply to operate. A more efficient and power saving system is necessary to develop a truly portable system.

Despite the increase in the number of detectable compounds, one-dimensional gas chromatography is still limited in terms of the number of compounds that can be separated by the system. Further, there is a significant need for the ability to separate 1000s of compounds efficiently using a portable system. To address this issue, researches have been working on developing portable real-time two dimensional-gas chromatography devices. In the next section we review some of the portable multi-dimensional gas chromatography systems that have been reported in literature.

2.2. Portable Multi-dimensional Gas Chromatography systems and Thermal modulators

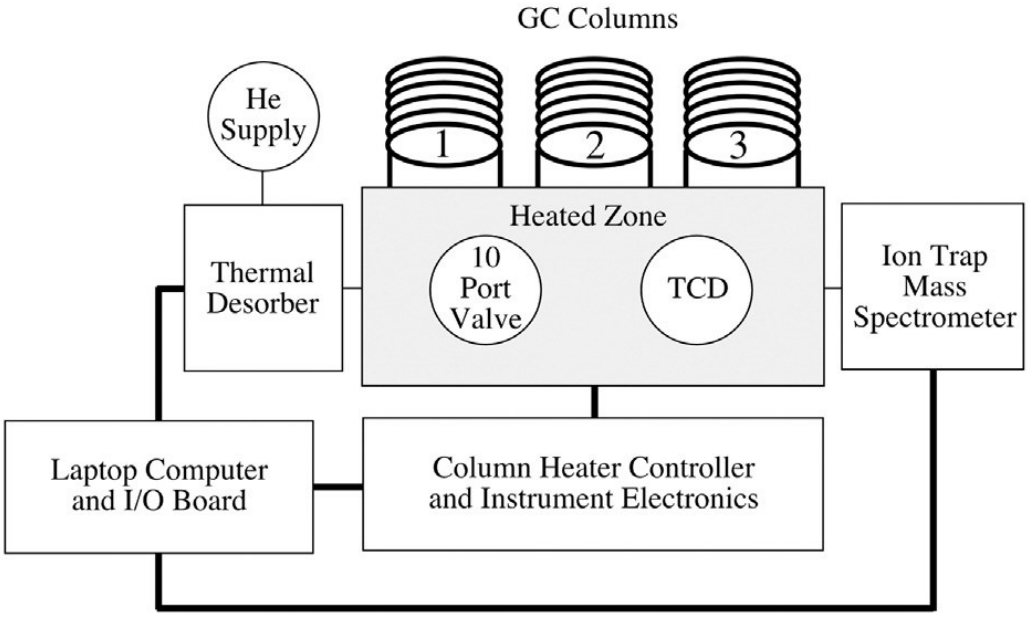

Figure 2.6 Schematic diagram of the overall MDGC chromatographic system comprising a laptop computer interface, column heater controller and instrument electronics, and chromatographic heated zone. The thick solid lines depict electrical connections. [43]

The first of such portable multi-dimensional gas chromatography systems was reported by Wahl et al [43]. Their system is capable of both on-dimensional and multi-dimensional analysis in one single package. It uses three chromatographic columns which can be configured in various two-dimensional configurations using a 10-port valve system. Because of the valve-switching methodology, no effluent is lost, and comprehensive two-dimensional gas chromatography can be performed in this system. Because of the valving scheme, the system can be switched from heart-cut to comprehensive analysis by a simple change in the software methodology.

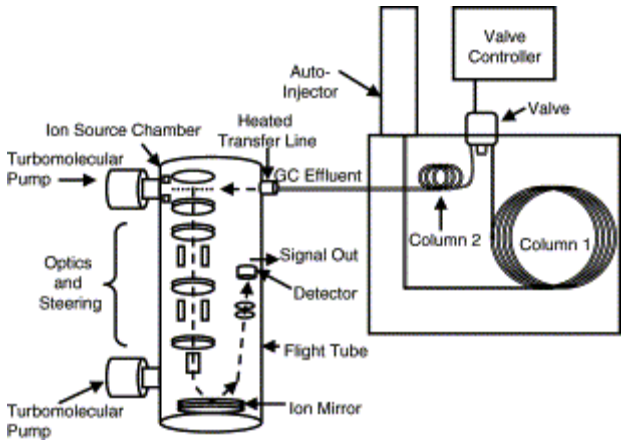

Figure 2.7Valve-based GC×GC/TOFMS instrument schematic. Both columns are housed inside the same oven. A stand-alone pulse generator (valve controller) is utilized in the system to simplify the instrumentation and to promote portability. Modulation occurs via a sample loop on a six-port high-speed mini-diaphragm valve. [44]

In 2003 Sinha et al [44], proposed a valve-based comprehensive two-dimensional gas chromatograph coupled to a time-of-flight mass spectrometer. They demonstrated a new compact, stand-alone, valve-pulse generator device and used it to separate a complex mixture containing a mixture of fuel components, natural products and organo-phosphorus compounds. A stand-along pulse generator that was designed in house was used to control the pulse width, the period of actuation, and the total duration of the analysis. This new device replaced the LabVIEW program and the computer that was previous used to control the valve, and made the system much more portable. Conventional capillary columns, a 60 m x 250 μm i.d. DB-5 column from Agilent was used as the first dimension column, while a 3 m x 180 μm i.d. RTX-2330 capillary column, was used as the second dimension capillary. A Time of Flight Mass spectroscopy system was used to detect the compounds. Synovec et al [45], also reported another valve based system to promote portable two dimensional gas chromatography around the same time. Most valve base systems are not comprehensive since

only 5-10% of the effluent is transferred to the second dimension. To address this issue, they developed a total transfer system, where 100% of the effluent is transferred to the second dimension, without adding complexity to the system. It relies on simply blocking one of the appropriate ports of the high-speed six port diaphragm valve that is used as the modulator between column 1 and 2. Using this valve, the researchers demonstrate good peak capacity for real complex samples: gasoline and Eucalyptus oil where compounds were spread out over much of the two-dimensional separation space.

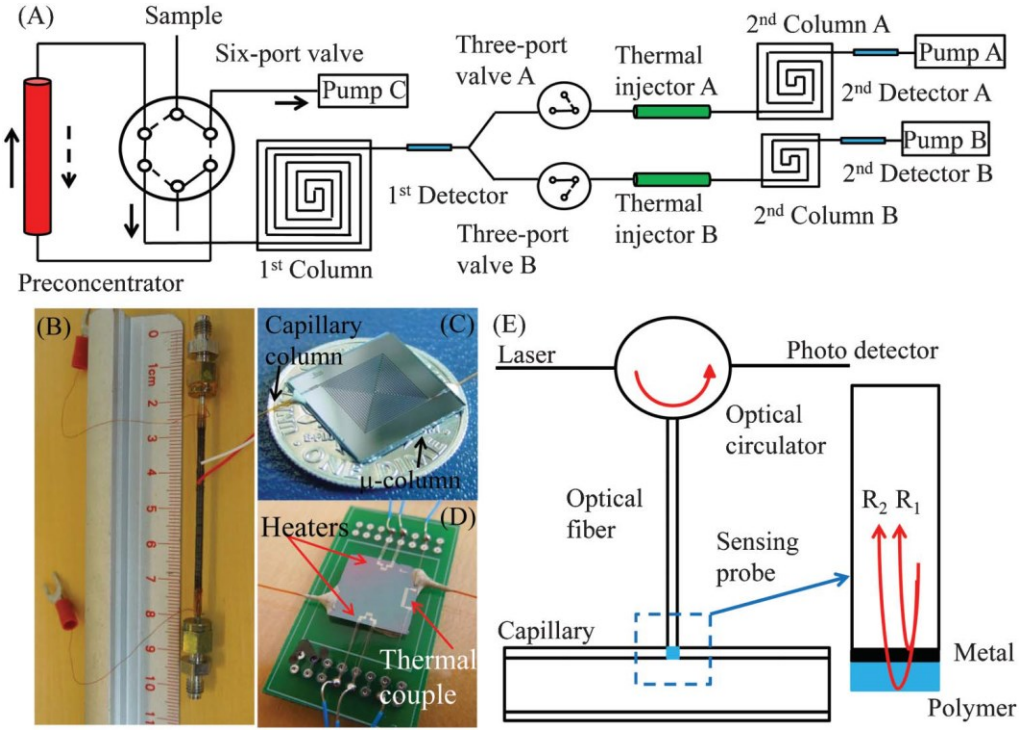

Figure 2.8(A) Schematic of the proposed smart 1 6 2 channel 2-D mGC with dual 2nd columns. A preconcentrator was connected to the 1st column through a six-port valve. During sampling (as shown by the dashed lines), sample was drawn into the preconcentrator by Pump C. During analysis (as shown by the solid lines), the trapped sample in the preconcentrator was released at high temperature and delivered onto the 1st column by a back-flush flow. The 1st column was connected to both 2nd columns by a Y-connector. Each of the 2nd columns had a three-port valve to control its connection with the 1st column. In this manner, the effluent from the 1st column was sent to the two 2nd columns alternately. (B) Photo of the preconcentrator. (C) Photo showing the front of the micro-fabricated column. (D) Photo showing the back of the micro-fabricated column. (E) Schematic of the on-column gas detector (the 1st and 2nd detectors were the same) using an optical fiber whose end-face was coated with a layer of vapor sensitive polymer. [46]

Liu et al [46] at the University of Michigan proposed a novel smart multi-channel two-dimensional micro-gas chromatography for rapid workplace VOC measurement. In this design, a non-destructive on-column detector and a flow-routing system is installed between the first dimension and multiple second dimensional separation columns. The effluent from

the first dimension is monitored in real-time and decision is made to route the effluent to one of the second dimensional columns for further separation. The greatest benefit of this system is the enhanced separation capability of the second dimension column and hence the overall 2-D GC performance. All the second dimensional columns are independent of each other, and their characteristics can be optimized for best separation performance. This smart μGC also eliminates the high power requirement as in thermal modulators, and provides high peak amplitude enhancement, a simplified 2-D chromatogram re-construction and potential scalability to higher dimensional separation.

To address this challenge we have been working on developing a portable Comprehensive Two-dimensional Gas Chromatography system (GC × GC) system. As the above literature review shows, the major bottle neck towards realizing a portable comprehensive two-dimensional gas chromatography system is the intermediary modulator. Valve-based systems are portable, but cannot always perform comprehensive two-dimensional gas chromatography. On the other hand, conventional thermal modulators use very high amounts of cryogenic coolants and cannot be easily miniaturized. A new technology that has recently been used widely is the thermos-electric-cooler (TEC). Using such a multi-stage TEC cooler, we previously showed a micro-scale thermal modulator [19, 17, 18, 47, 48]. This device operates with approximately 20 W of power, and as a result, can be potentially used in portable comprehensive two-dimensional gas chromatography. Based on this thermal modulator, we demonstrate the first microscale portable comprehensive two-dimensional gas chromatography using our microscale thermal modulator. However, since the performance of our thermal modulator is still not comparable to conventional thermal

modulators, we propose the first multi-physics model for thermal modulation and use it to propose design modifications for improved two-dimensional gas chromatography.

Chapter 3. Comprehensive Two-Dimensional Gas Chromatographic Separations with a Micro-fabricated Thermal Modulator

3.1. Introduction

Numerous reports have appeared over the past decade or so on micro-scale gas chromatograph (μGC) components [22, 41, 49, 7, 50, 51, 9, 27, 52, 53] [54, 55, 56] subsystems [30, 32, 42], and systems [57, 33, 35, 34, 36, 42, 40, 58, 59], consisting of one or more microfabricated Si devices. The low power requirements, small size, and eventual low production cost of μGC systems favor their use in field or clinical settings for measuring volatile and semi-volatile organic compounds (SVOC), such as explosive markers, chemical warfare agents, indoor air pollutants, and breath biomarkers of disease or toxic chemical exposure. Although the scaling laws governing GC separations generally favor miniaturization [60], inherent limitations on the maximum length and minimum diameter of the (micro)columns, as well as the minimum injection bandwidth, place limits on the achievable peak capacity (n_p) and resolution (R_s). One approach to relieving these constraints on performance entails the use of comprehensive two-dimensional gas chromatography (GC×GC).

GC×GC is a highly effective method for separating the components of complex mixtures of (S)VOCs [61]. A junction-point modulator couples a relatively long first-

dimension (^{1}D) column to a relatively short second-dimension (^{2}D) column having a different stationary phase. As each compound elutes from the ^{1}D column it is re-injected in a series of narrow bands that elute through the ^{2}D column rapidly enough to preserve the ^{1}D separation. Pneumatic modulation is achieved by tapping a second carrier gas source into the junction point and toggling a series of valves that transfer the effluent from the ^{1}D column to the ^{2}D column at very high frequency [45, 62]. Re-injection bandwidths as narrow as 22 ms can be obtained but little or no focusing occurs, and therefore the peak amplitude enhancement (*PAE*; i.e., the modulated/unmodulated peak-height ratio) is minimal [62].Thermal modulation is achieved by alternately bathing a small section of capillary at the junction point in a cooled gas to trap and focus peak segments from the ^{1}D column, and then heating to transfer them to the ^{2}D column [6, 63, 11, 64]. Re-injection bandwidths as narrow as 50 ms and *PAE* values as high as 70 have been reported by virtue of the refocusing that occurs with the thermal modulator (TM) [61, 11, 64]. Plotting the ^{1}D retention times against the ^{2}D retention times provides a 2-D chromatogram that conveys the net differential retention of the mixture components on the two columns.

The primary difficulties faced in trying to miniaturize GC×GC systems with commercial TM subsystems are the need for large quantities of consumable cooling fluids and the power demands for both heating and cooling, which can be on the order of kW [65, 66]. As part of an on-going effort concerned with the development of μGC systems and components in our laboratories [22, 7, 9, 27, 66, 32, 31, 33, 36, 42] [58, 59], we recently described a microfabricated TM (μTM) that operates with relatively low power and without cryogenic fluids [17, 18, 67]. The μTM chip consists of two series-coupled, convolved-

square-spiral, deep-reactive-ion-etched (DRIE) Si microchannels (stages) with an anodically bonded Pyrex cap, a crosslinked PDMS wall coating, and individual thin-metal-film heaters and temperature sensors. The chip is mounted on a thermoelectric cooler (TEC), which is used for focusing. Highlights of that work include modulated peaks with full-width-at-half-maximum (*fwhm*) values as low as 70 ms (for n-heptane) and *PAE* values as high as 50. Testing performed to date, however, entailed only a ^{1}D column so that the modulated peaks emerging from the μTM could be characterized without the influence a ^{2}D column.

In this article, we describe a GC×GC system that uses a μTM of similar design to that reported previously. Relatively short commercial ^{1}D and ^{2}D capillary columns are used in anticipation of developing a μGC×μGC system for (S)VOCs. The effects of varying the stage temperatures, modulation period, stage-heating offset period, and volumetric flow rate are examined with respect to several performance metrics using a small set of VOCs as test analytes. The reproducibility of the 2-D separations provided under a given set of conditions is examined and then a structured chromatogram is produced and assessed. Finally, a fast GC×GC 21-component VOC mixture separation is presented. The implications of the results for using this type of μTM in benchscale GC×GC systems and in portable μGC×μGC systems for fast analysis of (S)VOC mixtures are considered.

3.2. Experimental results

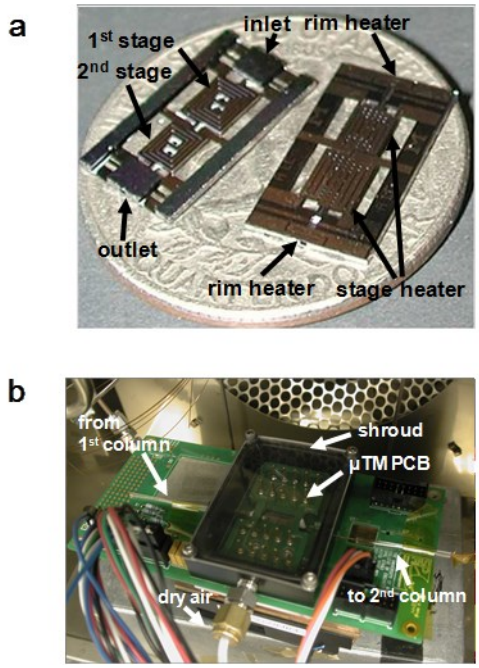

Figure 3.1. (a) Photograph of the microfabricated two-stage thermal modulator (μTM), with labels identifying the essential features; (b) Photograph of the fully assembled μTM mounted on a printed circuit board (PCB). The TEC is located beneath the μTM PCB and the ^{1}D and ^{2}D columns are beyond the field of view.

3.2.1 μTM preparation.

The design, thermal analysis, and fabrication of the μTM device has been described previously [17, 18]. Figure 3.1a shows a photograph of the device. The 13×6 mm μTM chip consists of two square-spiral, boron-doped Si microchannels, 4.2 cm (stage 1) and 2.8 cm (stage 2) long, with cross-sections of 250 (w) × 140 (h) μm and wall thicknesses of 30 μm. A 100-μm thick Pyrex cap is anodically bonded to the top surface, sealing the microchannels and providing additional mechanical strength to the Si frame. There is a 0.5-mm long microchannel interconnection segment between the two stages. Connections to upstream and

downstream capillaries are made at opposing sides of the rim. Four Ti/Pt resistive heaters and temperature sensors are patterned on the Pyrex surface; one set beneath each stage and beneath the inlet and outlet ports on the rim.

Two 5-cm long sections of deactivated fused-silica capillaries having 250 μm i.d. and 100 μm i.d., were connected to the inlet and outlet ports, respectively, with epoxy (Hysol Epoxy Patch 1C, Rocky Hill, CT). The interior walls of the microchannels (and connecting capillaries) were coated with a 0.3 μm thick cross-linked film of polydimethylsiloxane (PDMS, OV-1, Ohio Valley, Marietta, OH) from a 1:1 n-pentane:dichloromethane solution (0.6% w/v PDMS, 0.005% w/v dicumyl peroxide), using a static coating and thermal cross-linking method described previously [9].

3.2.2 μTM Mounting.

The μTM chip was mounted with epoxy (EE129-4, Epoxy Technology, Billerica, MA) and wirebonded to a custom printed circuit board having a central rectangular cut out that allowed access to the underside of the chip. Two microfabricated Si spacer structures (7.5 × 4.5 mm, and 7.5 × 3.5 mm, for the first and second stage, respectively) were affixed to the Pyrex beneath each stage using thermally conductive paste (Silicon Heat Sink 340, Dow Corning, Midland, MI). Each spacer has a central mesa structure the cross section of which matches that of the overlying stage. The air gap between the mesa and the device substrate (Pyrex) was 19 μm. In addition, a pair of 3×3 mm, 450-μm thick Si slabs was inserted between each Si spacer and the TEC surface to localize the cooling to the regions beneath the stages. A thin layer of thermally conductive paste was spread on both surfaces of the Si slabs

to ensure good thermal contact from the TEC to the device. This assembly was inverted and manually mounted and aligned on the top surface of the four-stage TEC (SP2394, Marlow Industries, Dallas, TX). A small axial fan (E1U-N7BCC-03, Sundial Micro, Ontario, CA) was placed below the TEC to facilitate heat dissipation. Finally, a shallow, rectangular glass shroud with a thick frame was bolted to the top side of the PCB on which the μTM was mounted. A barbed fitting in one wall of the frame permitted a tube to be connected for purging the μTM and TEC surfaces with dried house air to prevent ice formation.

3.2.3 Performance Testing.

The μTM-TEC testing platform was place inside the oven of a bench-scale GC (Model 6890, Agilent Technologies, Santa Clara, CA). Resistance values of the integrated temperature sensors were calibrated using the GC oven. The TEC was operated continuously at an applied power of 21 W, which yielded a minimum stage temperature, T_{min}, of -40 °C with the rim heaters deactivated and an ambient temperature of 23 °C. Reducing the power to the TEC allowed for higher T_{min} values. Modulations entailed applying 100-ms voltage pulses independently to each stage heater through two solid-state relays (D1D12, Crydom, San Diego, CA). The voltage applied to each stage was adjusted manually between 55 and 60 V to achieve the desired maximum stage temperature, T_{max}, which ranged from 195 to 250 °C. A custom Visual C# program was used to control the timing of the applied voltages, as well as to read the temperature sensors via a DAQ card (NI USB-6212, National Instruments, Austin, TX) installed on a laptop computer. A constant voltage was applied independently to

each rim heater and adjusted to maintain the ports at the ambient temperature when the TEC was on.

Inlet and outlet capillary sections were connected to commercial fused-silica capillary columns by means of press-tight connectors. The ^{1}D column was a 6-m long, 0.25-mm i.d. capillary, with 0.25-μm thick stationary phase of PDMS (Rtx-1, Restek Corp., Bellefonte, PA) and the ^{2}D column was a 0.5-m long, 0.1-mm i.d. capillary with a 0.1-μm thick stationary phase of polyethylene glycol (PEG, Rtx-Wax, Restek). The temperature of the ^{1}D column corresponded to that of the GC oven. The ^{2}D column was wrapped with insulated Cu wire (100 μm o.d., EIS, Inc., Atlanta, GA) and then heat-resistant thin polyimide tape (McMaster Carr, Santa Fe Springs, Ca). A fine-wire thermocouple (Type K, Omega, Stamford, CT) was placed between the capillary and heater coil. For all tests the ^{2}D column was maintained at ~80 °C. Note that the outlet capillary segment affixed to the μTM chip was coated with PDMS and was at oven temperature for all testing. The distal end of the ^{2}D column was connected to the FID via a 5-cm segment of deactivated fused silica capillary (100 μm i.d.). For some testing, the ^{2}D column was bypassed and the TEC was deactivated so that the ^{1}D peak widths could be measured.

Test compounds were > 98% pure (Sigma-Aldrich, Milwaukee, WI) and used without further purification. Vapor mixtures were prepared by injecting 1 μL of each component into a 10-L Tedlar bag (SKC Inc., Eighty-Four, PA) filled with a known volume of dry N_2. A sample of this test atmosphere was drawn by a small diaphragm pump (UN86, KNF Neuberger, Trenton, NJ) through a 112-μL sampling loop connected to a six-port valve. The valve and loop were housed in a heated (80 °C) enclosure on the GC chassis. Actuating the

six-port valve injected the contents of the loop to the ^{1}D column of the GC×GC subsystem via a short section of deactivated fused-silica capillary. Using He as the carrier gas, the volumetric flow rate, F, was adjusted by varying the GC inlet pressure and was measured at the end of the ^{2}D column with a bubble flow meter.

The data sampling rate and temperature of the FID were 200 Hz and 250 °C, respectively. ChemStation software (Rev.B.01.01, Agilent Technologies, Santa Clara, CA) was used for data acquisition, GRAMS32 (Version 6.0. ThermoScientific, Pittsburgh, PA) was used for 1-D data processing, and GC Image (Rev 2.2, Zoex, Houston, TX) was used for 2-D data processing and display of 2-D chromatograms. Estimates of the linear velocity, u, and hold-up time, t_M, as a function of F were determined for both columns using FlowCalc 2.0 (Agilent Technologies).

3.3. Results and Discussion

Several μTM operating variables must be set for a GC×GC analysis, and each has an effect on performance. The stage-heating offset, O_s, is the time delay between heating of the first and second stage heaters, which can affect sample transfer efficiency. The modulation period, P_M, is the time between successive first-stage heating events (i.e., modulations), and it must be considered together with the retention time, t_R, on the ^{2}D column which, in turn, is affected by the F value, ^{2}D column temperature, and the analyte-stationary phase interactions. The values of T_{min} and T_{max} affect the efficiencies of trapping and remobilization, and the rates at which T_{min} and T_{max} are achieved affect the minimum achievable P_M as well as the re-injection bandwidth for the ^{2}D column separation. The rate at

which T_{max} is reached for the μTM design used here is determined by the magnitude and duration of the applied heater voltage, and was as high as 2300 °C/s for the range of T_{min} and T_{max} values studied. The rate at which T_{min} is reached is determined by the thermal mass of the stage and the net thermal resistance of all heat dissipation pathways [17]. Although the thermal time constant for cooling the μTM was ~ 0.34 s, regardless of T_{max}, it required ~3-4 s to fully return to T_{min}.

Thermal crosstalk between the rim and each stage and between the two stages can also affect performance. If no voltage were applied to the rim heaters, then the inlet and outlet ports would reach temperatures similar to T_{min}, creating a cold spot in the sample transfer path. By applying a constant bias in the range of 2-3 V to each rim heater, the temperatures of the inlet and outlet ports were adjusted to match that of the GC oven (i.e., 25 or 33 °C). The inter-stage thermal crosstalk was ~7-10% for the μTM design used in this study under the conditions employed. This is as much as 3% higher than that for the device described in Ref. 42 owing to the shorter interconnection microchannel employed (i.e., 0.5 mm vs. 1 mm). As a result, heating the first stage led to a transient increase of ~16-19 °C in the value of T_{min} for the second stage during each modulation over the ranges of T_{max} and T_{min} values studied. Increasing O_s from the default value of 600 ms to 1800 ms prolonged the transient temperature and reduced the trapping efficiency of the 2nd stage. Reducing O_s to 200 ms gave performance similar to that for O_s = 600 ms, indicating that inter-stage heat transfer is rapid.

Performance was assessed with respect to the *fwhm* of the primary modulated peaks, t_R values and critical-pair resolution in the ^{2}D column (R_{s2}), the modulation ratio (M_R, i.e.,

number of detectable ^{2}D peaks per ^{1}D peak), n_p, and the extent of breakthrough and wrap-around. The latter two phenomena were assessed qualitatively by careful inspection of the 2-D chromatograms. Breakthrough occurs when the trapping capacity of the μTM is exceeded in one or both stages. It is accompanied by the appearance of vertically broadened signals in the 2-D chromatogram at ^{1}D retention times that are earlier than expected, and it results in unpredictable ^{2}D retention times. Wrap-around occurs when P_M is shorter than the retention time on the ^{2}D column. It results in compounds eluting in a later modulation cycle at an unpredictable, though reproducible, ^{2}D retention time. R_{s2} is defined as $(t_{R2} - t_{R1})/w_A$, where t_{R2} and t_{R1} are the ^{2}D retention times of adjacent compounds, assuming co-elution in the first dimension, and w_A is the average base peak width of the primary modulated peaks [68]. Values of R_{s2} for the ("critical") n-octane/hexanal pair were used to compare the performance under certain operating conditions.

The peak capacity represents the hypothetical number of perfectly spaced peaks that could be separated at a specified value of R_s: $n_p = 1 + N^{1/2}/(4R_s)\ln(t_{Rn}/t_M)$ [69], where N is the plate number derived from the equation $5.545(t_R/fwhm)^2$, $R_s = 1$ for this study (arbitrary), and t_{Rn} is retention time of the last retained peak. For GC×GC separations, $n_{p,GC\times GC}$ is the product of the peak capacity for each dimension, i.e., $n_{p1} \times n_{p2}$ [61], and P_M is used instead of t_{Rn} for the ^{2}D column [66].

3.3.1 Modulator temperatures.

The influence of T_{min} and T_{max} on performance was evaluated using the following seven VOCs, the boiling points (*bp*) of which range from 80 to 174 °C: benzene, isoamyl

alcohol, hexanal, n-octane, 2-methyl-2-hexanol, 2-heptanone, and n-decane. The values of O_s, P_M, and F used initially were 0.6 s, 6 s, and 0.9 mL/min, respectively.[42] Four different combinations of T_{min} and T_{max} were tested; as the value of T_{min} was adjusted the corresponding value of T_{max} was also adjusted so as to maintain a span (i.e., $\Delta T = T_{max} - T_{min}$) of 220-230 °C.

For the first tests, with T_{min} = -27 °C and T_{max} = 195 °C, the ^{1}D column temperature was 25 °C and the 2-D chromatogram in Figure 3.2a was obtained. MR values were between 2 and 3 for all compounds, all 2D tR values were < 2.5 s, Rs2 was 1.7, and the separation required 4.4 min. Importantly, the most volatile test compound, benzene, was trapped efficiently in the μTM under these conditions. The ^{2}D t_R values of the polar compounds were generally larger than those of the hydrocarbons, as expected, and the *fwhm* value of the primary modulated peak of each compound ranged from 82 ms (n-octane) to 300 ms (n-decane). The tailing observed along the 2D axis could arise from any of several of factors, including the low value of T_{min}, the relatively thick PDMS wall coating in the μTM, and the short segment of downstream interconnecting capillary**,** which was at the oven temperature of 25 °C.

For the second test condition (Figure 3.2b), the GC oven (^{1}D column and capillary interconnect) temperature was increased to 33 °C, and the lowest T_{min} value that could be maintained was -20 °C. The value of T_{max} was therefore increased to 210 ºC. Under these conditions, breakthrough of benzene occurred; it eluted from the ^{2}D column as a broadened signal in the modulation cycle preceding that in which it was expected, and gave an anomalous ^{2}D t_R value of ~5.4 s. This can be attributed to the inter-stage thermal crosstalk,

which led to a transient increase in the second-stage T_{min} value to −1°C during each modulation and reduced the trapping capacity for benzene. The ^{2}D t_R and M_R values of the remaining test compounds were similar to those in Figure 3.2a, but the ^{1}D retention times were shorter due to the higher ^{1}D column temperature. In addition, there was less ^{2}D peak tailing due to the higher T_{min}, T_{max}, and interconnect temperatures; values of *fwhm* of the primary modulated peaks decreased slightly for the more volatile compounds (e.g., 72 ms for n-octane) and significantly for the less volatile compounds (e.g., 197 ms for n-decane). The R_{s2} value increased to 2.4 while the separation time decreased to 2.9 min.

For the data shown in Figure 3.2c, T_{min} was increased to 0 ºC (transient second-stage T_{min} = 16 °C) and T_{max} was increased to 230 °C while maintaining the column temperatures as in the previous run. In this case, both benzene and n-octane showed evidence of breakthrough from the second stage, and *fwhm* values increased 2- to 3-fold for all other compounds except n-decane, for which *fwhm* decreased by ~10% (i.e., 180 ms) in spite of the higher value of T_{min}. Apparently, the increase in *fwhm* for the four other compounds arises from a reduction in focusing within the second stage of the modulator and a consequent increase in the re-injection bandwidth. Accordingly, the ^{2}D t_R and M_R values, and total separation time were the same as those for Figure 3.2b. Due to n-octane breakthrough, R_{s2} could not be calculated. The separation required < 1 min.

For T_{min} = 20 ºC (transient second-stage T_{min} = 35 °C) and T_{max} = 250 °C, all compounds except for n-decane broke through the modulator (data not shown). The *fwhm* of n-decane remained at 180 ms, suggesting that these conditions would be suitable for compounds of similar and somewhat lower volatility than n-decane. Note that *fwhm* for n-

decane did not change upon reducing T_{max} to 210 ºC, which indicates that the re-injection bandwidth was not limited by this factor.

From the preceding results, values of T_{min} = -20 °C and T_{max} = 210 °C seemed to provide the best performance for this set of compounds, with the exception of benzene. With these modulator temperatures and the other operating conditions used in this series of experiments, $n_{p,\mathrm{GCxGC}}$ was 216 on the basis of the n-decane t_R and *fwhm* values (n_{p1} = 18; n_{p2} = 12) and 60 on the basis of 2-heptanone t_R and *fwhm* values (the latter allows comparisons with data from the next series of experiments).

3.3.2 Flow rate.

In GC×GC, it is generally necessary to compromise between optimal carrier gas velocities for the ^{1}D and ^{2}D columns, because they are connected in series and F cannot be adjusted independently. In general, F should be adjusted such that the maximum ^{2}D t_R value is less than P_M. This places a constraint on the minimum F value. At higher F values, several issues can arise. First, the trapping capacity of the modulator can be exceeded because of sample overloading or because insufficient time is available for the first stage to cool down after the first modulation heating event. Second, M_R values can be reduced because the peaks eluting from the ^{1}D column are narrower [68]. Third, the retention on the ^{2}D column could be reduced to a point where resolution is compromised. These factors, thus, place constraints on the maximum F value.

Golay plots generated separately for each column using He as carrier gas, (n-octane, k = 2.7, 33 °C for ^{1}D; and n-tridecane, k = 2, 80 °C for ^{2}D) indicated optimal velocity values,

u_{opt}, of 37 and 14 cm/s for the ^{1}D and ^{2}D column, with H_{min} values of 0.028 and 0.017 cm, respectively. The corresponding values of N are 3570 and 5500 plates/m, respectively. This corresponds to F values of 1.2 mL/min for ^{1}D column, and 0.06 mL/min for ^{2}D column (via FlowCalc). The effect of F was explored for a subset of 5 test compounds (i.e., benzene, isoamyl alcohol, hexanal, n-octane, and 2-heptanone) at discrete F values of 0.1, 0.4, 0.9, and 1.5 mL/min. The corresponding theoretical values of u for the ^{1}D and ^{2}D columns were as follows: 3 and 25 cm/s, 13 and 79 cm/s, 30 and 170 cm/s, and 45 and 201 cm/s, respectively. Thus, u_{opt} for the ^{1}D column is bracketed by the two highest values of F and u_{opt} for the ^{2}D column is exceeded at all values of F. Values of the other relevant operating variables are given in the caption of Figure 3.2.

As shown in the 2-D chromatograms in Figure 3.2d-f, increasing F leads to a commensurate decrease in the ^{1}D column t_R values of all compounds. Notwithstanding the breakthrough of benzene under these conditions, the effects on the ^{2}D column separation vary. At F = 0.1 mL/min the ^{2}D t_R values exceeded P_M and all compounds exhibited wrap around, however, all compounds were well separated (data not shown). Due to the broadness of the ^{1}D peaks at this low flow rate, the M_R values were > 3 and the separation required 4.4 min. The large *fwhm* values of the primary modulated peaks of the compounds are also attributed to the low F in the ^{2}D column (e.g., n-octane *fwhm* = 627 ms).

At F = 0.4 mL/min (Figure 3.2d), all compounds were effectively separated in 1.6 min. R_{s2} was 2.7, M_R values ranged from 2.5 to 3.5, and the *fwhm* for the primary modulated peak of n-octane was 130 ms. On the basis of 2-heptanone, the $n_{p,GC\times GC}$ for this flow rate is 200 (n_{p1} = 25; n_{p2} = 8). At F = 0.9 mL/min (Figure 3.2e), the compounds were also

effectively separated, R_{s2} was 2.5, M_R values ranged from 2 to 3, and the separation required 1.1 min. The *fwhm* for the primary modulated peak of n-octane was 76 ms. On the basis of 2-heptanone, the $n_{p,GC\times GC}$ for this modulation period is 180 (n_{p1} = 18 and n_{p2} = 10); slightly lower than at 0.4 mL/min. Increasing F to 1.5 mL/min (Figure 3.2f) led to very short t_R values on the ^{2}D column. R_{s2} was not calculated due to breakthrough of n-octane, however, the resolution among the other compounds was lower than that at 0.9 mL/min. At this F, the base peak widths from the ^{1}D column decreased to where M_R values were < 2. The separation required <1 min.

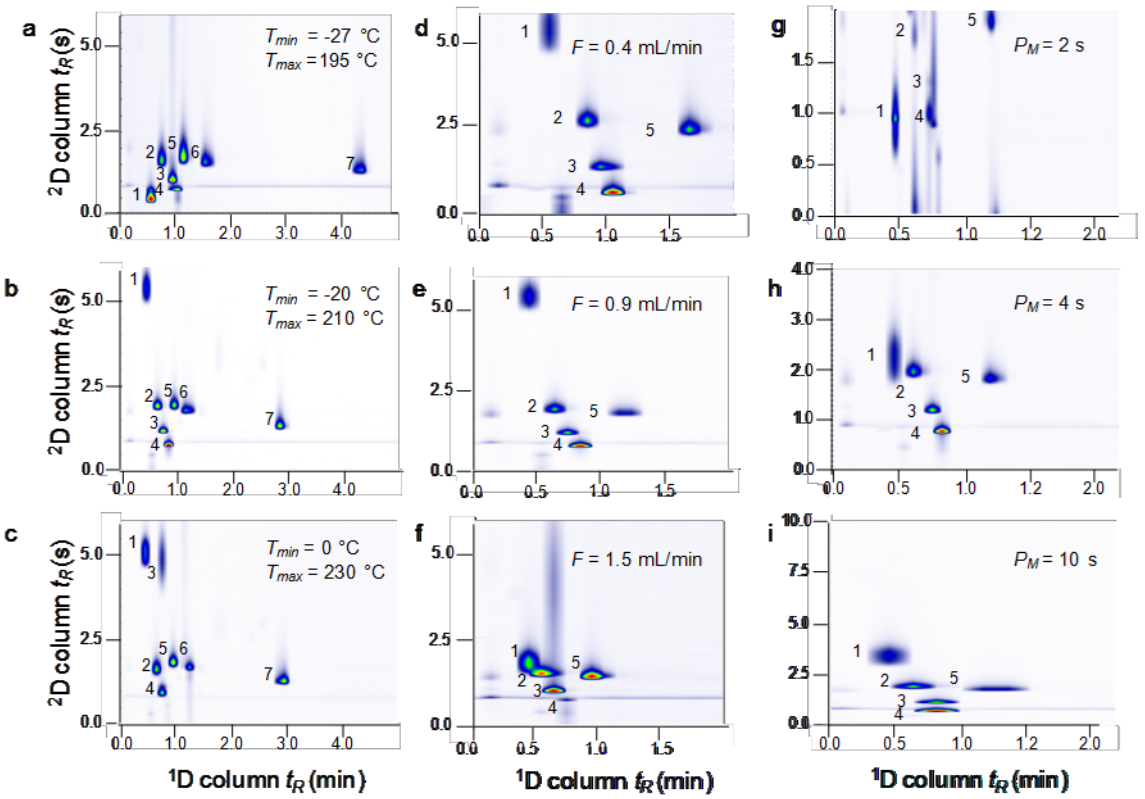

Figure 3.2. 2-D chromatogram showing the effect of the modulator temperatures (a, b, c), volumetric flow rate (d, e, f), and modulation period (g, h, i) on the quality of separations; ^{1}D column temperature = 33 °C (25 °C for (a)), ^{2}D column temperature = 80 °C. Conditions for a, b, and c: F = 0.9 mL/min, P_M = 6 s, O_s = 600 ms. Conditions for d, e, and f: P_M = 6 s, O_s = 600 ms, T_{min} = -20 °C, T_{max} = 210 °C. Conditions for g, h, and i: F = 0.9 mL/min, O_s = 600 ms, T_{min} = -20 °C, T_{max} = 210 °C. Compounds: 1, benzene; 2, isoamyl alcohol; 3, hexanal; 4, n-octane; 5, 2-methyl-2-hexanol; 6, 2-heptanone; 7, n-decane.

Although similar results were obtained for F values of 0.4 and 0.9 mL/min, the latter was deemed preferable because it reduced the analysis time by 30% with minimal decreases in R_{s2} (8%) and $n_{p,GCxGC}$ (10%). In addition, the linear velocity in ^{1}D for F = 0.9 mL/min is 30 cm/s, which is closer to u_{opt} (37 cm/s). At the same time, however, the linear velocity in ^{2}D is 170 cm/s, which is 12 × u_{opt} (14 cm/s). At 0.4 mL/min, the ^{2}D linear velocity, 74 cm/s, is only 5·$u_{opt,}$ but the ^{1}D linear velocity of 13 cm/s is 0.3·u_{opt} (37 cm/s). Thus, both conditions involve tradeoffs in chromatographic efficiency.

3.3.3 Modulation period

For the next series of tests, P_M was varied from 2 to 10 s while keeping all other variables at the values shown in the caption of Figure 3.2e. The same subset of five test vapors was used. The shortest P_M value of 2 s (Figure 3.2g) resulted in breakthrough for all compounds due to insufficient time for cooling the μTM stages between successive heating events. There was also some evidence of wrap-around for those compounds with t_R (^{2}D) close to 2 s. At P_M = 4 s (Figure 3.2h), all compounds were effectively separated, R_{s2} was 2.4, M_R values ranged from 2.2 - 3, and the separation required 1.1 min. The *fwhm* for the primary modulated peak of n-octane was 80 ms. On the basis of 2-heptanone, the $n_{p,GC\times GC}$ for this modulation period is 171 (n_{p1} = 18; n_{p2} = 9.5). The data for P_M = 6 s was already presented in Figure 3.2e. R_{s2} was 2.2, M_R values ranged from 2.0 - 3.0, and the ^{2}D t_R values were similar to those with P_M = 4 s. Despite the slightly smaller values of M_R and R_s, a P_M of 6 s is considered preferable to 4 s because it allows more time for the ^{2}D separation and a slightly higher $n_{p,GC\times GC}$ (i.e., 180, based on 2-heptanone, see above).

At P_M = 10 s (Figure 3.2i), all compounds were effectively separated and only benzene suffered breakthrough. At this P_M value breakthrough might have been expected due to the limited capacity of the μTM, however, none was observed for other compounds. R_{s2} was reduced to 1.6 and M_R values were < 1.5 for all compounds, which is less than optimal, since the resolution in ^{2}D is degraded. The separation required 1.1 min. The *fwhm* of the principal modulated peak for n-octane was 78 ms. The $n_{p,GC\times GC}$ value determined on the basis of 2-heptanone increases to 234 (n_{p1} = 18; n_{p2} = 13) primarily by virtue of using the value of P_M as the default retention time in the peak capacity calculation. It is clear from Figure 3.4c

that one would want to operate at a lower flow rate to take full advantage of such a long P_M setting.

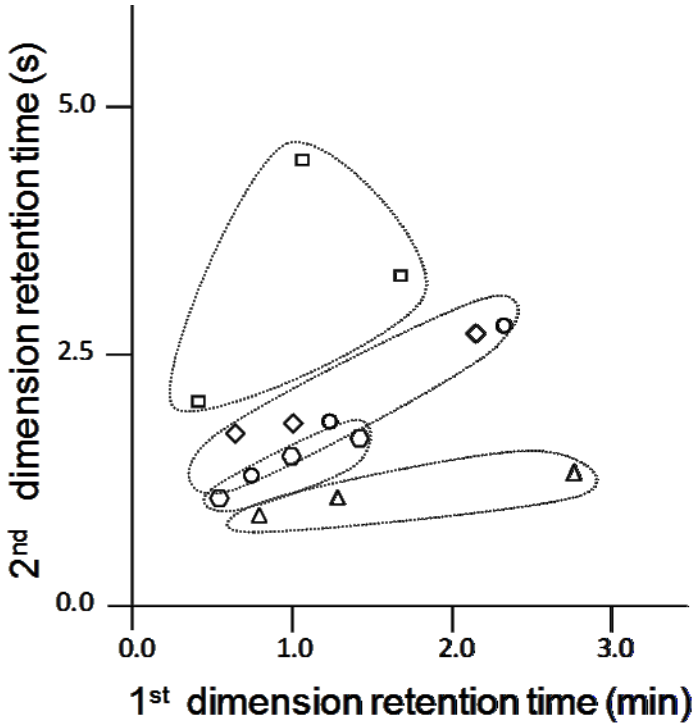

Figure 3.3. Structured chromatogram of compounds from several functional group classes. Symbols designate subsets: triangles for alkanes (in order of ^{1}D t_R, n-heptane, n-octane, n-nonane); hexagons for aromatics (in order of ^{1}D t_R, toluene, m-xylene, cumene); circles for ketones (in order of ^{1}D t_R, 2-hexanone, cyclopentanone, 2-heptanone); diamonds for aldehydes (in order of ^{1}D t_R, hexanal, heptanal, benzaldehyde); and squares for alcohols (in order of ^{1}D t_R, 1-propanol, 1-hexanol, 2-heptanol).

Table 3.1 Reproducibility of t_R and area of modulated peaks in the ^{2}D column.[a]

compound	t_{R2} (s)	Peak area (pA·s)[b]			
		mod 1	mod 2	mod 3	A_t
benzene	1.31 (3.6)	0.08 (4.5)	0.70 (5.9)	n/a	0.78 (4.9)
hexanal	1.52 (4.7)	0.09 (5.7)	0.51 (0.8)	0.06 (6.7)	0.66 (2.6)
isoamyl alcohol	1.87 (2.9)	0.07 (5.9)	0.13 (5.4)	0.23 (6.0)	0.43 (5.0)
n-octane	2.57 (2.8)	0.41 (2.8)	0.17 (5.4)	0.08 (4.9)	0.66 (1.0)
2-heptanone	2.76 (2.2)	0.21 (5.5)	0.23 (4.7)	0.07 (3.6)	0.51 (1.3)

[a] From replicate sample-loop injections of test atmospheres containing 16-18 ng of each vapor (n = 4). Values in parentheses are RSDs (%). Conditions: ^{1}D column temp.: 33 °C, ^{2}D column temp. = 80 °C, F = 0.9 mL/min, T_{min}/T_{max} = -20/210 °C, P_M = 6 s, O_s = 600 ms, FID.

[b] mod 1, 2, and 3 refer to the series of modulated peaks for a given compound; A_t = total area of all modulated peaks.

3.3.4 Reproducibility.

To examine reproducibility, four replicate separations were performed for the same subset of five test compounds used in previous experiments under the conditions presented in Figure 3.2e. Table 3.1 shows the relative standard deviation (RSD) of the ^{2}D t_R values and total area of the modulated peaks. The former ranged from 2.2% for 2-heptanone to 4.6% for isoamyl alcohol and is largely a consequence of the lack of an automatic modulation event start timer for the GC×GC analysis. The tailing peaks obtained for isoamyl alcohol in the ^{2}D column contribute to its higher RSD value. The sums of the modulated peak areas show a similar degree of variability, with RSDs ranging from 1-5%. RSD values of the peak areas for individual modulated peaks, also shown in Table 3.1, are as high as 7%, undoubtedly due to changes in modulation phase associated with slight changes in the timing of the modulations [70].

3.3.5 Structured chromatogram

Figure 3.2 shows more clearly the effect of the different stationary phases of the two columns. A mixture of 12 compounds composed of sets of n-alkanes (n-heptane, n-octane, n-nonane), aromatics (toluene, m-xylene, cumene), aldehydes (hexanal, heptanal, benzaldehyde) and alcohols (1-propanol, 1-hexanol, 2-heptanol) was separated using the conditions described above (see Figure 3.2e).

The alkanes eluted in order of *bp* from the ^{1}D column and were well separated, but they were not retained significantly on the polar ^{2}D column. The aromatic compounds also eluted in order of *bp* from the ^{1}D column and were retained only slightly longer than the

alkanes on the ^{2}D column, due to p-π interactions with the ether moieties on the PEG stationary phase of the ^{2}D column. The ketones and aldehydes also showed *bp* separations on the ^{1}D column and moderate retention on the ^{2}D column that reflects their relative polarities and the dominance of dipole-dipole interactions with the PEG. Note that several of these compounds co-eluted with the aromatics and alkanes on the ^{1}D column, but they were separated on the ^{2}D column. As expected the alcohols, except 1-propanol, had the largest t_R values on the ^{2}D column by virtue of strong dipolar and hydrogen-bonding interactions with the PEG. The relative low ^{2}D t_R for 1-propanol can be explained by its high polarity and low volatility, which leads to second-stage breakthrough, as seen for benzene in previous experiments.

The grouping of homologues within a functional group class is a well-known feature/advantage of GC×GC analyses of complex samples, where compound-specific analyses are often not necessary or feasible [61]. Although a high degree of orthogonality is observed between the ^{1}D and ^{2}D column separations, the increase in ^{2}D retention time with increasing carbon number within a homologous group reflects some residual volatility-based separation. This could be reduced or eliminated with temperature programming of the ^{2}D column.

3.3.6 Fast GC×GC separation of a moderately complex mixture.

Figure 3.4a shows the chromatogram from the ^{1}D column (i.e., bypassing the μTM and ^{2}D column) of a 21-component test mixture containing compounds spanning a *bp* range of 80 °C (benzene) to 178 °C (benzaldehyde). The column temperature was 33 °C and *F* was

set to 5 mL/min to obtain t_R values similar to those at 0.9 mL/min with the GC×GC set-up (Figure 3.4b). Peak assignments are based on individual runs of each component. The total analysis time was only 3 min. Overall, good peak shapes were obtained with some tailing of the more polar compounds. The following full or partially co-elutions are apparent: peaks 3/4 (1-propanol/n-heptane), 6/9/10 (n-octane/2-hexanone/cyclopentanone), 15/16 (cumene/heptanal), and 13/21 (2-heptanone /benzaldehyde). The n_p for this chromatogram is ~ 31 on the basis of the n-decane t_R value. Note that a relatively high value of F (i.e., 5 mL/min) was employed in this 1-D separation to achieve t_R values comparable to those in the GC×GC separation shown in Figure 3.4b. This is well above the optimal value. However, operating at F = 1.2 mL/min (i.e., u_{opt}) increased the total separation time 3-fold (i.e., to 9 min).

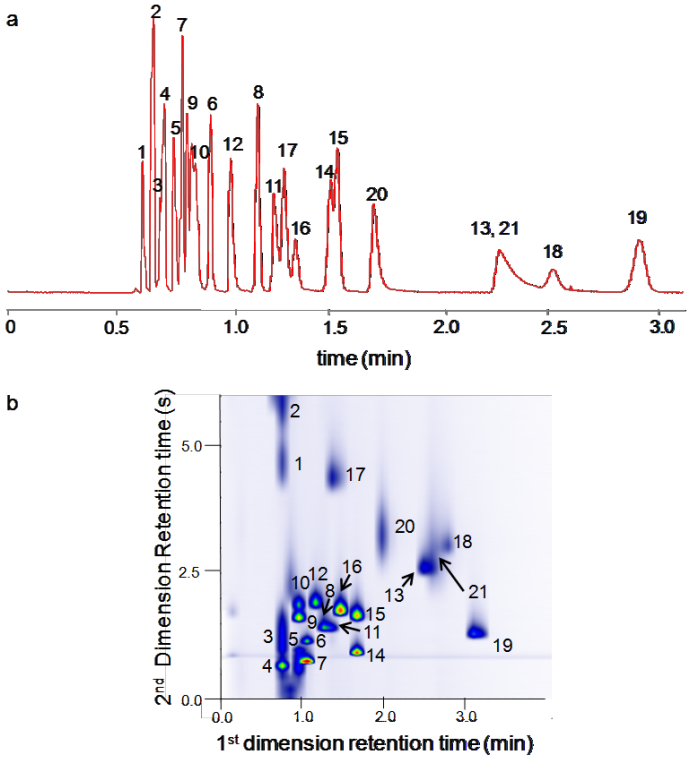

Figure 3.4. (a) 1-D chromatogram of a 21-component mixture (16-20 ng of each compound, injected as vapor). Conditions: 6-m, 0.25 mm i.d. PDMS (0.25 µm thickness); 33 °C (oven); F = 5 mL/min, FID. (b) GC×GC chromatogram of the same mixture. The ^{1}D column was same used for the 1-D chromatogram (33 °C), the ^{2}D column was a 0.5-m, 0.10 mm i.d. PEG (0.10 µm thickness, 80 °C), F = 0.9 mL/min, T_{min}/T_{max} = -20/210 °C, P_M = 6 s, O_s = 600 ms, FID. Compounds (*bp*, °C): 1, benzene (80); 2, trichloroethylene (87); 3, 1-propanol (97); 4, n-heptane (98); 5, toluene (111); 6, hexanal (119-124); 7, n-octane (125); 8, 2-hexanone (127); 9, cyclopentanone (130); 10, isoamyl alcohol (131); 11, m-xylene (139); 12, 2-methyl-2-hexanol (141); 13, 2-heptanone (150); 14, n-nonane (151); 15, cumene (152); 16, heptanal (153); 17, 1-hexanol (155-159); 18, octanal (171); 19, n-decane (174); 20, 1-heptanol (175); 21, benzaldehyde (178).

Figure 3.4b shows the GC×GC chromatogram for the same mixture with the same modulator settings and operating conditions as used in the preceding section. Peaks 1, 2, and 3 correspond to the most volatile members of the mixture, benzene, trichloroethylene and 1-propanol, respectively. They all showed evidence of breakthrough, as expected (*vida supra*). The peaks of the polar compounds (i.e., peaks 17, 18, 20, 13, and 21) were broader than those

of the non-polar compounds due to the longer ^{2}D t_R values. Values of *fwhm* of the primary modulated peaks ranged from 75 ms (n-heptane) to 900 ms (benzaldehyde). All of the overlapping peaks in the ^{1}D separation (Figure 3.4a) are resolved in the ^{2}D dimension except for 15/16 (cumene/heptanal), which remain only partially resolved in the 2-D plot. The $n_{p,GC\times GC}$ is ~ 367.

3.4. Conclusions

This is the first study to demonstrate GC×GC separations with a μTM. Short ^{1}D and ^{2}D columns were employed in anticipation of using microfabricated columns to assemble a μGC×μGC system, which resulted in fast separations even for the moderately complex mixtures tested. The effects of the key operating variables T_{min}, T_{max}, O_s, P_m, and F on the quality of isothermal GC×GC separations were rationalized in terms of the trapping capacity and transfer efficiency of the μTM, and the retention time on the ^{2}D column. Results demonstrate that under proper operating conditions the performance of this robust μTM rivals that of some commercial modulators requiring much higher operating power or consumable cryogenic fluids.

Due to the need to control the ^{1}D column temperature by means of a conventional GC oven in this series of experiments, the lowest value of T_{min} achievable was limited by the oven temperature, which in turn reduced the trapping efficiency of the more volatile compounds tested. This problem will be easily resolved in the planned μGC × μGC system by using on-chip heaters and temperature sensors to control the ^{1}D and ^{2}D microcolumn temperatures. Thermal crosstalk between stages also contributed to breakthrough of the more

volatile compounds, and the relatively slow cooling time of the μTM stages limited the minimum P_M to about 4 s. These issues should be resolved by increasing the length of the inter-stage interconnection channel and reducing the air gap between the μTM and the TEC (at the cost of somewhat greater heating power dissipation), respectively.

Although a T_{max} of 210 °C was sufficient to remobilize even the least volatile compounds tested here, a higher T_{max} would be required to analyze mixtures containing components with boiling points > 200 °C (e.g. essential oils, pesticides, and diesel fuel). Furthermore, progressive ramping of T_{min} and T_{max} would be required to analyze more complex mixtures. The former may require use of a different stationary phase in the modulator due to the possibility of excessive bleed at higher temperatures. The latter could be addressed by implementation of temperature controllers to coordinate T_{min} and T_{max} with the (micro)column temperature program over the course of the separation, while maintaining a constant value of ΔT [33]. These modifications would increase the range of compounds and the effective peak capacity of a μGC × μGC system.

Chapter 4. μGC × μGC: Comprehensive Two-Dimensional Gas Chromatographic Separations with Microfabricated Components

4.1. Introduction

The quantitative analysis of airborne volatile/semi-volatile organic compounds (S/VOC) is critical to solving numerous vexing problems, including mapping and remediating environmental pollution, [71] assessing human exposures, [72] diagnosing metabolic abnormalities, [73] combating terrorism, [74] and ensuring indoor air quality. [75] Performing such measurements directly in the field or clinic can improve the quality and quantity of data collected and can facilitate rapid interventions. Since reliable determinations of S/VOCs in complex mixtures generally require temporal/spatial separation prior to detection, gas chromatography (GC) is one of the most effective approaches to such analyses.

Advances in commercial, field-deployable GC instrumentation have led to significant improvements in performance, reliability, and portability, [76, 77, 78, 79] and research on GC microsystems (μGC) fabricated using Si-micromachining processing techniques [37] continues to produce innovative designs that further reduce size and power requirements. [33, 80, 35, 34, 81, 82, 83, 84] Such microsystems represent the most promising path to realizing miniature, low-cost, ubiquitous, near-real-time air monitors for S/VOC mixtures. Yet, the inherent limitations on the maximum length and minimum diameter of μGC separation

columns under pressure-driven flow place inherent constraints on peak capacity and resolution which, in turn, may limit the complexity of the mixtures that can be effectively analyzed.

Comprehensive two-dimensional gas chromatography (GC × GC) is widely viewed as the most effective method available for separating the components of highly complex S/VOC mixtures [85, 61] In GC×GC, a first-dimension (^{1}D) column is coupled through a modulator to a shorter second-dimension (^{2}D) column with retention selectivity complementary to that of the ^{1}D column. Each mixture component eluting from the ^{1}D column is re-injected in a series of narrow bands into the ^{2}D column at a rate that preserves the ^{1}D separation order. A 2-D contour plot depicting the separation in each dimension can be generated. Pneumatic [62, 45] or thermal [6, 13, 11, 66] modulators (TM) can be used, and each has advantages and limitations [86] In the latter, a cryogenically cooled fluid is typically used to trap and focus sequential segments of each analyte peak eluting from the ^{1}D column, and then a resistive or convective heater is used to reintroduce them to the ^{2}D column [13, 11, 12]. Rapid cycling between minimum (T_{min}) and maximum (T_{max}) temperature set-points produces the desired modulation. The primary advantages of GC × GC, particularly with thermal modulation, are the higher resolution and detectability that can be realized from the taller, sharper peaks produced, relative to 1-D GC systems [85, 61, 87].

In regard to μGC, adding an independent, second-dimension separation stage (i.e., μGC × μGC) is a logical approach to overcoming the limitations on analytical performance imposed by the inherently short μcolumns. Toward that end, Kurabayashi, et al. recently reported on a microfabricated TM (μTM) that operates at much lower power levels than

conventional TMs and that does not use any cryogenic fluids [17]. This μTM incorporates two, series-coupled, spiral Pyrex-on-Si microchannel stages with independent thin-metal-film meander-line heaters on each stage. It is mounted in proximity to a stacked, solid-state thermoelectric cooler (TEC). Rapid heating and cooling are possible and μTM-stage T_{min} values in the range of -20 to -35 ^{o}C and T_{max} values of 250 ^{o}C (or higher) are achievable. We have used this device to perform GC × GC separations with conventional capillary columns [18, 32], but testing to date has been performed under isothermal conditions (i.e, fixed values of T_{min}, T_{max}, and ^{1}D and ^{2}D column temperatures) that favored trapping and re-mobilization of more-volatile compounds. Less volatile analytes displayed much broader modulated peaks (*fwhm* ~seconds). Temperature programming of all components would expand the range of compounds for which effective μGC × μGC separations could be performed. Several other noteworthy efforts toward multi-dimensional μGC subsystems, all of which use pneumatic modulation or flow switching, have been reported over the past few years, as well. [88, 89, 46, 81]

Traditionally, the ^{1}D column is coated with a nonpolar stationary phase and the ^{2}D column is coated with a more polar or polarizable phase. For the latter, room temperature ionic liquids (RTILs) have been used to good effect [90]. Several members of a relatively new class of RTILs, having trigonal tricationic core structures and a bis(trifluoromethylsulfonyl)imide (NTf_2) anion, have been explored as GC stationary phases recently by Armstrong et al [91, 92]. A subset of these exhibits sub-ambient melting points, high decomposition temperatures, low bleed, and retention properties complementary to PDMS, [92] and thus are interesting prospects not only as ^{2}D μcolumn wall coatings but also

as possible μTM wall coatings (note: with a discrete μTM one could potentially use different phases in the μTM and the ^{2}D μcolumn in a μGC×μGC system).

As a further step toward the realization of a field portable μGC × μGC system having fluidic and analytical components arranged as shown in the block diagram in Figure 4.1, the work described here entailed the fluidic integration and testing of wall-coated ^{1}D and ^{2}D Si-microfabricated μcolumns with a wall-coated μTM. Conventional injection methods were used along with flame ionization detection (FID). PDMS was used in the ^{1}D μcolumns and the μTM, and both a trigonal tricationic RTIL and a commercial poly(trifluoropropyl methylsiloxane) (PTFPMS, OV-215) were investigated as ^{2}D μcolumn phases. After describing the deposition of the various stationary phases and characterization of the individual coated μcolumns, the results of testing the assembled subsystem with a simple mixture of alkanes under isothermal and temperature programmed conditions using the RTIL-coated ^{2}D μcolumn are presented. The separation of a more complex mixture of polar and non-polar compounds is then demonstrated and the retention behavior of the RTIL is further evaluated. Finally, using an OV-215 coated ^{2}D μcolumn, the separation of a moderately complex mixture of 36 compounds is presented. Results are considered in terms of their impact on the design and function of a fully integrated μGC × μGC system.

4.2. Experimental Section

Test compounds and starting materials for the RTIL synthesis were >98% pure (Sigma-Aldrich, Milwaukee, WI) and used without further purification. PDMS (OV-1) and PTFPMS (OV-215) were obtained from Ohio Valley Specialty Chemicals (Marietta, OH).

The RTIL was synthesized by a published method [92] and characterized by standard methods, as described in Figure 4.2-Figure 4.9, Table 4.1below. A commercial capillary column, coated with the same RTIL as that synthesized for this study and used as the stationary phase in one of the ^{2}D µcolumns, was tested for comparison (100 µm i.d., 0.5-m long, 0.08 µm SLB-IL76 phase, Supelco, Bellefonte, PA).

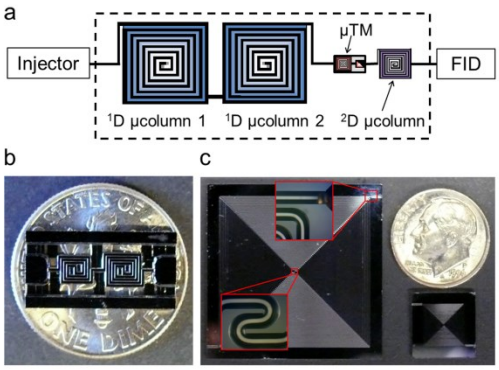

Figure 4.1. a) Block diagram of the µGC×µGC test set-up (dashed box represents the GC oven); b) the 2-stage µTM on a U. S. dime; c) 3-m ^{1}D µcolumn (left of dime) and 0.5-m ^{2}D µcolumn (below dime). Insets show enlargements of the ^{1}D µcolumn inlet and the center where the channel changes from a clockwise to an anticlockwise spiral.

4.2.1 Structure of the RTIL

The structure of the trigonal tricationic room-temperature ionic liquid (RTIL) that was synthesized and used as the ^{2}D µcolumn stationary phase is shown in Figure 4.2, [92].

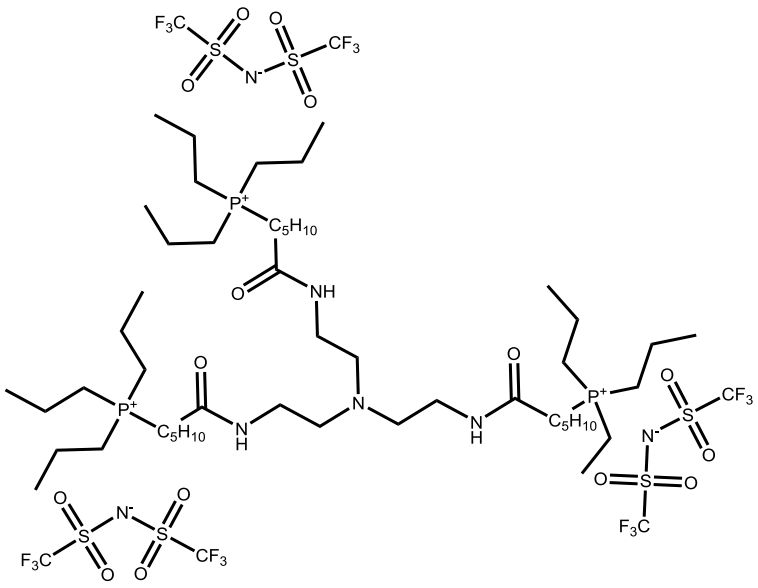

Figure 4.2 Structure of Tris[2-(6-aminopropylphosphoniumhexaamido)ethyl]amine tris[bis(trifluoromethylsulfonyl)imide] (RTIL).

4.2.2 Elemental analysis

Analyses for C, H, N, and F were performed by Atlantic Microlab Inc. (Norcross, GA). Duplicate measurements of C, H, and N were performed. Table 4.1shows the results. Experimental values agree closely with theoretical values.

Table 4.1 Elemental analysis of the RTIL (values are % mass).

Element	Theor.	Measured		Error[a]
C	38.93	38.5	38.5	-0.4
H	6.19	6.16	6.04	-0.09
N	5.57	5.32	5.28	-0.27
F	19.44	19.7	--[b]	+0.3

[a] difference of average measurement from theoretical; [b] duplicate was not collected.

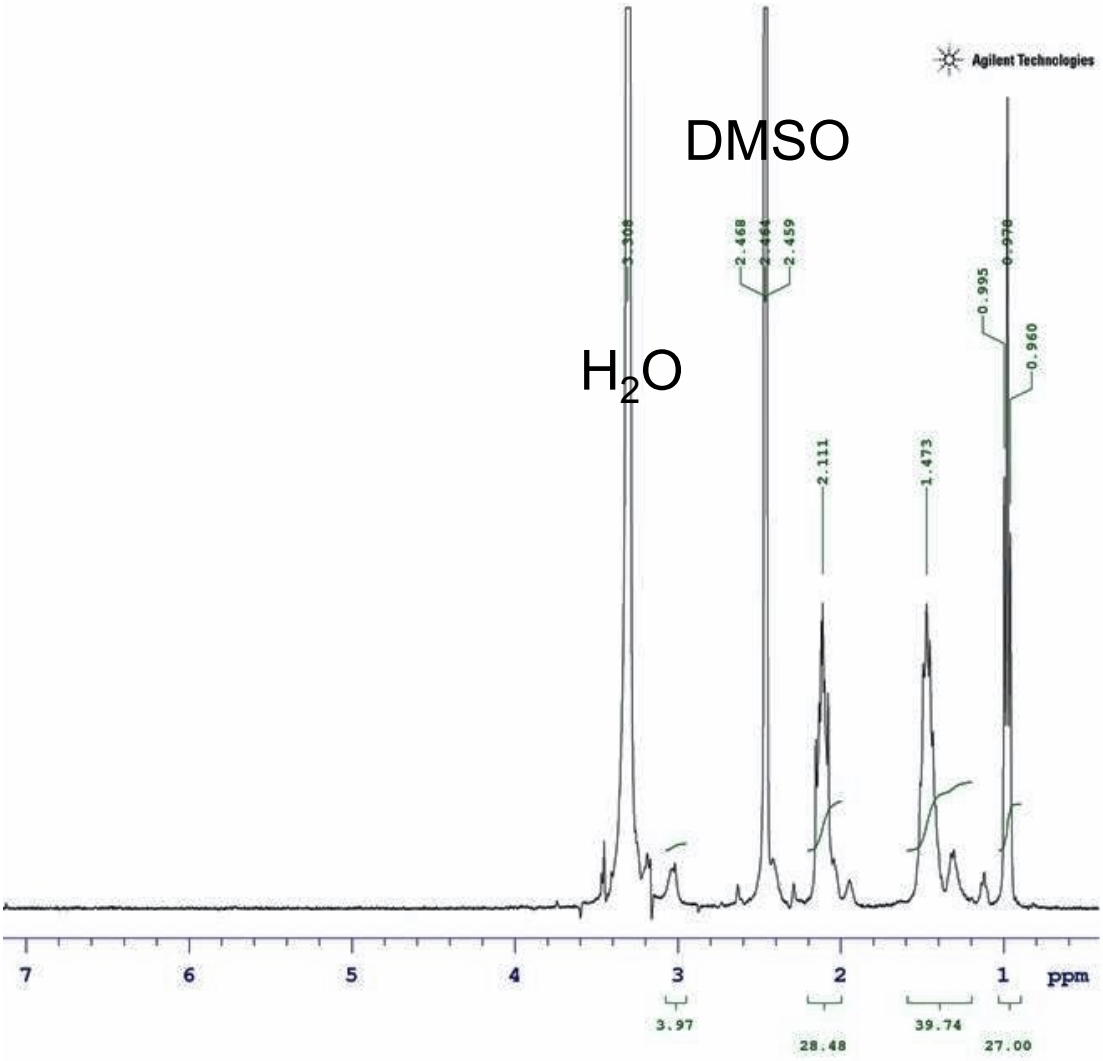

Figure 4.3 ^{1}H NMR (400 MHz, DMSO): δ(ppm) = 3.06 (br s, 4H), 2.11 (m, 28H), 1.47 (m, 40H), 0.98 (t, 27H). Multiplicities are reported as follows: singlet (s), triplet (t), multiplet (m), broad (b). All NMR spectra were recorded at room temperature.

4.2.3 ^{1}H NMR analysis

The ^{1}H NMR spectrum of the RTIL in DMSO-d6 was collected on a Varian MR400 spectrometer (400 MHz). Chemical shifts (δ, ppm) are relative to tetramethylsilane (TMS).

Chemical shifts and integrated intensities are consistent with those reported in the literature; [S-1] peaks due to residual water and other minor impurities are also apparent (Figure 4.3).

4.2.4 Phase transitions

Differential scanning calorimetry (DSC) was performed on a 13-mg sample of the RTIL crimp-sealed in an aluminum pan using a TA Instruments DSC Q2000. Scans were performed using the following non-isothermal protocol: pre-melting (equilibrate at -90 °C for 5 min); heating scan (linear ramp from -90 to 40°C @ 10°C/min); cooling scan (linear ramp from 40 to -90°C at 10 °C/min); repeat heating and cooling scans for a total of 10 scans. Figure 4.4presents the results. Phase transition temperature of -27 °C is close to the literature value of -31 °C [92].

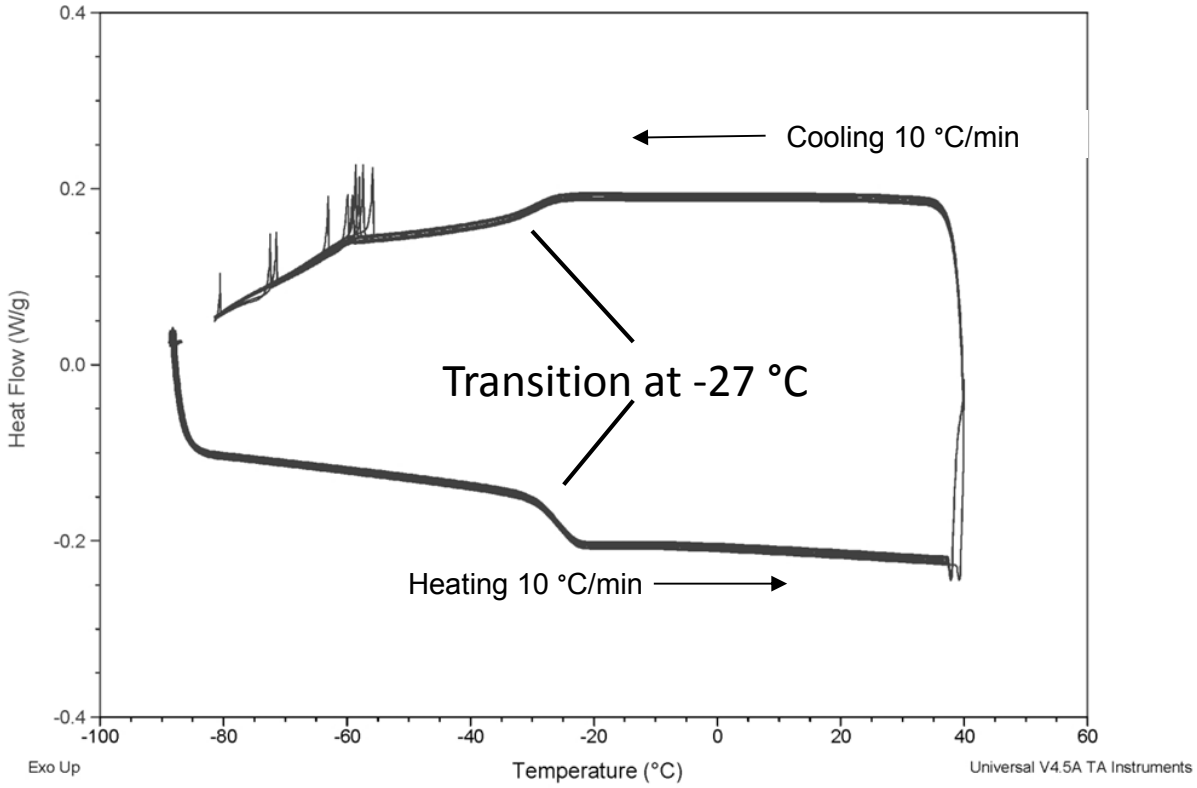

Figure 4.4 DSC thermogram for the RTIL. The solid-to-liquid phase transition occurs between -25.3°C and -28.8°C. 10 scans overlaid.

4.2.5 Thermal stability

Thermogravimetric analysis (TGA) was used to determine the thermal stability of the RTIL using a Perkin Elmer Pyris 1 instrument. Samples (~ 10 mg) were heated in platinum pans from 30 to 600°C at 10°C/min in both N_2 and air sheath gases. Results are presented in Figure 4.5 as mass loss vs. temperature. Values of 1% and 5% mass loss under N_2 were 290 and 370 °C respectively. These were 2.1% higher and 4.9% lower than the values reported in literature [92]. Values of mass loss in air are similar to those in N_2, confirming the high-temperature air stability of this RTIL.

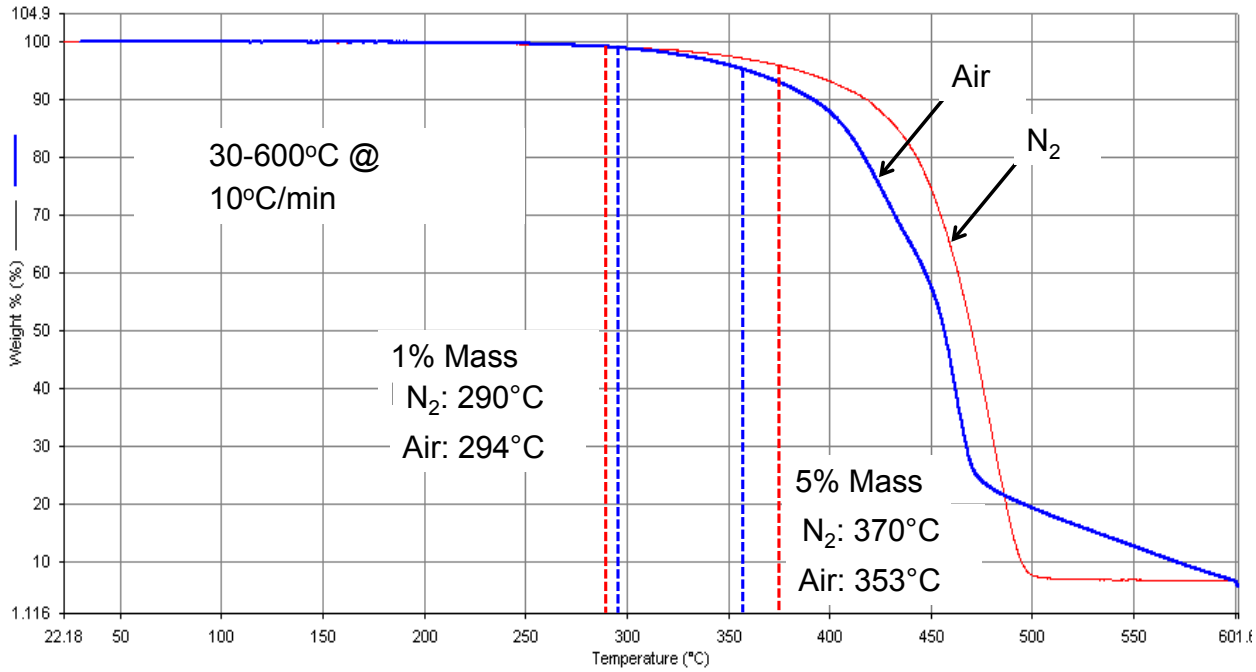

Figure 4.5. TGA curves for the RTIL heated at 10 °C/min with a sheath gas of N2 (red curve) and air (blue curve).

4.2.6 Devices:

Figure 4.1b shows the microfabricated devices employed. The two-stage µTM was described previously [18, 17, 47].The 13×6 mm Si chip contains a single deep-reactive-ion-etched (DRIE) Si µchannel with a cross section of 250 (w) × 140 (h) µm along the length of which are two convolved square-spiral segments, 4.2 cm (stage 1) and 2.8 cm (stage 2) long, separated by a 1.0 mm long straight segment. A 100-µm thick Pyrex cap is anodically bonded to the top surface of the entire chip to seal the µchannel. Four meander-line Ti/Pt resistive heaters are patterned on the Pyrex surface; one above each µTM stage and one each on the rim above the inlet and outlet ports. Ti/Pt RTDs are patterned beside the heaters to measure temperature.

The μTM was connected to upstream and downstream (μ)columns through 10-cm sections of deactivated fused silica capillary (250 μm i.d., upstream; 100 μm i.d., downstream) inserted into expansion ports on the chip and sealed with epoxy (Hysol 1C, Rocky Hill, CT). The device was epoxied Pyrex side up and wire-bonded to a custom carrier printed circuit board (PCB) with a hole cut out beneath the device for thermal isolation. This sub-assembly was inverted and mounted such that the Pyrex surface of the μTM was suspended directly above the TEC (SP2394, Marlow Industries, Dallas, TX). Two small slabs of Si were placed on the TEC beneath the μTM stages and two more small Si spacers were placed on the slabs. The slabs and spacers were held in thermal contact with the TEC surface with thermal grease, and the μTM was positioned with a height gauge to within ~40 μm of the spacers. The spacer and slab help to focus the cooling on the two μTM stages, while the small air gap reduces power for heating [17]. A plastic shroud through which a constant stream of dry air is passed during operation to prevent atmospheric water condensation on the device is secured around the μTM.

The basic design and fabrication of the μcolumns used here have also been described previously. [8, 3] Each μcolumn consists of a DRIE-etched Si channel with an anodically bonded Pyrex cap. Thin-film Ti/Pt heaters and RTDs patterned on the back side of the Si permit temperature ramping, although this feature was not used in the current study. The ^{1}D separation stage consisted of two series-coupled 3.1 × 3.1 cm μcolumn chips with convolved square-spiral DRIE channels, 3-m long and 250 × 140 μm in cross section, wall-coated with a PDMS stationary phase. The ^{2}D separation stage consisted of a 1.2 × 1.2 cm μcolumn chip with a similarly shaped DRIE channel, 0.5-m long and 46×150 μm in cross section, wall-

coated with either the RTIL or OV-215. Fluidic connections were made through ~5-cm segments of fused silica capillary (250 μm i.d. for 3-m μcolumns, 100 μm i.d. for 0.5-m μcolumns) epoxied into expansion ports in the Si chips.

4.2.7 Stationary Phase Deposition.

The ^{1}D μcolumns and μTM were statically coated individually with PDMS from a solution that also contained 1% (w/w) dicumyl peroxide as the crosslinking agent using a published procedure [7, 9]. PDMS concentrations were adjusted to produce an average (nominal) wall-coating thickness of 0.20 μm for the ^{1}D μcolumns and 0.30 μm for the μTM. The PDMS in the μcolumns was cross-linked by heating at 180 °C for 1h under N_2 in a GC oven. The PDMS in the μTM was cross-linked by heating at 180 °C for 1h under N_2 using the on-chip stage heaters in order to avoid rupturing the capillary-chip union from expansion of the adhesive. An unavoidable consequence of the method is that the connecting capillaries were coated (in both the μcolumn and μTM) and crosslinked (only in the μcolumn).

Prior to (statically) coating one of the ^{2}D μcolumns with the RTIL, it was pre-treated with NaCl to promote adhesion according to a published method [93].

4.2.7.1 RTIL and OV-215 deposition on the ^{2}D μcolumns

In preparation for pretreating the 0.5-m ^{2}D μcolumn prior to RTIL coating, a colloidal suspension of NaCl was prepared by rapidly dispensing 3 mL of saturated NaCl in methanol into 8 mL of 1,1,1-trichloroethane (TCA). After rinsing the μcolumn with dichloromethane and methanol, the suspension was passed through the μcolumn at 2-3 cm/s under a positive pressure of N_2, leaving a thin layer of the salt on the inner walls. After drying under N_2, a

rough, (visually) uniform film of NaCl remained on the walls. The μcolumn was then statically coated with the RTIL from a dichloromethane solution (8 mg/mL) to yield a nominal average RTIL-film thickness of 0.1 μm.

A second pretreatment using cyanopropyltetramethyldisiloxane (CPTMS) was attempted according to a published method [94]. First, the μcolumn was rinsed sequentially with dichloromethane and methanol, and then dried under N_2. Then, a 20% solution of aqueous HCl was passed through the μcolumn for 30 min at 0.1 mL/min, followed by rinsing with 1 mL of methanol and drying with N_2. Next, 1 mL of 10 % CPTMS in methanol was passed though the μcolumn. After drying under N_2 for 30 min, the ends of the μcolumn were sealed with silicone septa and it was heated at 300 °C for 24 hr. The μcolumn was then rinsed with 1 mL each of methanol, dichloromethane, and diethyl ether, and dried under N_2.

In preparation for coating with OV-215, the ^{2}D μcolumn was pretreated with (3,3,3-trifluoropropyl)methylcyclotrisiloxane (TFPCMS) according to a published method [9]. First, the μcolumn was rinsed sequentially with dichloromethane and methanol, and then dried under N_2. Then, a 20% solution of aqueous HCl was passed through the μcolumn for 30 min at 0.1 mL/min, followed by rinsing with 1 mL of methanol and drying with N_2. Next, 1 mL of 1% TFPCMS in dichloromethane was passed though the μcolumn. After drying under N_2 for 30 min, the ends of the μcolumn were sealed with silicone septa and it was heated at 300 °C for 24 hr. The μcolumn was then rinsed with 1 mL each of methanol, dichloromethane, and diethyl ether, and dried under N_2. The OV-215 was then deposited statically from a 0.35% (w/w) solution in 4:1 diethyl ether: ethyl acetate that also contained 1% (w/w)

dicumyl peroxide. Crosslinking at 180 °C for 1 hr in a GC oven produced a wall coating of OV-215 with an average (nominal) thickness of 0.08 μm.

Figure 4.6a shows a portion of an uncoated μcolumn for reference. Figure 4.6b shows the corresponding portion of a second μcolumn that was statically coated with the RTIL after pretreatment with CPTMS. This method should have produced a polar surface which could be wetted by the RTIL; however, as evidenced by the droplets of RTIL Figure 4.6b, this was unsuccessful. Figure 4.6c shows the NaCl/RTIL coated μcolumn. The surface roughness on the channel walls I attributed to the NaCl crystals. The absence of droplets implies good RTIL wetting of the NaCl surface. Figure 4.6d shows portions of the OV-215 coated μcolumn; the hazy appearance of the channel is taken as evidence of a uniform coating.

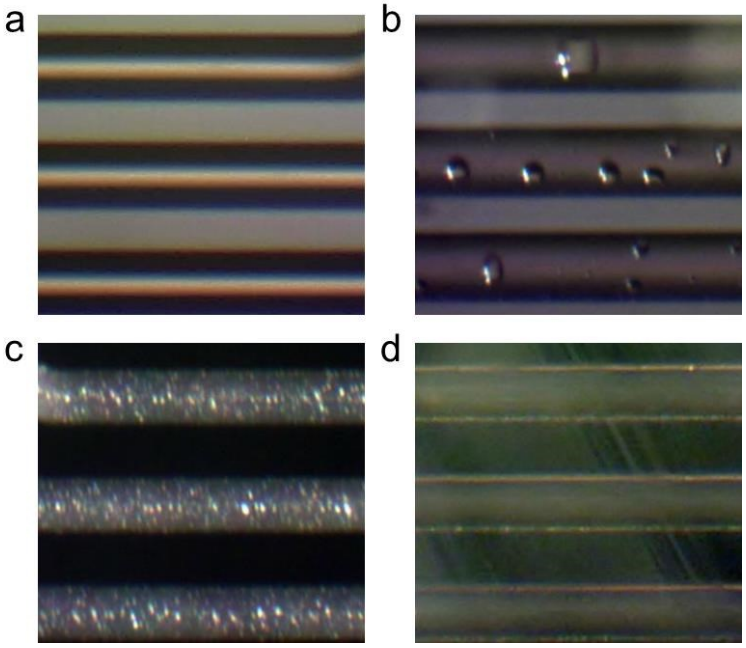

Figure 4.6 Optical micrographs of μcolumns (20X magnification); a) an uncoated 0.5 m μcolumn; b) the CPTMS pretreated 0.5 m μcolumn with RTIL droplets; c) the NaCl/RTIL coated 0.5 m μcolumn; d) the OV-215 coated 0.5 m μcolumn.

The nominal average RTIL-film thickness was 0.1 μm. Details of the procedure used for pretreatment, coating, and cross-linking of OV-215 on a separate ^{2}D μcolumn are also provided above [9]. The calculated average OV-215 thickness was 0.08 μm.

4.2.8 Chromatographic Efficiency

The separation efficiency of each (μ)column was determined by measuring the retention time, t_R, and the full-width-at-half-maximum (*fwhm*) of each peak as a function of average carrier gas velocity, $\bar{u}$, using one of two probe compounds and N_2 as carrier gas. Methane hold-up times were used to determine $\bar{u}$. Peaks were approximately Gaussian and the total plate count, $N = 5.545(t_R/fwhm)^2$, and plate height, $H = L/N$, were calculated from the data for each column of length L.

4.2.9 System Integration and Testing

The two 3-m ^{1}D μcolumns were epoxied to individual carrier PCBs and wire-bonded to pads on the PCB. A cut-out in the PCB beneath each column provided a degree of thermal isolation. These μcolumns were connected in series through the attached capillaries using press-fit unions. The ^{2}D μcolumn was placed on a resistor-embedded polyimide heater pad (Omega Engineering, Inc., Stamford, CT) to which thermal grease was pre-applied. A fine wire thermocouple was inserted between them to monitor the temperature and polyimide tape was used to maintain intimate contact between the heater and μcolumn chip.

The capillaries affixed to the μTM were connected to those on the ^{1}D and ^{2}D μcolumns by means of press-fit unions, and the entire μGC × μGC subsystem was placed in the oven of a bench scale GC (Agilent 6890, Agilent Technologies, Palo Alto, CA). The

outlet of the ^{2}D μcolumn was connected to the FID of the GC. Helium was used as the carrier gas. The temperature of the ^{1}D μcolumns was controlled by the GC oven. This also set the ambient temperature of the TEC, which affected the T_{min} and T_{max} of the μTM stages, respectively (discussed below). The temperature of the ^{2}D μcolumn was offset by ~20 °C above that of the oven by use of the heater pad. Note: the on-chip μcolumn heaters were not used in these experiments to avoid the need for computer control.

Test atmospheres of a mixture of C_7-C_{10} n-alkanes were generated in 10-L FlexFilm® bags (SKC Inc., Eighty Four, PA) pre-filled with N_2 into which 10 μL of neat liquid samples of each mixture component was injected and allowed to evaporate, leading to vapor concentrations in the range of 140 to 185 ppm for each alkane. A test atmosphere was similarly generated for separations run subsequently with a 16-component vapor mixture. Samples were drawn by a small diaphragm pump through a 250- or 112-μL sample loop, via a 6-port valve maintained at 30 °C, and then injected into the ^{1}D μcolumn through a 10-cm segment of capillary. For tests with the 36-component mixture, a solution containing 10 μL of each analyte in 3 mL of CS_2 was prepared, and 0.1 μL was injected directly into the GC inlet via syringe to the ^{1}D column.

A modulation period, P_m, of 5 or 6 s was used, depending on the ^{2}D retention times of the analytes. The offset between heating of the first and second stages of the μTM was 500 ms [18, 47]. Operating the TEC at 8 V produced T_{min} values of -22 and -28 °C, for stage 1 and stage 2, respectively, in a 30 °C GC oven. Modulations entailed applying 100-ms voltage pulses independently to each stage heater. The voltage applied to each was ~45 V and was adjusted to achieve a T_{max} of ~210 °C at an ambient (oven) temperature of 30 °C. A constant

voltage was applied independently to each μTM rim heater and adjusted to maintain the ports at 20 °C at an ambient of 30 °C. Due to a small degree of thermal crosstalk between the stages and the rims, the rim temperature increased 5-7 °C when the proximal stage was heated. Applying 4.5 V to the ^{2}D μcolumn resistive heater pad yielded a temperature of 50 °C at an oven temperature of 30 °C.

Chromatographic data were collected using ChemStation software (Rev.B.01.01, Agilent Technologies, Santa Clara, CA). A custom Visual C# program was used to control the timing of the applied voltages (via two solid-state relays), as well as to read the temperature sensors via a DAQ card (NI USB-6212, National Instruments, Austin, TX) installed on a laptop computer. The data sampling rate from the FID was 200 Hz and it was held at 250 °C. OriginPro 9.1 (OriginLab, Northampton, MA) and GC Image (Rev 2.2, Zoex, Houston, TX) were used for chromatographic data processing and display of 2-D chromatograms, respectively.

4.3. Results and Discussion

4.3.1 (μ)Column Efficiencies:

4.3.1.1 Golay plots of the (μ)columns

The μcolumns used in this study were first characterized through the construction of Golay plots. The μcolumns were placed in a GC oven and attached to the split/splitless inlet and the FID detector. A small amount of the headspace of a vial containing the probe compound and methane (see

Table 4.4 for probe compounds) was injected via gas-tight syringe. From the resulting FID chromatogram, probe compound retention time (t_r) and *fwhm* (w_h) were used to calculate the height equivalent to one theoretical plate (H) using the following equations:

$$H = N/L \qquad 4.1$$

$$N = 5.45 \times \left(\frac{t_r}{w_h}\right)^2 \qquad 4.2$$

The retention time of methane was used to calculate the average flow velocity (ū) which was plotted against *H* to yield the Golay plots in Figure 4.7.

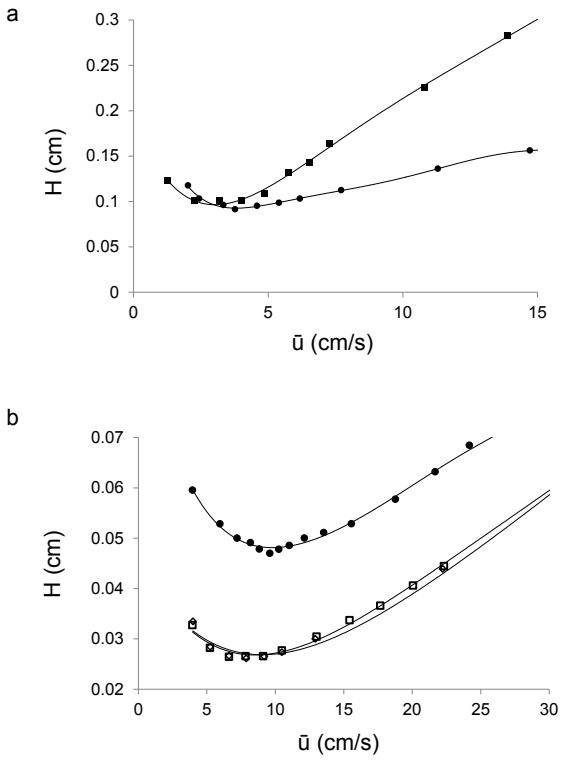

Figure 4.7. Golay plots for (μ)columns used in this work. a) 0.5 m commercially coated, SLB-IL76, 100 μm id capillary (squares) and 0.5 m μcolumn (46 × 150 μm cross section) coated with RTIL (circles); b) 3 m μcolumns (150 × 240 μm cross section) wall-coated with PDMS (unfilled squares and diamonds) and 0.5 m μcolumn (46 × 150 μm cross section) wall-coated with OV-215 (circles). See

Table 4.4for conditions and results.
Golay plots (i.e. H vs. $\bar{u}$) for all (μ)columns are presented below in Figure 4.7and the test conditions and results are summarized in

Table 4.4. Values of k' ranged from 1.1 – 4.9. The RTIL-coated μcolumn retained the probe analyte (MIBK) much more strongly than did the IL-76 capillary, which required increasing the oven temperature by 30 °C to obtain approximately the same value of k'. The maximum number of plates, N_{max}, of 3,800 plates/m calculated for the two OV-1-coated dual 3-m ^{1}D μcolumn ensemble (with each 3-m μcolumn tested individually) was ~25% lower than reported previously for similarly coated 3-m μcolumns [8]. On the basis of N_{max}, the separation efficiencies were in the order OV-1 μcolumn > OV-215 μcolumn > RTIL μcolumn ≈ IL-76 capillary.

4.3.2 Preliminary Testing with the RTIL-coated ^{2}D (μ)Column.

Initial tests of the microsystem used the RTIL-coated ^{2}D μcolumn and entailed isothermal (30 °C) and temperature ramped (30-80 °C at 5 °C/min) separations of C_7 to C_{10} vapors. For the latter, the oven temperature was constrained to 80 °C to avoid overheating the ancillary electronic components on the μTM PCB. The raw μGC × μGC chromatograms are presented in Figure 4.8. For the isothermal separation (Figure 4.8a), the number of modulations per peak (i.e., the modulation number, M_N) were 3, 2, 4, and 8 and *fwhm* values were 160, 280, 530 and 1020 ms for C_7, C_8, C_9, and C_{10}, respectively. These *fwhm* values are significantly smaller than those reported by Kim, et al., who used the same type of μTM without a ^{2}D column installed, but a much lower carrier gas flow rate of 0.38 mL/min [18]. The insets in Figure 4.8a show enlarged views of the bases of the modulated peaks. No breakthrough was evident, but there was some tailing. The *fwhm* values for C_9 and C_{10} are relatively large owing to the low operating temperature. For C_{10}, which showed moderate

tailing, the base peak widths approached the value of P_m (i.e., 5 s). Although the conditions were less than optimal, these results serve to demonstrate that the integrated microsystem was operating as intended.

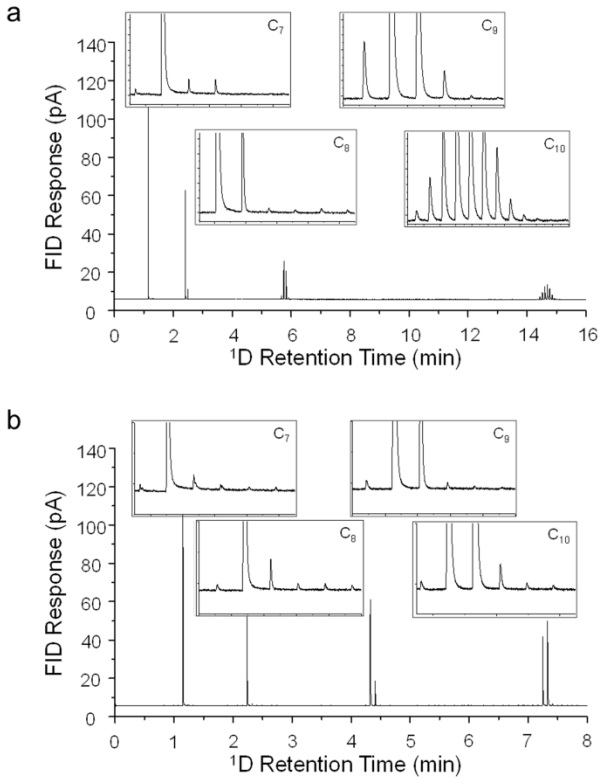

Figure 4.8. Raw chromatograms of the 2-D separations of n-alkanes C_7 through C_{10} obtained with the microsystem shown in Figure 4.1a with stationary phases of OV-1 for the ^{1}D µcolumns and the RTIL for the ^{2}D µcolumn: a) isothermal separation with the ^{1}D µcolumn at 30 °C and the ^{2}D µcolumn at 50 °C; b) temperature ramped separation (30-80 °C at 5°C/min, see Figure 4.9). Conditions: loop-injection (~ 9 ng of each analyte vapor); 1.5 mL/min of He; P_m = 5 s. All insets span a 3-pA FID response range and a 30-s time interval, except the isothermal C_{10} inset, which shows a 60-s interval.

The separation was then repeated with a modest oven temperature ramp from 30 to 80 °C at 5 °C/min. Figure 4.9 shows the temperature profiles for the microsystem components. The ^{1}D µcolumn temperatures were taken as those of the GC oven. The ^{2}D µcolumn was offset ~20 °C from that of the ^{1}D µcolumn and lagged the oven temperature ramp by only 0.5

°C/min. The T_{min} and T_{max} values of the μTM stages also increased linearly but at rates significantly lower than that of the oven. The same was true of the average rim temperature (as noted above, the rim temperature temporarily rose 5-7 °C above the reported temperature as the adjacent stage was heated). This was not unexpected, since the large thermal mass of the TEC attenuates the effect of changes in ambient temperature on the μTM. Operation in this manner is similar to that of one version of the LMCS modulator developed by Marriott et al [65]. wherein the T_{min} and T_{max} values were gradually increased over the course of a separation so as to maintain a T_{min} low enough for efficient trapping but high enough to efficiently remobilize the progressively less volatile eluates.

Figure 4.8b shows the raw 2-D chromatogram of the C_7-C_{10} alkane mixture for the temperature-ramped separation. Values of t_R for C_9 and C_{10} were much shorter, as expected, while those for C_7 and C_8 were about the same because they elute after only a slight change in temperature. Accordingly, values of M_N were ~2, 2, 3, and 5 and values of *fwhm* were 161, 217, 294 and 346 ms for C_7, C_8, C_9 and C_{10}, respectively. That is, the M_N and *fwhm* values for C_7 and C_8 did not change much, while those for C_9 and C_{10} decreased significantly. The reductions in M_N were due to the narrower ^{1}D peaks entering the μTM.

With temperature ramping, the *fwhm* values for the modulated C_7 peaks did not change, relative to the isothermal separation, while those for C_8, C_9, and C_{10} decreased by ~20, 45, and 65%, respectively. By running a series of additional separations with the μTM maintained at a constant baseline temperature and the ^{2}D μcolumn set at several higher (discrete, isothermal) temperatures, the influence of ramping the μTM temperature on the *fwhm* values could be separated from that of the ^{2}D μcolumn temperature. The effect of the

μTM temperature ramp on the *fwhm* values of the modulated peaks was found to be negligible for C_8, moderate for C_9, and predominant for C_{10}. Although the range of this temperature ramp was very narrow, the value of increasing the temperature of the μTM and the μcolumns as the separation proceeds is apparent. Since the increase in T_{max} was only ~14 °C, it is likely that the ~40 °C increase in T_{min} was the more important parameter affecting remobilization. Obviously, a means of heating the μTM independently would be needed to decouple it from the ambient (e.g., oven) temperature and to allow higher temperatures to be achieved without damaging the electronic components on the μTM PCB. Extending analyses to less volatile analytes would undoubtedly also require increasing the rim temperatures to avoid cold spots at the inlet and outlet of the μTM.

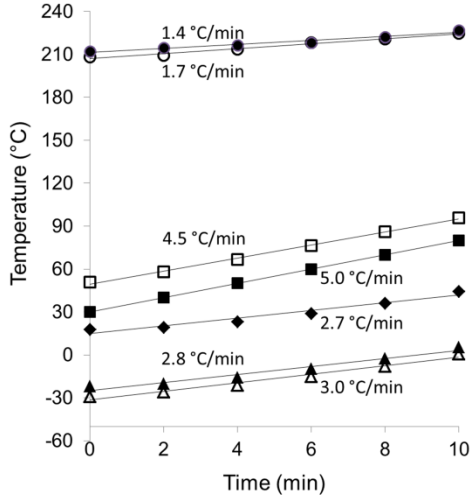

Figure 4.9. Temperature profiles of the μcolumns and μTM for the 5 °C/min oven ramp used to generate the chromatogram in Figure 4.8b. Legend: unfilled circles, stage-1 T_{max}; filled circles, stage-2 T_{max}; unfilled squares, ^{2}D μcolumn; filled squares, ^{1}D μcolumn (assumed to be the same as the oven); filled diamonds, rim temperature; filled triangles, stage-1 T_{min}; unfilled triangles, stage-2 T_{min}.

Table 4.2. Retention times and peak widths for compounds in Figure 4.8 of the main text.

No.	Analyte	^{1}D t_r(min)	^{2}D *fwhm* (msec)
1	Benzene	0.3	480
2	isopropanol	0.5	1100
3	C_7	0.7	80
4	1,4-dioxane	0.7	532
5	MIBK	0.9	700
6	Toluene	1.0	330
7	cyclopentanone	1.2	1010
8	C_8	1.4	120
9	*m*-xylene	2.1	450
10	2-heptanone	2.5	990
11	C_9	2.9	185
12	Cumene	3.1	450
13	C_{10}	5.2	280
14	*d*-limonene	5.6	410

Table 4.3 Vapor pressures, retention times, and peak widths for compounds in Figure 4.10 of the main text.

	Analyte	p_v (kPa)	^1D t_R (min)	^2D *fwhm* (ms)		Analyte	p_v (kPa)	^1D t_R (min)	^2D *fwhm* (ms)
1	2-propanol	5.8	1	100	19	3-heptanone	0.53	6.5	270
2	1-propanol	2.7	1.3	110	20	2-heptanone	0.51	6.7	300
3	2-butanol	2.4	1.4	100	21	heptanal	0.47	6.9	300
4	benzene	12.7	1.7	110	22	C_9	0.59	7.4	210
5	cyclohexene	11.9	1.9	90	23	cumene	0.60	7.6	240
6	C_7	6.1	2.3	90	24	a-pinene	0.53	8.3	240
7	1,4-dioxane	5.3	2.3	150	25	benzaldehyde	0.17	8.4	340
8	MIBK	2.6	2.8	230	26	octanal	0.27	10.3	310
9	isoamyl alcohol	0.5	3.2	380	27	dicyclopentadiene	0.31	10.8	260
10	toluene	3.5	3.2	160	28	mesitylene	0.20	10.9	280
11	cyclopentanone	1.5	3.6	310	29	C_{10}	0.17	11.1	270
12	2-hexanone	0.5	3.8	250	30	*d*-limonene	0.21	11.4	270
13	hexanal	1.5	3.9	240	31	nitrobenzene	0.035	12.5	480
14	perchloroethylene	2.5	4.2	170	32	2-nonanone	0.080	13.7	400
15	C_8	1.9	4.3	150	33	nonanal	0.035	14.1	400
16	2-me-2-hexanol	0.3	5.3	280	34	C_{11}	0.055	14.6	300
17	ethylbenzene	1.3	5.6	210	35	decanal	0.027	19.9	640
18	*m*-xylene	1.1	5.9	210	36	C_{12}	0.028	20.9	490

4.3.2.1 Mixture Separation with the RTIL-coated ^2D (μ)Column:

Next, a mixture of 14 compounds spanning a range of functional group classes was separated. The temperature ramp used was the same as that in Figure 4.8b and Figure 4.9. The resulting 2-D contour plot is shown in Figure 4.10and the values of t_R and *fwhm* for the 14 analytes are listed in Table 4.2 in the Supporting Information. As shown, the alkanes (compounds 3, 8, 11, and 13) eluted early from the ^2D μcolumn, as expected, and give sharp peak clusters, with *fwhm* values ranging from 80 (C_7) to 280 ms (C_{10}). The alkene d-limonene and the set of four aromatics (compounds 1, 6, 9, 12, 14) were all retained slightly

longer than the alkanes and had *fwhm* values of 410-480 ms, with little or no tailing evident. The diether 1,4-dioxane had slightly wider modulated peaks (*fwhm* = 532 ms). Unfortunately, 2-propanol and the set of three ketones (compounds 2, 5, 7, 10) had relatively long retention times and all gave very broad modulated peaks (*fwhm* ranged from 700 to 1100 ms); in fact, 2-propanol peak wrapped around to the next modulation period. Values of M_N ranged from 2 (2-propanol) to 5 (C_{12}).

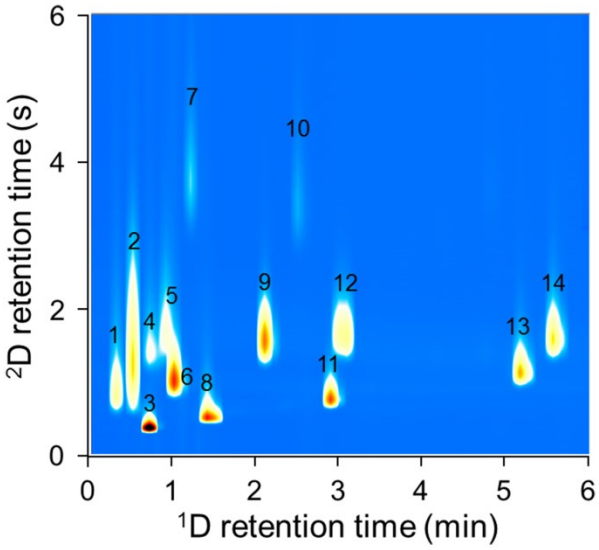

Figure 4.10 14-compound 2-D contour plot generated with the microsystem with OV-1 coated ^{1}D µcolumns and RTIL coated ^{2}D µcolumn. Conditions: loop injection (10-20 ng of each analyte vapor); 1.5 mL/min of He; 30 °C with 5 °C/min oven ramp to 80°C; P_m = 6 s. Peak assignments: **1**, benzene; **2**, 2-propanol; **3**, C_7; **4**, 1,4-dioxane; **5**, 4-methyl-2-pentanone; **6**, toluene; **7**, cyclopentanone; **8**, C_8; **9**, *m*-xylene; **10**, 2-heptanone; **11**, C_9; **12**, cumene; **13** C_{10};, **14**, *d*-limonene.

Although benzene gave well-focused modulated peaks for this analysis, in replicate runs it would occasionally show partial breakthrough, consistent with our previous tests of benzene with this µTM [67]. Since the value of T_{min} reached at the outset of each run was just barely sufficient to trap benzene, even a slight mis-registration in the timing of the cooling

cycle of the μTM and the elution of the benzene peak from the ^{1}D μcolumn can lead to breakthrough. Running a similar mixture isothermally with the ^{1}D μcolumn at 33 °C and the ^{2}D μcolumn at 120 °C gave modulated *fwhm* values similar to those reported above. (Note that the increase ^{1}D t_R values for the alkanes in Figure 4.10, compared to Figure 4.8, is attributed to the insertion of a slightly longer section of 100-μm id interconnecting capillary between the μTM and the ^{2}D μcolumn and the consequent increase in pressure and decrease in velocity in the ^{1}D μcolumn.)

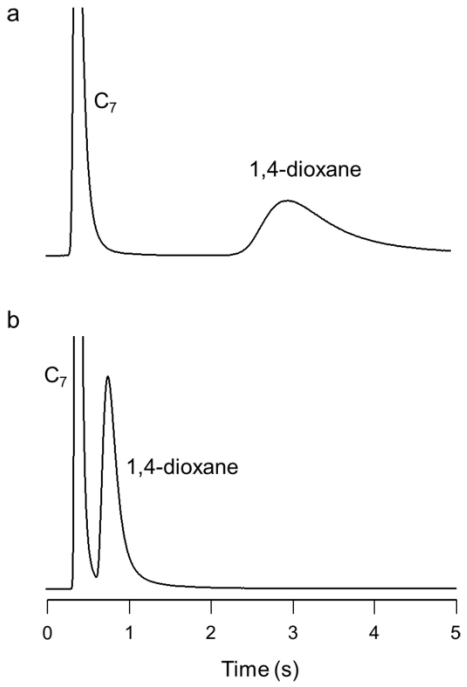

Figure 4.11 Comparison of single raw modulated chromatograms of C_7 and 1,4-dioxane using a) the RTIL-coated ^{2}D μcolumn and b) a commercial IL-76 coated ^{2}D capillary column (0.1 mm i.d., 0.5-m long). The same OV-1coated ^{1}D μcolumns were used for both a) and b). Conditions: loop injection (~ 10 ng of each analyte vapor); 1.2 mL/min of He; isothermal ^{1}D μcolumns (33 °C) and ^{2}D μcolumn (55 °C); P_m = 6 s.

Table 4.4.Summary of test conditions and results of Golay plots generated with the (μ)columns and stationary phases.[a]

Phase	L (m)	Probe	k'	H_{min} (mm)	$\bar{u}_{opt}$ (cm/s)	N_{max} (plates/m)
OV-1	3	C_8	4.6	0.26	7.8	3800
OV-1	3	C_8	4.9	0.26	8.8	3800
OV-215	0.5[b]	MIBK[c]	1.4	0.39	8.4	2500
RTIL	0.5[b]	MIBK	1.1	0.76	3.5	1300
IL-76[d]	0.5	MIBK	1.2	1.0	2.5	1000

[a]$k' = (t_R-t_M)/t_M$ where t_M is the methane holdup time; H_{min} and $\bar{u}_{opt}$ are from the minima in the Golay plots in Figure 4.6 in the Supporting Information; [b]for both of these columns, H_{min} was calculated assuming L = 0.6 m to account for the coated interconnecting capillaries. (μ)column temperature was 30 °C except for the RTIL (60°C); commercial capillary column (0.1 mm i.d.); [d]MIBK = 4-methyl-2-pentanone.

4.3.2.2 Commercial IL-76 Capillary vs. RTIL μColumn.

To explore further the retention characteristics of the RTIL, a set of targeted separations was also performed after replacing the RTIL-coated ^{2}D μcolumn with the commercial IL-76 coated capillary (100 μm id, 0.5 m long), which has a slightly thinner RTIL film (0.08 μm) and yielded an N_{max} value about 30% lower than that of the RTIL μcolumn (see

Table 4.4). The critical pair, C_7 and 1,4-dioxane, which co-eluted from the ^{1}D μcolumn, was selected to explore the differences in performance between the RTIL μcolumn and the IL-76 capillary column.

Representative raw chromatograms from a single modulation of this pair of compounds with the RTIL coated μcolumn and the IL-76 coated capillary column are shown in Figure 4.11a and b, respectively, for an isothermal separation (initial ^{1}D μcolumn = 30 °C; ^{2}D μcolumn = 55 °C). For C_7, the ^{2}D t_R values were about the same whereas the *fwhm* value with the μcolumn was roughly twice that with the capillary. For 1,4-dioxane, the t_R value on the μcolumn was about ~3 times longer (i.e., 3 s and 1 s, respectively) and the *fwhm* value was about ~7 times larger with the μcolumn than with the capillary (i.e., 770 ms and 115 ms, respectively). These differences cannot be accounted for solely by the nominal 20% difference in RTIL film thicknesses. Although small errors in the deposition solution concentration could be contributory, we suspect that the roughness in the NaCl film in the μcolumn results in localized pooling of the RTIL during deposition on the μcolumn walls, and that this was responsible for the excessive retention of the more polar 1,4-dioxane. Since the alkane does not partition significantly into this material, there is less of an effect on its retention and band shape. Re-running this separation at progressively higher ^{2}D μcolumn temperatures did not resolve the problem: even at 120 °C, the 1,4-dioxane peak had a *fwhm* value of 470 ms, which is too broad for effective μGC×μGC.

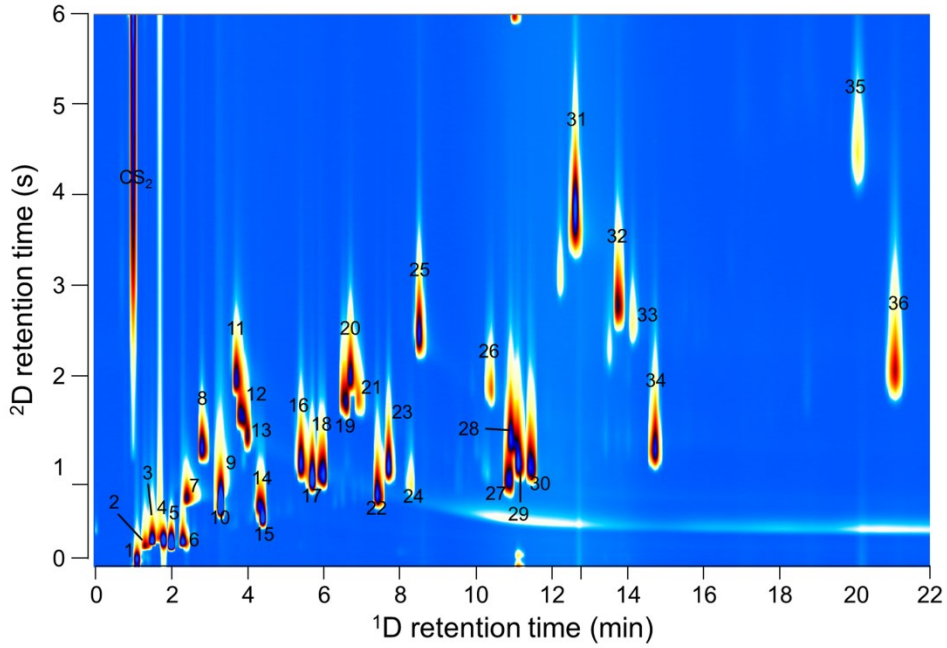

Figure 4.12 36-compound 2-D contour plot generated with the microsystem with OV-1 coated ^{1}D µcolumns and an OV-215 coated ^{2}D µcolumn. Conditions: syringe injection (0.3 µg of each analyte in CS_2); 100:1 split; 1.5 mL/min of He; 1 min hold at 30 °C (oven), then 30-80 °C at 5 °C/min (oven), then 10 min hold at 80°C (oven); ^{2}D µcolumn offset +20 °C using resistive heater; P_m = 6 s. Peak assignments: **1**, 2-propanol; **2**, 1-propanol; **3**, 2-butanol; **4**, benzene; **5**, cyclohexene; **6**, C_7; **7**, 1,4-dioxane; **8**, 4-methyl-2-pentanone; **9**, isoamyl alcohol; **10**, toluene; **11**, cyclopentanone; **12**, 2-hexanone; **13**, hexanal **14**, perchloroethylene; **15**, C_8; **16**, 2-methyl-2-hexanol; **17**, ethylbenzene; **18**, m-xylene; **19**, 3-heptanone; **20**, 2-heptanone; **21**, heptanal; **22**, C_9; **23**, cumene; **24**, α-pinene; **25**, benzaldehyde; **26**, octanal; **27**, dicyclopentadiene; **28**, 1,2,3-trimethylbenzene; **29**, $C_{10;}$ **30**, *d*-limonene; **31**, nitrobenzene; **32**, 2-nonanone; **33**, nonanal; **34**, C_{11}; **35**, decanal; **36**, C_{12}.

4.3.2.3 Mixture Separation with OV-215 coated ^{2}D (µ)Column.

Next, the RTIL coated ^{2}D µcolumn was replaced with an OV-215 coated µcolumn of the same length and a mixture of 36 compounds was analyzed. A GC oven temperature program consisting of a 1-min hold at 30 °C followed by 5 °C/min ramp to 80 °C and a 10-min hold at 80 °C provided reasonably good separations. As before, a heater was placed in intimate contact with ^{2}D µcolumn to offset its temperature by 20 °C above that of the oven.

To facilitate peak identification, compounds were added to the mixture progressively a few at a time. As such, it was possible to evaluate run-to-run retention time reproducibility for most of the peaks. Working from the contour plots, ^{1}D t_R values never varied by more than one modulation period (6 s), and ^{2}D t_R values, measured relative to that of 1-propanol, varied by < 10% (RSD) with the exceptions of C_7 (14%) and isopropanol (12%). The separation required 22 min and the range of ^{2}D t_R values was 0.1 – 4.4 s, indicating fairly good use of the 2-D space. The resolution in the 2nd dimension, which was rather low for the earliest eluting compounds (i.e., compounds 1-6), improved with increasing ^{1}D t_R values. Notably, numerous pairs of compounds that co-eluted from the 1st dimension were separated in the 2nd dimension (e.g., compounds 6 and 7, 9 and 10, 14 and 15, and 27 and 28), and the cluster consisting of compounds 19-21, which partially co-eluted in the 1st dimension were well resolved in the 2nd dimension. The excessively broad peak for benzene (compound 4) reflects μTM breakthrough, which occurred in 7 of the 13 replicates in which benzene was analyzed. Breakthrough of compounds 1-3 was also observed in some of these replicate runs.

Values of *fwhm* ranged from 90 (compound 6, C_7) to 640 ms (compound 35, decanal) and, with the exception of the alkanes, were smaller than those obtained with the RTIL stationary phase (see Table 4.2 and

Table 4.3); among the polar compounds *fwhm* values were 2-11 times smaller using the OV-215 ^{2}D μcolumn. For the alkanes, the temperature program used in Figure 4.12 led to slightly lower elution temperatures in most cases and, hence, similar or slightly larger (i.e., ≤ 12%) *fwhm* values. The horizontal streak at a ^{2}D t_R value of ~0.5 s is attributed to PDMS bleed from the μTM, which reached maximum intensity at ~10 min into the run. i.e., the point at which the μTM reached its highest T_{max} value of 224 °C.

4.3.2.4 Structured chromatogram

Figure 4.13shows the peak apex plot associated with Figure 4.12in the main text. Figure 4.14shows an enlarged view of one region of Figure 4.12, highlighting the repeating pattern evident for ketones/aldehydes/alkanes. See the text in the main body of the article for discussion of these figures.

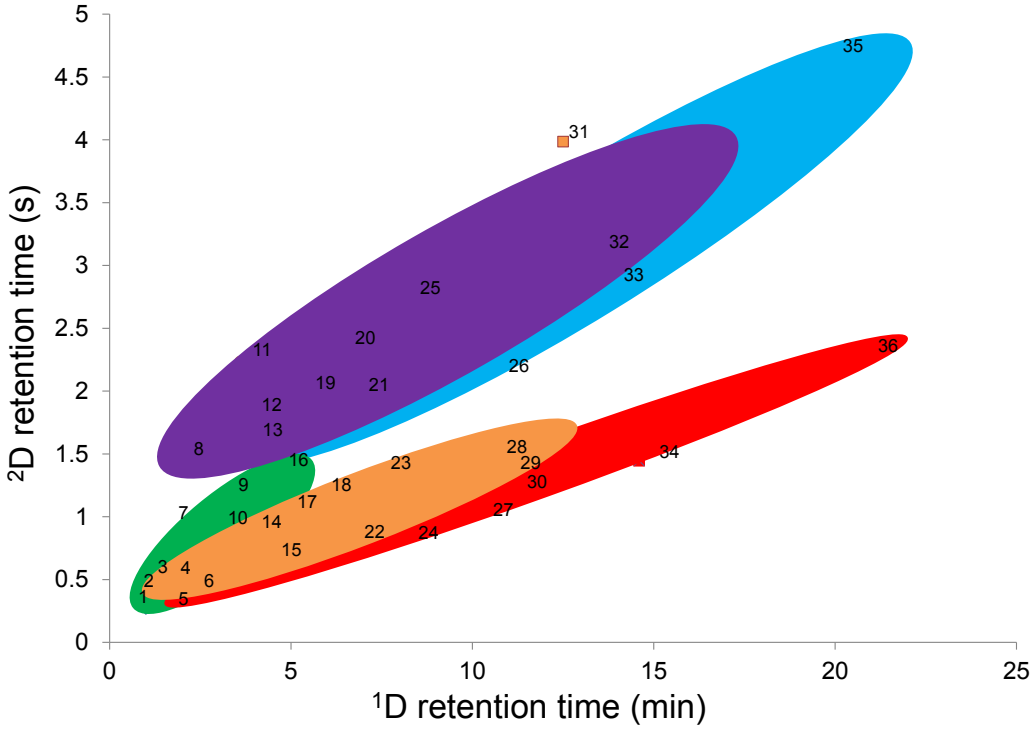

Figure 4.13 Structured chromatogram generated from the 2D chromatogram in Figure 4.12 of the main text. See

Table 4.3for peak identification.

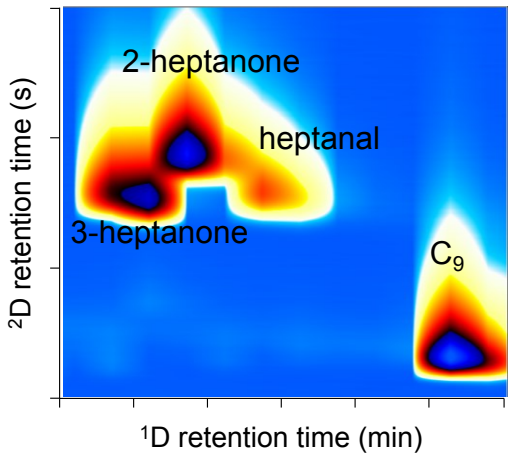

Figure 4.14 Expanded region of Figure 4.12 in the main text showing the elution pattern of ketones/aldehydes in relation to the alkane 2 carbons longer.

The separation of mixture components into functional group bands, a so-called "structured chromatogram", is a hallmark of GC × GC. Structure can be seen in Figure 4.12, but the contour plot shown in Figure 4.13 (Supporting Information) illustrates this much more clearly; shaded ellipses were used to delineate different members of a given functional group. An interesting feature is that groups of carbonyl compounds (2-hexanone/hexanal; 2-heptanone/3-heptanone/heptanal; 2-nonanone/nonanal) eluted in a recognizable pattern with respect to each other and with a ^{1}D retention time slightly shorter than that of the n-alkane two carbons longer; the enlargement of one section of the contour plot presented in Figure 4.14 shows this pattern, which is also evident in Figure 4.12. More general patterns are evident as well. For example, the group consisting of alkenes and alkanes overlapped slightly with the group of aromatic hydrocarbons, while both were well separated from the aldehydes and ketones, which overlapped considerably due to the short ^{2}D μcolumn used and their similar polarities. The alcohols were not very distinct from either of these two main groups,

falling between the two. Notably, the ^{2}D t_R value for nitrobenzene exceeded that for all other compounds except decanal.

4.4. Conclusion

This inaugural study of μGC × μGC separations with Si-microfabricated separation and modulation components has revealed several important factors affecting the operation and performance of these microsystem components. Effective separations of moderately complex mixtures were possible using relatively short 1st and 2nd dimension μcolumns statically coated with a pair of complementary commercial siloxane polymers and a simple temperature program spanning a very modest temperature range of 50 °C. Modulated peaks had *fwhm* values between 90 and 500 ms and M_N values between 2 and 5 for compounds spanning a 700-fold vapor pressure range. Replicate analyses showed high retention-time fidelity.

The deposition of a trigonal tricationic RTIL onto the walls of the ^{2}D μcolumn was challenging and the technique is still being optimized. Our best efforts thus far yielded films that were apparently much thicker than expected. As a result, although the retention selectivity of the RTIL was quite different from that of the OV-1 ^{1}D μcolumn phase, polar analytes were retained much too strongly. On the basis of tests with a commercial capillary with the same stationary phase, refinements in the pretreatment and deposition techniques should lead to improved retention properties for this RTIL in our ^{2}D μcolumns. Extension of this approach to testing selected other trigonal tricationic RTILs with similar thermal stability is planned, followed by implementation as the stationary phase in the μTM. The expectation

that one or more of such RTILs will provide low bleed rates at elevated temperatures in the μTM should allow an increase in T_{max} and a commensurate reduction in the vapor pressures of analytes that can be effectively remobilized.

Tests thus far have been performed with the entire assembly inside a conventional GC oven, utilizing bench-scale components for sample injection and detection. On-going work is directed at placing the μTM outside of the oven or using locally heated, low-thermal-mass columns to decouple the temperatures of the subsystem components. We are also exploring the use of a micromachined preconcentrator-focuser for injection and a microsensor array for detection, as further steps toward an autonomous, field portable μGC × μGC system.

Chapter 5. First-principle modeling and characterization of thermal modulation in comprehensive GC×GC using a microfabricated device

5.1. Introduction

Resolving analytes in highly complex mixtures poses a significant challenge for analytical chemists. Peaks of such complex mixtures tend to overlap each other, a phenomenon known as peak crowding. Securing large peak capacity commonly entails increasing the column length, decreasing the column diameter, or a combination of both [5]. The use of a column with such a great excess of peak capacity can ease some of the problems but the costs are high in terms of analysis time, detection limits and instrument requirements. In contrast, two-dimensional gas chromatography (GC×GC) is a promising alternative approach that enables complex mixtures to be resolved with higher separation capacity and selectivity than the conventional approach described above. Furthermore, the GC×GC technique potentially permits development of a miniaturized GC lab-on-a-chip system incorporating a microfabricated thermal modulator (μTM) for real-time field deployment under limited resources without the separation performance compromised by reduced column lengths [17, 47].

In GC×GC two columns with independent separation mechanisms, namely the first dimension (^{1}D) column and the second (^{2}D) dimension column, are used to separate the gas species (Figure 5.1). This multi-dimensional analytical approach results in two distinct retention-time parameters by which the analytes can be identified with larger capacity. Various different column combinations have been tried since the 1990s, such as a combination of non-polar coating in the ^{1}D column and a polar coating in the ^{2}D column [95]; a polar coating in the ^{1}D column and non-polar coating in the ^{2}D column [96], and various degrees of polarity in the ^{1}D column and ^{2}D column [97]. A combination of a non-polar ^{1}D column and a polar ^{2}D column is one of the most popular combinations used. The main advantage is that the use of a non-polar column allows the virtual direct transfer of methods that have already been developed in the context of conventional GC. In addition, while the analytes are separated in the ^{1}D on the basis of their different volatilities, the fast and consequently essential isothermal ^{2}D separation neutralizes any further boiling-point contribution, and separation is only governed by specific polarity-based interactions. That is, the two chromatographic processes are independent, and the separation is orthogonal. More recently, it has been found that a polar/medium polar ^{1}D and a polar ^{2}D column can provide valuable results especially when highly polar or iogenic analytes are among the key components of a mixture [98].

An intermediate modulator device placed at the junction between the ^{1}D and ^{2}D plays a key role in realizing GC×GC analyses (Figure 5.2). While different types of modulators exist, thermal modulators (TMs) have become widely used due to their ability to provide comprehensive modulation resulting in increased analyte detectability relative to other

modulator types. This device cuts and re-concentrates the effluent peak from a long ^{1}D column, at a time interval known as the modulation period (P_M) and re-injects them onto a short ^{2}D column as sharp sub-bands [85]. This prevents recombination of the species that have been partially separated in the ^{1}D after their re-injection to the ^{2}D as well as expands their detection limit. However, Blumberg et al. [99, 87] show that while the theoretical peak capacity of GC×GC is much higher than that of the conventional GC, current experimental studies show GC×GC only achieves moderately improved separation capability. The modulator device is the key bottleneck in reaching the desired separation performance of GC×GC. To reach the maximum possible potential of GC×GC operated by thermal modulation, a TM needs to inject very sharp effluent bands with full-width at half height (FWHH) as narrow as 10 ms into the ^{2}D with a short channel length of 1-2 cm at a flame ionization detector (FID) data acquisition rate of ~ 1kHz [99, 87]. Hence, there is significant room for improving the peak capacity obtainable using GC×GC by optimizing the performance of the modulator to realize the ideal GC×GC operation above. Since, the FWHH of the modulated peak is the critical parameter determining the effective peak capacity of the GC×GC system, we use that as the performance metric of the system in our study.

To our best knowledge, no rigorous theoretical model exists that provides a good design guideline for TMs. This prevents researchers from achieving optimal performances for TMs based on a thorough understanding of physics governing the thermal modulation process. Hence, they usually resort to the expensive route of blindly reducing the minimum trapping temperature, with the aim to achieve small FWHH of injection. This paper presents a theoretical basis to predict the behavior of a microfabricated TM device (μTM) developed

in our previous study [17, 47]. The goal of this paper is to understand the physics governing the operation of the device, so as to develop better and more efficient μTMs in the future. Towards this end, we have experimentally validated our model for the μTM device. This study proposes improved operational principles and design features to develop a high-performance μTM.

5.2. Materials and Methods

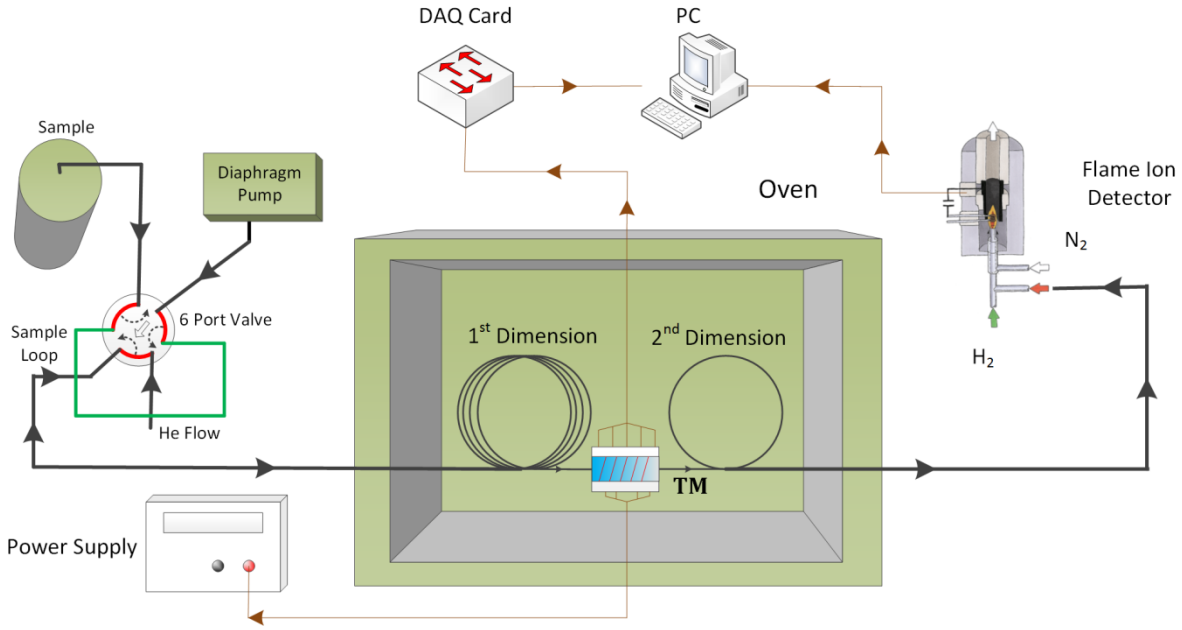

Figure 5.1. Schematic of a typical GC × GC system incorporating thermal modulator (TM) and two columns with their internal surfaces coated with complementary stationary phases for analyte separation. Additional components of the system include a sample injection unit, a temperature-controlled oven, a gas sensor (flame ion detector), a computer system for programmable TM operation and data acquisition, and a power supply.

5.2.1 Thermal Modulator Operation

A cycle of the thermal modulation process consists of cooling and heating periods. In the cooling period, analyte species eluting from the ^{1}D in a carrier gas (mobile phase), such

as CO_2, N_2, or air, become trapped and focused into the organic coating film (stationary phase) of a modulator channel stage (Figure 5.3C). This period is followed by the heating period, where the trapped species are rapidly heated, thermally desorbed from the stationary phase, and reentered into the mobile phase for their injection to the ^{2}D (Figure 5.3D). The thermal modulation process repeats the cycle to generate a series of narrow analyte pulses separated in the ^{2}D. Commercial TMs use cryogenic consumables (liquid N_2/CO_2), or cryogenic refrigeration-based cooling to trap the eluent and a resistive or convective heating pulse to release the trapped species from the stationary phase [100].

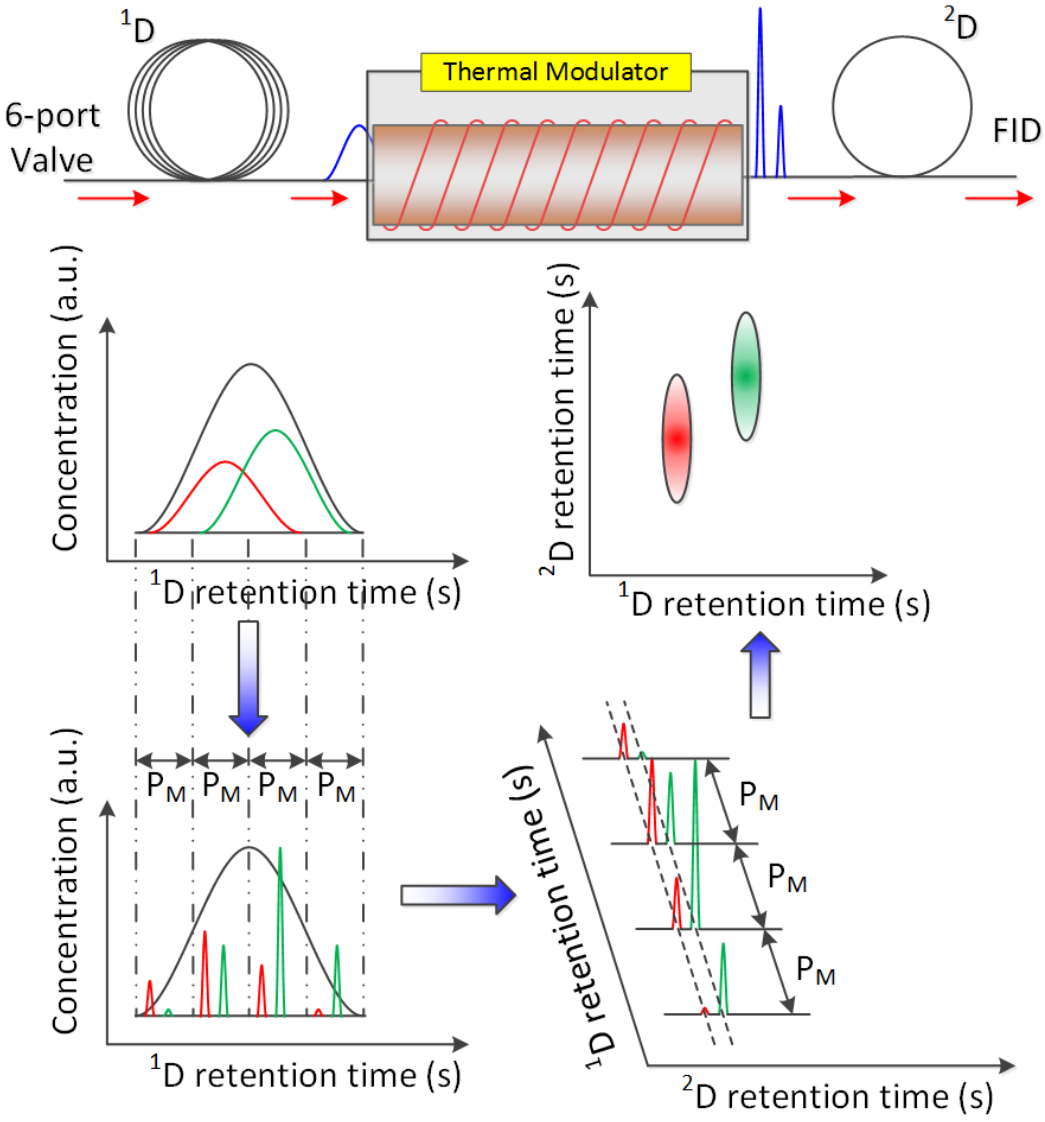

Figure 5.2**.** GC × GC operation enabled by a junction modulator between the ^{1}D and ^{2}D columns. Thermal modulators (TMs) are the most widely employed modulator devices in GC × GC. The modulator cuts the ^{1}D peak consisting of co-eluted gas compounds into sharp peak bands, each containing a smaller amount of analytes and injects the bands to the ^{2}D column. The ^{2}D column further separates the co-eluted compounds, which yields signal peaks in the ^{2}D column retention time for each band. Mapping the obtained signal peaks with respect to both the ^{1}D retention time and the ^{2}D retention time results in the two-dimensional (2D) gas chromatogram and allows for high-resolution analysis of complex gas compound mixtures at large capacity.

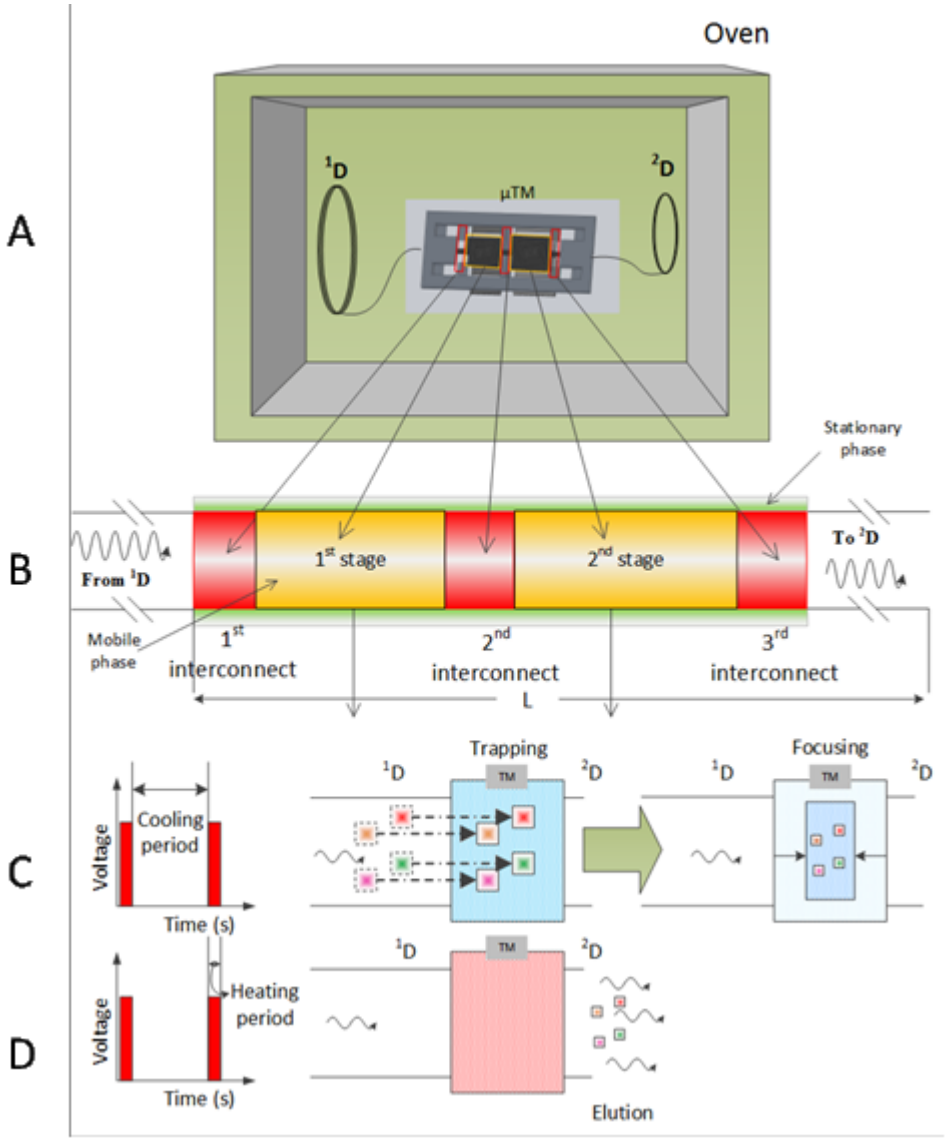

Figure 5.3 (A) Illustration of the microfabricated thermal modulator (µTM) device modeled by this study. The ^{1}D, ^{2}D columns and the µTM are kept inside a temperature-controlled oven. This helps prevent unpredictable influences of ambient temperature fluctuations on the chromatogram. (B) Simplified model of the µTM depicting the locations of interconnects and the two stages during the cooling period (C) and heating period (D). The unmodulated species flowing in from ^{1}D are presented as large colored rectangles. (C) The species are trapped and focused simultaneously as they move into the µTM when the heaters are turned off (cooling period). This happens because the cold stationary phase in the cold stage (blue rectangle), instantaneously traps all incoming species. (D) Upon application of the heating pulse, the hot stationary phase (red rectangle) releases the analyte molecules, which flow out with the carrier gas.

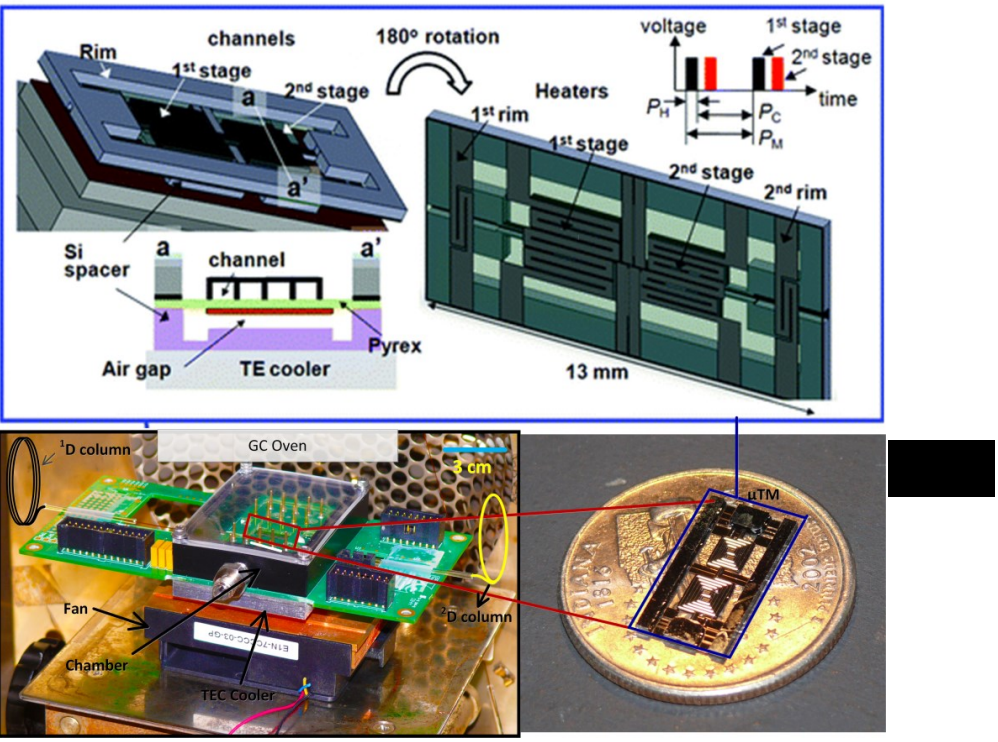

Figure 5.4 (A) Perspective-, side-, and back-view diagrams of the μTM, showing its essential structural features and mounting configuration. The device primarily consists of two trapping stages, rims at the inlet/outlet, and interconnects. The interconnects provide a continuous flow path between the rims and the stages and between the stages. The lengths of the first and second stage microchannels, and of each inerconnect are 4.2 cm, 2.8 cm, and 1 mm, respectively. The microchannel cross-section is 150 (h) × 250 μm (w) throughout, and the wall thickness is 30 μm. Inset (upper right) shows the voltage–time relationship of a representative modulation period, P_M, for the resistive heater on each stage of the device (P_H and P_C are the heating and cooling segments of the modulation period, respectively). (B) Photographs of the fully assembled μTM mounted on a printed circuit board. The μTM is mounted on top of a TEC and covered by a shroud of flowing dry air, to prevent any condensation. The TEC in turn is cooled by a heat sink attached to a fan. (C) Optical image of the μTM placed on a US quarter coin, for scale. (Reprinted with permission from Kim et al.[2] Copyright 2011 American Chemical Society)

5.2.2 Microfabricated Thermal Modulator (μTM)

Recently, our study has demonstrated GC×GC analyses using a μTM operated with a solid-state thermoelectric cooler (TEC) [17]. The study shows that our device allows for thermal modulation requiring no cryogenic consumables at much lower power consumption than commercial devices. Integrating the μTM with other MEMS GC components is expected to open the door to field-deployable, portable GC×GC [48]. The μTM consists of a silicon-glass chip bonded using anodic bonding. We mounted the device on a PCB board (Figure 5.4C). A thermoelectric cooler (TEC) (Model SP2394, Marlow Industries, Dallas, TX) provides cooling for the chip device. Our study attached the TEC to a bottom PCB board. These two PCB boards were then aligned and joined using male and female pins (Figure 5.4B). The μTM incorporates two microfluidic channel stages, and inlet and outlet ports on a silicon/Pyrex-based chip. The device has several integrated on-chip heaters on its rims (rim heaters) and stages (stage heaters). We heated the inlet and outlet ports individually using the rim heaters. The stages were heated by their own integrated on-chip heaters. Resistance Temperature Detectors (RTD) were also placed on the stages and the rims (Figure 5.4A), to obtain the stage and rim temperatures as a function of time [17, 47]. After mounting, our μTM was temperature calibrated, cross-linked and attached to ^{1}D and ^{2}D columns to perform the next set of experiments. Our previous study employed a two-stage modulation scheme for the μTM, which alternately activates the heaters of the two TM stages in different timings to mitigate sample loss due to incomplete trapping during the thermal transitions. However, as the first step of our modeling study, we assumed synchronous operations of these stages in this paper to maintain our simulation task relatively simple.

5.2.3 Mass Transport Model for µTM Operation

Historically, there have been numerous attempts by researchers to model the process of gas chromatography. Lapidus, Amundson and van Deemter [101, 102] developed an analytical expression for the solute concentration in the column, using error functions. Martin and Synge used moment analysis on the domain equations to arrive at an expression for the height equivalent to theoretical plate (HETP) [103]. Giddings later used statistical mechanics to model the kinetic non-equilibria that develop at the gas-liquid interface [104]. In this paper, we have built our theoretical model upon the aforementioned study by Lapidus, Amundson and van Deemter, along with temperature dependent stationary/ mobile phase properties to simulate a single-stage TM.

Our μTM was placed inside a GC oven, which provided consistent environmental conditions necessary to obtain repeatable measurements (Figure 5.3A). We modeled our device as consisting of three interconnects, two stages and the ^{2}D column (Figure 5.3B). The interconnects provided a continuous flow path between the capillary column and the stages and also connected the two stages together. Here, our model assumed that the interconnects were at a constant temperature shift ($\Delta T_{interconnect}$) from the ambient temperature in the oven (T_{oven}), while the stages oscillated between the minimum temperature (T_{min}) for analyte trapping and the maximum temperature (T_{max}) for analyte elution. The ^{2}D was assumed to be uncoated according to the convenience of our experimental setup used in this study and operating at T_{oven}. Our μTM design only heated the rims and the two stages with the integrated heaters while keeping the interconnects unheated. We knew that the interconnect temperature ($T_{interconnect}$) was much lower than the T_{oven} because of

convective cooling due to a continuous heat flow path from the unheated interconnects to the TEC. We accounted for these cold interconnects in our model by incorporating small sections of low temperature along the length of the μTM (Figure 5.3B). The stages acted so as to trap and focus any incoming species from the ^{1}D column within the stationary phase while the low temperature interconnects act similar to a coated capillary column maintained at a constant low temperature.

Figure 5.5A and Figure 5.5B illustrate the trapping and elution processes occurring in the stages, respectively. At the start of the modulation cycle, the temperature of the stages is at the maximum temperature (T_{max}). Upon shutting down the square heating pulse, the temperature exponentially decays to the minimum temperature (T_{min}). During the cooling period (Figure 5.5A), the incoming analyte species (represented by the Gaussian curve at the inlet of the TM) carried by an inert gas from the ^{1}D column is rapidly trapped into the stationary phase of the modulator. This results in a high concentration at the inlet, which exponentially decays towards the outlet. During the subsequent heating period where the heater is activated (Figure 5.5B), the analyte species trapped in the stationary phase elutes rapidly from the stationary phase into the mobile phase and elutes out of the capillary channel as a sharp band. The heating and cooling periods are repeated at regular intervals of time equal to P_M and convert a broad peak entering the μTM into a series of sharp peaks entering the ^{2}D column. Typically, species that are separated in GC×GC have a wide range in polarity and volatility. Although we could apply the model developed here for a wide range of species separated in GC×GC, we specifically chose octane as a model species in this study. The volatility and polarity of octane lie in the middle range of those of chemical

analytes typically analyzed in GC×GC. Published data are readily available in literature regarding the properties of octane in conjunction with its interactions with a poly-dimethylsiloxane (PDMS) stationary phase.

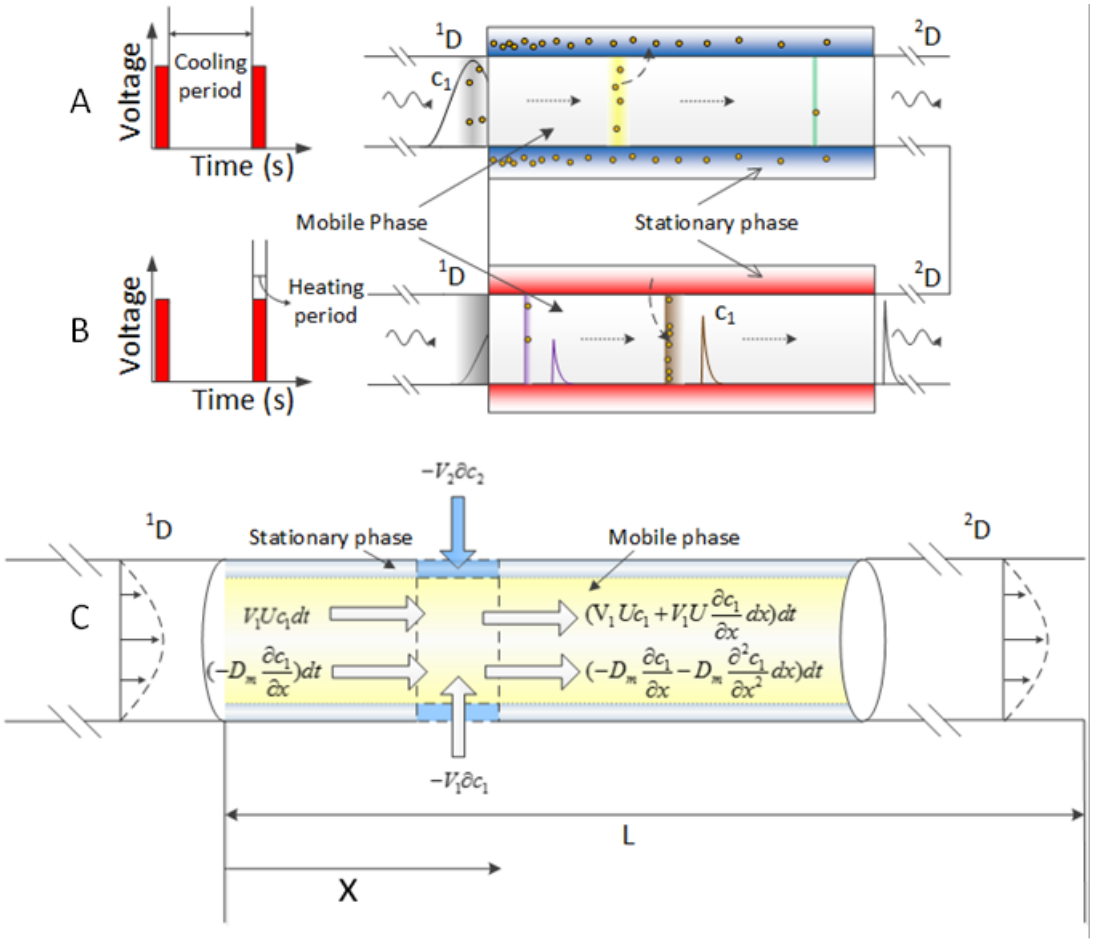

Figure 5.5 Schematic of a single-stage thermal modulator operation between ^{1}D and ^{2}D columns. (A) Analyte trapping process under cooling period. As the analyte with Gaussian peak shape, moves from the ^{1}D into the TM stage, the stationary phase (blue rectangle) adsorbs the analyte species due to its cold temperature, while the concentration in the mobile phase decreases. (B) Analyte elution process under heating period. Upon application of the heat pulse, the hot stationary phase (red rectangles) releases the species as a sharp pulse, which flows out of the thermal modulator. (C) Mass balance in a differential control volume (the dotted box), which is governed by diffusion and convection.

To derive the governing equations described later, we applied mass balance of the analyte species for the mobile and stationary phases of the TM capillary during the thermal modulation cycle (Figure 5.5C). Here, we used a one-dimensional species conservation model. The species conservation equation within the capillary channel is given as[14]

$$V_1 \frac{\partial c_1}{\partial t} + V_2 \frac{\partial c_2}{\partial t} = V_1 \left(D_m \frac{\partial^2 c_1}{\partial x^2} - U \frac{\partial c_1}{\partial x} \right) \quad 5.1$$

$$c_2 = K c_1 \quad 5.2$$

where c_1 is the concentration profile of the analyte in the mobile phase, c_2 is the concentration profile of the analyte in the stationary phase, V_1 is the volume of the mobile phase, V_2 is the volume of the stationary phase, D_m is the effective dispersion coefficient, U is the average velocity of the carrier gas in the channel, K is the partition coefficient of octane-PDMS combination, t denotes the time axis and x denotes the local position within the channel with $x = 0$ at the inlet of the μTM. At a very small time scale, the concentration in the stationary phase and in the mobile phase does not necessarily equilibrate. However, the time scale of the thermal modulation process is much larger than the equilibration time constant, thus we assumed a quasi-equilibrium condition for the species at the interface between the mobile and stationary phases during the dynamic modulation process [104]. The first two terms on the left in Eq. 5.1represent the transient variation of the total species concentration in the mobile and stationary phases, respectively. The first term on the right in Eq. 5.1 represents the effect of diffusion in the mobile phase, while the last term represents the mass transport due to convection in the mobile phase. In this model, we neglected the mass transfer due to convection or diffusion through the stationary phase. The expressions for D_m, V_1, V_2, K, and U are provided in Supplementary Information.

The flow regime through the modulator and ^{2}D column was determined by using the Mach number. When the Mach number is << 1, the flow can be considered incompressible with a linear pressure drop. The average Mach numbers of the flow through the modulator and the ^{2}D column given by $Ma = \frac{U}{\sqrt{RT}}$ were 0.0015 and 0.0042, respectively. Hence, we used Hagen-Poissuelle incompressible equations to determine the flow through the channel.

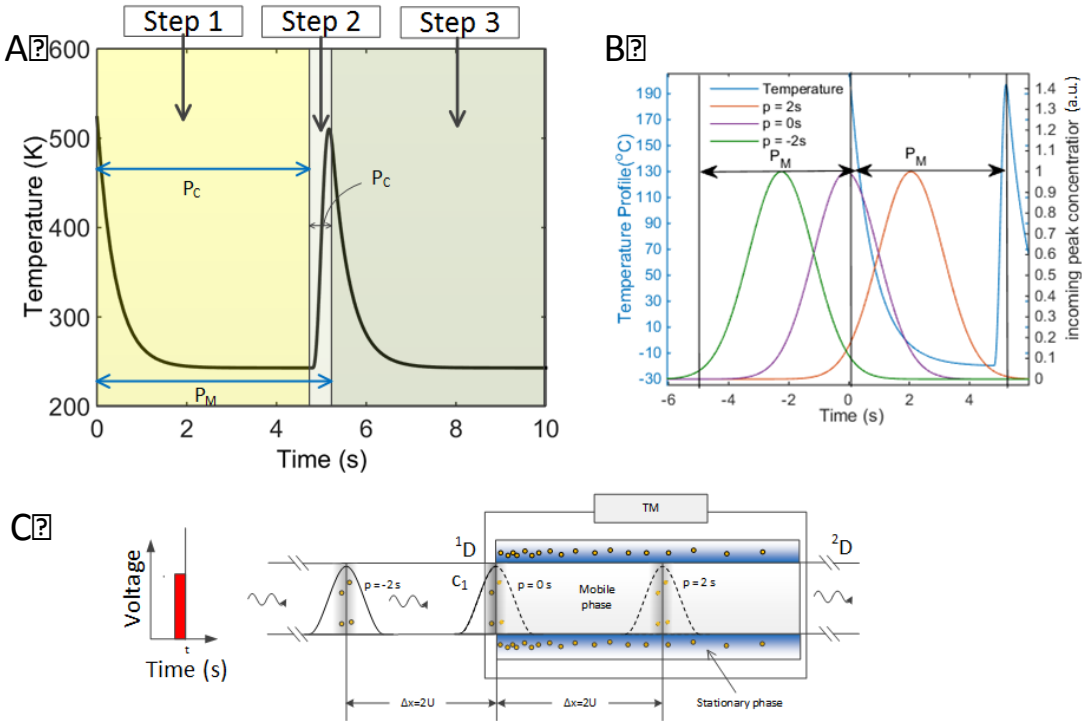

Figure 5.6 (A) Variation of modulator temperature with time for a modulation period of 5s. Three steps of the modulation process are indicated: *Step 1* – cooling period (0-4.8 s); *Step 2*– heating period (4.8-5.0 s); and *Step 3* – cooling period (5-10 s). (B) Incoming unmodulated peak from ^{1}D, at various values of p. The temperature profile is also shown to demonstrate the location of the incoming ^{1}D peak relative to the heat pulse on the time axis. (C) Schematic demonstrating the location of peak maximum relative to the heating period (p) on the x-axis. The modulating heat pulse occurs at time = t s. If $p = 0\ s$, the concentration peak maximum is located right at the edge between the TM and the ^{1}D. For $p = -2\ s$, the concentration peak maximum is yet to arrive at the junction between the TM and the ^{1}D, while for $p = 2\ s$, the concentration peak maximum has already passed through the intersection between the TM and the ^{1}D.

5.2.4 Boundary Conditions and Initial Conditions

The boundary condition at the inlet is given by an incoming Gaussian flux as follows:

$$-D_m \frac{\partial c_1}{\partial x} + U c_1 = \exp\left(-\left(\frac{t-p}{\sqrt{2}\sigma_{1D}}\right)^2\right), at\ x = 0 \qquad 5.3a$$

where p is the location of the incoming peak maximum with respect to the start of the first cooling period in seconds, and σ_{1D} is the standard deviation of the peak moving out of the ^{1}D column and into the μTM measured in seconds. During real GC×GC experiments, the position of the incoming peak cannot be precisely determined with respect to the voltage pulses. Hence, multiple experiments performed with our μTM will yield incoming peak maxima located at a random locations with respect to the onset of the cooling period. We numerically simulated three instances of the incoming peak positioned at equal time intervals away from each other, to illustrate the idea of p (Figure 5.6B). The concept of p can also be represented in the spatial domain. A peak with $p = -2s$, has a peak maximum located $2s$ away from the starting of the cooling period on the time axis (Figure 5.6B). Assuming that the peak moves through the ^{1}D at a constant velocity of $U\ m/s$, its peak maximum is located $2U$ away from the entrance of the TM and within the ^{1}D. Similarly, a peak with $p = 0s$ has a peak maximum located right at the entrance of the TM, while a peak with $p = 2s$ has a peak maximum which has already been modulated and is located hypothetically away from the entrance of the TM towards the ^{2}D.

At the outlet of the ^{2}D column, we assumed that the flux due to diffusion was zero because the spatial variation in the species concentration was negligible at the end of a sufficiently long channel of length L. Thus, the boundary condition at the outlet is given by:

$$-D_m \frac{\partial c_1}{\partial x} = 0, at\ x = L \qquad 5.3b$$

We assumed that the simulation started at the end of the heating period at the temperature of T_{max} (alternatively, the beginning of the first cooling period), where there is no species trapped in the stationary phase. Thus, the initial condition is given by

$$c_1(t = 0, x) = 0 \qquad 5.4$$

A mesh independency study shows that a mesh size of 10^{-5} m is sufficiently small to provide reliable results, for the length of the modulator studied. Using this model, we first studied a simplified model of our μTM, assuming no coldspots, to demonstrate the process of generation of the peaks during the thermal modulation. Our simulations were performed with COMSOL Multiphysics 4.4 (COMSOL Inc., Stockholm, Sweden) in conjunction with MATLAB R2014b (The Mathworks Inc., Matick, MA).

5.2.5 Device Characterization

We performed experiments to characterize the analyte modulation performance of our μTM operating as a single-stage device. A bubble flow meter was used to perform flow vs. pressure calibration for an inlet gage pressure range between 7 and 13 psi. Five sets of data were obtained at each inlet pressure, and the flow rates were then averaged to obtain the calibration curve. We then used this calibration curve, to interpolate the inlet pressure required to obtain flow rates between 1 mL/min and 2 mL/min, at increments of 0.5 mL/min, and verified it using the bubble meter. Using these pressures, we performed 1D chromatography experiments with the μTM in line with a 250 μm i.d., 6 m long column

(Rtx-1, Restek Corp. Bellefonte, PA) coated with PDMS used as ^{1}D and a 100 μm i.d., 30 cm long uncoated column used as ^{2}D. The test atmosphere was created in a 10 L FlexFilm bag (SKC Inc., Eighty Four, PA). Any residual impurities were purged from the bag, by rinsing it three times with dry N_2. The bag was then filled to a capacity of 9L with purified N_2. 0.3 μL of neat liquid samples of n-octane (Sigma-Alrich) was injected to create a bag concentration of 5 ppm. Samples were drawn through a 112 μL sample loop connected to a 6 port valve (Model DC6WE, Valco, Houston, TX) and injected using a small sampling pump (UN86, KNF Neuberger, Trenton, NJ). Five separate ^{1}D chromatograms were obtained for each flow rate, and averaged to obtain the standard deviation of the incoming ^{1}D peak to the μTM. Using this experimental setup, we performed GC x GC experiments, and analyzed the FWHH of the modulated peaks. Finally, the experimentally obtained FWHH was compared to the theoretically predicted FWHH.

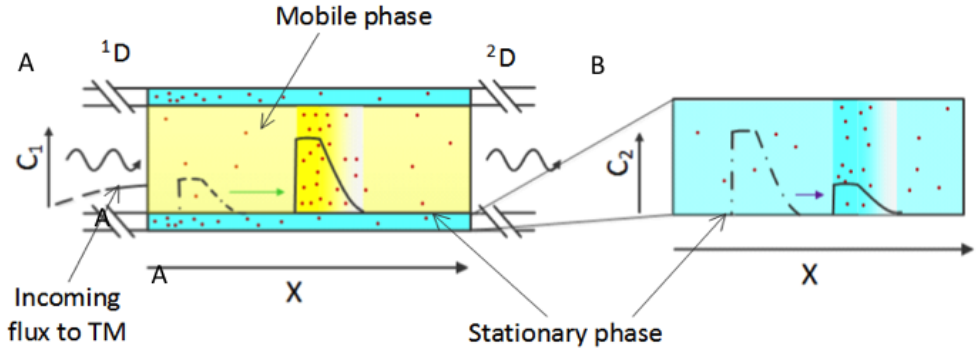
Mobile phase
A
1D
2D
B
C1
C2
A
A
X
X
Incoming
flux to TM
Stationary phase

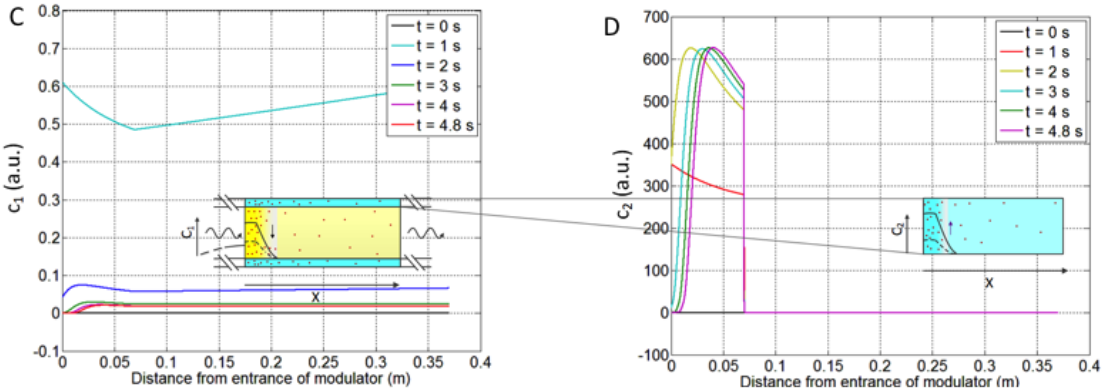
C
D
t = 0 s
t = 1 s
t = 2 s
t = 3 s
t = 4 s
t = 4.8 s
c1 (a.u.)
c2 (a.u.)
Distance from entrance of modulator (m)

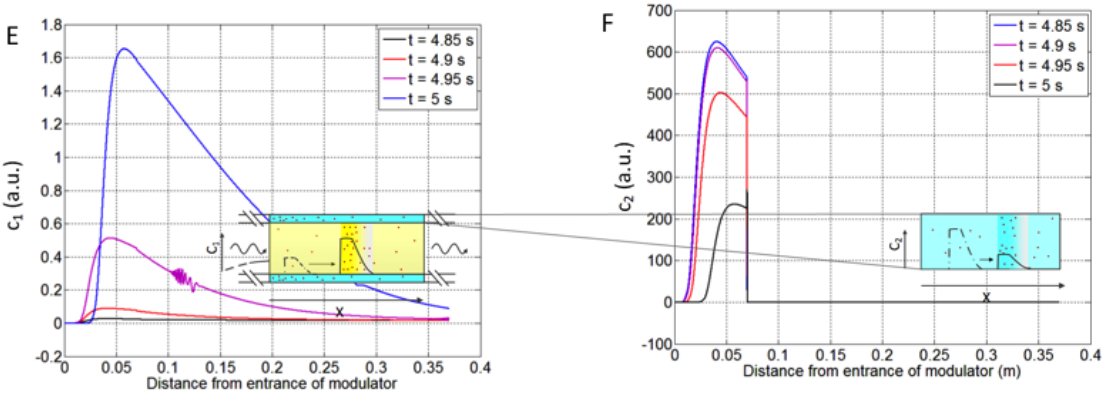
E
F
t = 4.85 s
t = 4.9 s
t = 4.95 s
t = 5 s
c1 (a.u.)
c2 (a.u.)
Distance from entrance of modulator
Distance from entrance of modulator (m)

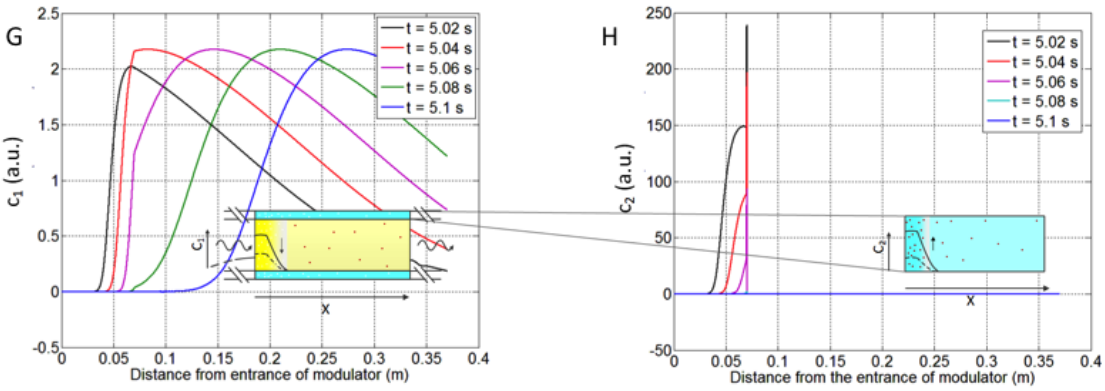
G
H
t = 5.02 s
t = 5.04 s
t = 5.06 s
t = 5.08 s
t = 5.1 s
c1 (a.u.)
c2 (a.u.)
Distance from entrance of modulator (m)
Distance from the entrance of modulator (m)

Figure 5.7Theoretically predicted concentration profile of the species within (A) the mobile phase c_1 and (B) the stationary phase c_2 during different periods in the modulation cycle. The peaks represent the spatial profiles of c_1 and c_2. The red dots represent the analyte molecules, the yellow region represents the carrier gas flow, and the aqua region represents the stationary phase. As c_1 increases, c_2 decreases simultaneously. c_1 in (C) *Step 1*, (E) *Step 2*, and (G) *Step 3*. c_2 in (D) *Step 1*, (F) *Step 2*, and (G) *Step 3*. *Step 1* entails partitioning and trapping of the species from the mobile phase to the stationary phase at t = 0-4.8s. *Step 2* entails partitioning and release of the species from the stationary phase into the mobile phase, accumulation and peak formation of the species in the modulator channel, and elution of the species from the modulator at t = 4.8-5.0 s. In *Step 3*, the next cycle of partitioning and trapping starts at t = 5.0 s and continues until t = 10s. Since the peak elutes out of the μTM after around t = 5.1 s, concentration profiles beyond t= 5.1 s are not shown in (G) and (H).

5.3. Results and Discussions

Table 5.1 Base parameters (unless otherwise stated)

Parameter	**Value**
T_{max}	481.5 K
T_{min}	259.95 K
T_{oven}	306 K
$\Delta T_{interconnect}$ w.r.t. T_{oven}	-36 K
Flow	1.5 mL/min
p	1.2 s
σ_{1D}	0.7524 s
d_{TM}	150 μm
W_{TM}	250 μm
d_{2D}	100 μm
$Length_{1st\ stage}$	4.2 cm
$Length_{2nd\ stage}$	2.8 cm
$Length_{interconnect}$	1.5 mm
$Length_{2D}$	30 cm
τ	0.77 s
Stationary Phase Thickness	0.3 μm

5.3.1 Simulation of modulation process

To demonstrate the underlying process of thermal modulation, we simulated the spatial distribution of the analyte species (i.e., octane) concentration for different instances of time in three steps of the thermal modulation process (Figure 5.7). Table 1 provides a list of parameters used for the simulations, unless otherwise stated. Here we neglected the presence of low temperature interconnects, which allowed us to highlight the process of thermal modulation without the additional complexity caused by their presence.. To demonstrate these steps, we performed simulations with $P_M = 5\text{s}$, Flow rate $(Q) = 1.5\text{mL/min}$, $\sigma_{1D} = 0.7467\text{s}$ and $p = 0\text{s}$. Figure 5.7A and Figure 5.7B show a blow up of the insets in Figure 5.7E-F to highlight the various parts of the schematic. The inset schematics depict the physical phenomena occurring in the mobile and stationary phases in each step of the process. At the beginning of our simulation, the temperature was set at the maximum elution temperature (T_{max}). Hence, any species that flew in at the start of the cooling period passed out without being trapped. Our model predicted that as the temperature of the modulator decreased exponentially during the cooling period (*Step 1* in Figure 5.6A), more species started getting trapped. Thus, the analyte concentration in the stationary phase increased in magnitude, while the analyte concentration in the mobile phase decreased in magnitude. Towards the end of the simulation, the incoming flux to the TM decreased drastically, due to the Gaussian nature of the incoming flux. This led to a concentration hump being formed close to the inlet of the TM at $t = 4.8s$ (Figure 5.7C and Figure 5.7D). Even though the temperatures of the stationary and mobile phases were very low, it should be noted that the velocity of the peak was not zero. The peak moved towards the exit at a small but non-

negligible velocity, which was clear by looking at the peak maximum for the analyte concentration in the stationary phase, in Figure 5.7D.

Our simulation showed that when the voltage pulse was applied to the TM (*Step 2* in Figure 5.6A), the species were rapidly removed from the stationary phase, and entered the mobile phase (Figure 5.7E and Figure 5.7F). The increase in magnitude in the concentration peak profile in the mobile phase was initially gradual, but speeded up with time. As the analyte concentration in the mobile phase increased, the analyte concentration in the stationary phase decreased proportionately. This happened because the partition coefficient decreased. Hence, desorption from the stationary phase increased exponentially with temperature. In this step, the temperature of the TM rose from T_{min} to T_{max} in about $0.2s$. Due to the constant flow of the carrier gas, the analyte desorbed from the stationary phase, and kept moving towards the exit of the TM. We could observe from the simulation results that the peak position for the mobile phase concentration at $t = 5s$ was located further towards the exit of the TM compared to that at $t = 4.85s$.

Our simulation indicated that when the elution peak moved from the TM to the ^{2}D column at the end of *Step 2* (in the beginning of *Step 3* in Figure 5.6A), almost all the analyte was already released into the mobile phase (Figure 5.7G-Figure 5.7H). Further, the cross-sectional area of the ^{2}D column was much smaller than that of the TM. Due to the compression effect, the concentration of the analyte increased, but slightly. This is clear by observing the peak concentration at $t = 5.02$ and $t = 5.04s$. The total amount of analyte remained the same, regardless of whether the analyte was located inside the mobile phase of the TM or the ^{2}D column. Hence, assuming that the concentration was approximately the

same, the total volume occupied by the analyte remained the same. Due to the smaller cross-sectional area of the ^{2}D column, this volume would occupy a longer section of the ^{2}D column, thus leading to the broad peak observed in the ^{2}D column at $t = 5.05$ to $t = 5.1s$. As expected, the concentration in the stationary phase inside the modulator decreased as the peak moved out of the TM. We used an *uncoated* column for the ^{2}D in our device characterization. As a result, the analyte concentration in the stationary phase of the ^{2}D column was virtually zero. We observed a slight amount of band broadening as the species moved through the ^{2}D column due to diffusion, however it was insignificant compared to the bandwidth of the modulated peak exiting the channel. The above simulations give us a physical and intuitive understanding of the process of thermal modulation, which will enable us to design a μTM with a much smaller FWHH.

Table 5.2. Experimental conditions

	Flow rate (mL/min)	$T_{max}(^oC)$ **(1^{st} stage)**	$T_{min}(^oC)$ **(1^{st}stage)**	$T_{max}(^oC)$ **(2^{nd}stage)**	$T_{min}(^oC)$ **(2^{nd} stage)**	$T_{av}(^oC)$ **(Rim, 1^{st}stage)**	$T_{av}(^oC)$ **(Rim, 2^{nd} stage)**	σ_{1D} **(s)**	$p\ (s)$
Exp. 1	1	208.4±1.8	-12.9±0.3	209.5±0.2	-14.0±0.1	29.7±0.7	27.4±0.9	1.0097± 0.0	2.3±0.8
Exp. 2	1.25	208.5±0.7	-12.7±0.2	209.0±1.6	-12.7±0.1	28.1±0.4	27.7±0.3	0.8599± 0.0091	5.3±0.2
Exp. 3	1.5	208.9±0.5	-13.3±0.9	208.2±0.6	-13.4±0.8	27.2±2.7	26.2±1.2	0.7524± 0.0066	1.2±0.1
Exp. 4	1.75	207.8±0.9	-10.7±0.3	209.3±0.6	-9.8±0.2	27.9±0.9	25.9±0.5	0.7529± 0.0023	1.8±0.2
Exp. 5	2	206.5±0.7	-11.9±0.2	209.4±1.1	-11.4±0.3	31.3±0.4	29.4±0.7	0.6324± 0.0026	4.3±0.1

5.3.2 Validation of Model with Experiments

We validated our model by performing experiments under five distinct conditions to obtain the FWHH of a modulated peak using our μTM. The experimental conditions used

here are outlined in Materials and Methods and Table 2. At the start of the experiments, the TEC was switched on along with the rim heaters, and the temperature was allowed to stabilize. Next we switched on the stage heaters and adjusted the voltage and heat pulse width needed by the stage and rim heaters to reach the desired temperature. We applied $55V$ and $47.5\,V$ to the first and the second stage heaters, respectively, with a pulse width of 135 ms to reach a T_{max} of 210^oC. A voltage of $9\,V$ was applied to the TEC to reach T_{min} of ~ -15^oC and ~ 2-3.5 V to the rim heaters to keep the temperature of the rims close to the oven temperature. We knew from experience that T_{min} and T_{max} tended to creep up over time when the TEC and heaters were activated. To determine the time required T_{min} and $T_{max}$to stabilize, we studied this temperature creep and found that ~ 120 s was sufficient for T_{min} and T_{max} to stabilize. As we mentioned before, the peak location of the incoming ^{1}D peak with respect to the heat pulse generating the modulated peak is extremely important in determining the FWHH of the modulated peak. However, it is challenging to accurately inject species at a fixed time interval with respect to the heat pulse since it would involve designing a completely new controller for the GC system. Hence, we performed a manual injection by carefully timing the injection precisely 250 s, after switching on the TM heaters. This time interval of 250 s was kept constant for all experiments. Since the time lag between switching on the heat-pulse and the actual injection into the column was kept constant, the location of the heating pulse maximum with respect to the ^{1}D peak (p) was constant for any given flow rate. Three separate modulated chromatograms were obtained for each experimental condition. The FWHH for the maximum peaks from these modulated chromatograms were averaged to obtain the FWHH for experiments.

To perform our simulations with high accuracy, we determined the parameters such as temperature, peak location etc, directly from the experiments (Table 2). Temperature data were acquired using a custom built NI-LabVIEW Interface. Chromatographic data were collected using ChemStation software (Rev.B.01.01, Agilent Technologies, Santa Clara, CA). The Flame-ion-detector (FID) was operated at 200 Hz and held constant at 250^oC. To obtain the location of the incoming peak from the ^{1}D to the μTM with respect to the heat pulse (p), we superimposed the modulated 1D chromatogram onto the unmodulated 1D chromatogram for the same flow rate (Figure 5.8). Because of the very small inner diameter of the ^{2}D column, the velocity of movement of the modulated peak through the ^{2}D column is expected to be very fast; hence the residence time of the peak in the ^{2}D column should be very small. As a result there should be minimum time lag between the occurrence of the heat pulse and the occurrence of the modulated peak on the FID display. Hence, the location of the modulated ^{1}D peak with respect to the unmodulated ^{1}D peak is a good estimate of the time stamp of the heat pulse. Using this procedure, we obtained the peak locations of the heat pulse with respect to the unmodulated peak for each flow rate. They were then averaged to obtain p for each velocity.

We performed parametric simulations assuming various shifts of the interconnect temperature from the oven temperature, $\Delta T_{interconnect}$, and we found excellent matches between the experiments and the simulations at $\Delta T_{interconnect} = -36^oC$ (Figure 5.9A). The presence of the cold interconnects changed the nature of the peak, and caused a dominant peak and a non-dominant peak to form (Figure 5.9B). Breakthrough during the operation of the μTM could be estimated by the concentration peak size at $t = 0\ s$. We also observed that

breakthrough for the case with cold interconnects was smaller, compared to the case without breakthrough (inset in Figure 5.9B). This is because the cold-interconnects act as trapping regions, and reduce the amount of species flowing through without getting trapped. The simulations revealed that the dominant peak in the simulated peak with cold interconnects was formed from species that were trapped in the second stage, while the non-dominant peak was formed by species trapped in the first stage. We also observed that the simulated peak without cold interconnects had a shorter retention time (time stamp of the peak maximum on the spectrum) compared to that of the case with cold interconnects. This happens, because the cold interconnects tend to retain species and release them slowly, thus increasing the effective retention of species in μTM stage. Further we observed that the peak with cold interconnects was larger than the case without interconnects. This is primarily due to the lower break through when cold interconnects are considered, as a result, more species elute within the modulated peak.

In actual experiments we did not distinctly observe the two peaks, possibly because the twists and turns in the spiral column merged the two peaks together. Since the half height of the dominant peak could fall below or above the second peak, using the standard method of evaluating the FWHH would result in an incorrect representation of the FWHH. Instead we used a Gaussian curve fitting method to evaluate the FWHH of the modulated peak [105]. Comparison of our simulation and experiments show a very close match in the trend as well as in the absolute value of FWHH (Figure 5.9). Error bars were calculated based on experiments repeatedly performed for each experimental condition. However, there was still some slight (< 10%) deviation between experiment and theory, which could be attributed to

multiple factors. First, we assumed that the temperatures of the stages were uniform along the length of the μTM and measured the temperature of the stages using RTDs located at the center of the stages. Hence, T_{min} of the stage channel walls on the outer periphery of the stage was mostly likely higher than T_{min}measured at the center of the stage, due to their closer proximity to the ambient environment. This led to higher trapping lengths and increased the FWHH of the modulated peak. Second, our simulations were based on a 1D model, which assumed that the analyte was in continuous contact with the stationary phase. In reality, analyte molecules traveled towards the stationary phase driven by differences in concentration between the center of the stage and the interface between the stationary phase and the mobile phase. This 3D nature of adsorption and desorption led to longer trapping lengths and deviations from our current 1D theory. Finally, we assumed a linear isotherm for our simulations. However, because of the high concentration inside the modulated peak, the linear isotherm assumption might have resulted in errors.

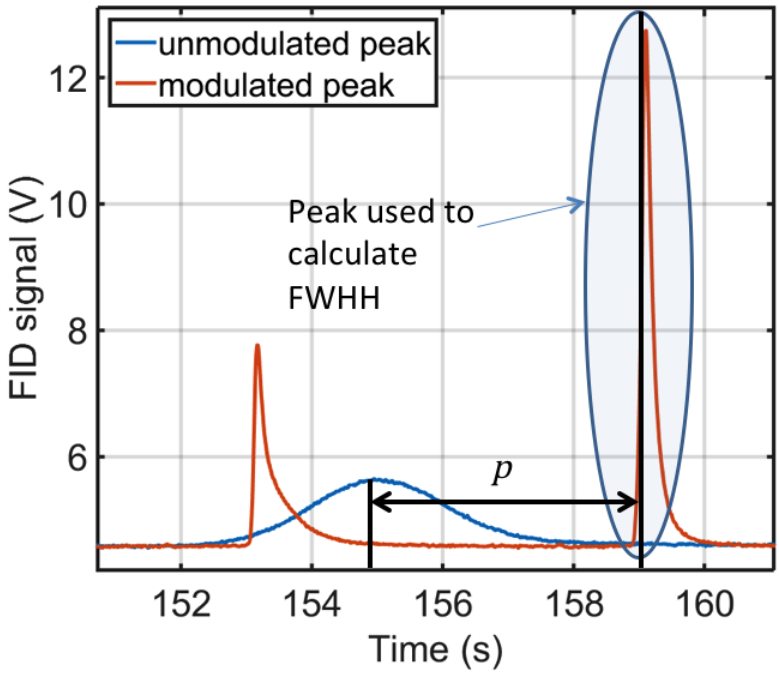

Figure 5.8 FID signal with and without modulation at a flow rate of 1 mL/min. The experimental value of FWHH is determined from the FWHH of the highest one among the modulated peak bands. p is determined assuming that the time stamp of the heat pulse is the same as that of the modulated peak and equal to the time interval between the peak maxima of the modulated and the unmodulated FID signal

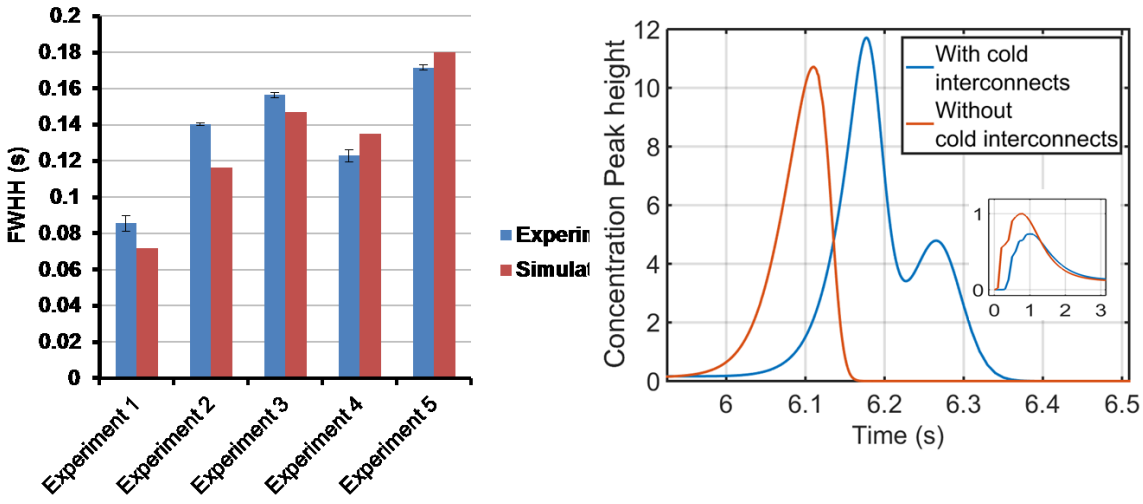

Figure 5.9 (A) Bar chart showing comparison of experimental and simulation results. Experiments performed with conditions shown in Table 2, and with a interconnect temperature of $-3^{o}C$. Experimentally determined values from Table 2, are used to run the simulations. (B) Comparison of modulated peak with and without cold interconnect, obtained with experimental conditions pertaining to Experiment 3. The presence of cold interconnect causes a second peak to appear. The inset in (B) shows breakthrough that happens at the beginning of the cooling period.

5.4. Conclusion

This study developed the *first* theoretical model for the thermal modulation process and applied it for predicting the performance of our μTM device operating as a single-stage. Our model assumed linear isotherms, Gaussian nature of the incoming peak from the ^{1}D column, and the presence of cold interconnects. Using the model, we first studied the fundamental physics of thermal modulation occurring in a single-stage TM without cold interconnects, accounting for three steps in the thermal modulation process: trapping, release and elution. Next, we incorporated the influence of cold interconnects and validate our model with experiments performed using our μTM. Excellent matches between experiment and simulation were found.

Our modeling work allowed us to see how device design features affect the analyte peak injection performance of the μTM. The results predict that an unheated cold interconnect between the first and second stages would give rise to analyte concentration to a greater extent than the trapping channels of these stages during the elution period of the thermal modulation. Extending this theory, we can deduce that in a two-stage asynchronous thermal modulator design, we need a second stage much shorter than that of our current μTM design. A device design with the shorter second stage channel can completely trap the eluent from the first stage. This design should also allow the second stage to be modulated faster as it cools down quickly to a lower temperature than the first stage owing to its lower thermal mass. Currently, the second stage channel of our μTM has a length of 2.8 cm. Reducing it nearly to the analyte trapping length, which is the minimum length required for completely trapping analyte compounds, would allow us to obtain better GC × GC results.

Our validated model can serve as a powerful tool to perform optimization of the design and operation condition parameters of the μTM. Our theoretical simulations expect to indicate performance trends of the μTM with parameters, including the depth, width, and length of the trapping stage channel, the interconnect length, the stationary phase thickness, the oven temperature, and the interconnect temperature. A study is currently underway to theoretically examine the influence of these parameters in depth, with the aim to fabricate a new generation of μTMs based on our study. We are also studying the physics behind operating our μTM as a two stage thermal modulator to develop better designs, which will help us obtain the highest possible GC × GC peak capacity.

Chapter 6. Effect of thermal time constant of primary stage on the peak capacity and breakthrough of a microscale thermal modulator

6.1. Introduction

One dimensional gas chromatography (1DGC) has existed in scientific literature since the early part of the 20th century and is widely used to separate complex mixtures [106]. It consists of a long capillary column, typically coated with a stationary phase usually polydimethlsiloxane (PDMS). The volatile organic compound (VOC) is sampled and injected at one end of the capillary, and separates into distinct bands as it is pushed through the column by the carrier gas. Recently, there has been a significant demand for portable devices to perform real-time monitoring [107]. While the portable one dimensional gas chromatography devices can perform such separation, they are limited in their capacity to separate very complex mixtures. [108, 109]

Two-dimensional gas chromatography (2DGC) was proposed by Phillips et al. [95] as a method to separate complex mixtures of VOCs with high separation capacity. 2DGC consists of two separate columns of different dimension and coated internally with different stationary phases. Typically a non-polar stationary phase such as PDMS is used in the primary column while a polar stationary phase (PEG) is used in the secondary column (provide reference). This is because using PDMS in the primary stage allows direct transfer of methods already

developed for 1DGC to the separation in the primary column of 2DGC. In between the primary and secondary column sits the modulator, which acts so as to trap and inject species as sharp bands into the second dimension. Thermal modulators are the primary type of modulators that exist, and current state of the art modulators can achieve full-width-at-half-height (FWHH) of the modulated peak down to 10 ms [86]. However, such performance requires use of extremely high amount of cryogenic consumable or high refrigeration power. Portable 2DGC can potentially separate a lot more compounds compared to one dimension GC [87], however the thermal modulator represents a significant bottleneck. To overcome this bottleneck we proposed, designed and fabricated the first thermal modulator.

Instead of using cryogenic cooling or high powered refrigeration systems, our device is made using MEMS techniques and uses thermoelectric cooling (TEC) for trapping the volatile organic compounds (VOCs). This allows us to scale the device significantly; as a result we can potentially achieve similar performance with significantly lower cooling power. For our device, we use thermoelectric cooling. Blumberg showed that optimal performance of 2DGC is achieved when the FWHH of the modulated peak is approximately 10 ms. Current state of the art modulators achieve this by using extremely high amounts of cryogenic consumables. Since that is not possible for portable gas chromatography systems, we developed a fundamental physics based model to understand the impact of all the design variables on the FWHH and peak capacity of the device. In this paper, we extend the previous model which was built for a single stage modulator to a dual stage modulator and study the impact of the thermal time constant of the first stage on the FWHH, breakthrough of the modulator; and the peak capacity of the 2DGC.

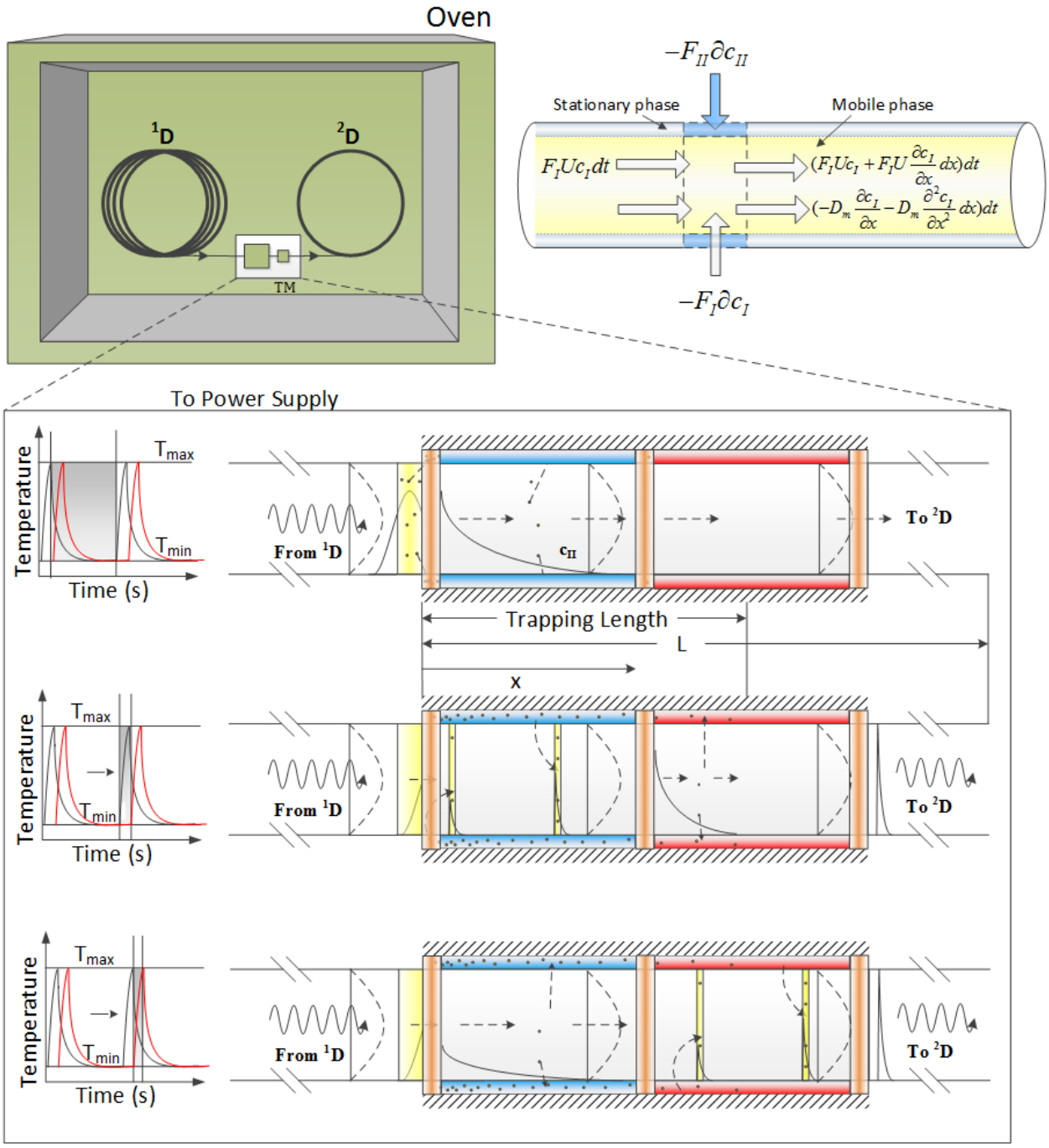

Figure 6.1 (A) Schematic of the microfabricated thermal modulator (μTM) device modeled by this study. The ^{1}D, ^{2}D columns and the μTM are kept inside a temperature-controlled oven. This helps prevent unpredictable influences of ambient temperature fluctuations on the chromatogram. (B) Diagram showing the conservation of mass, based on which this model is

built (C) Analyte trapping process under cooling period in the first stage. As the analyte with Gaussian peak shape, moves from the ^{1}D into the first stage of the TM, the stationary phase (blue rectangle) adsorbs the analyte species due to its cold temperature, while the concentration in the mobile phase decreases. (D) Analyte elution process under heating period of the first stage. Upon application of the heat pulse, the hot stationary phase (red rectangles) releases the species as a sharp pulse, which flows into the second stage of the TM. (E) Analyte elution process under heating period of the second stage. Upon application of the heat pulse, the hot stationary phase (red rectangles) releases the species as a sharp pulse, which elutes out of the TM and into the second dimension of the column.

6.2. Model

Our previous paper on single-stage thermal modulation describes the underlying physics and equations behind such a process. Here we provided a brief description of the previous model [110], its extension to a two-stage model and the calculation of the effective peak capacity.

Our μTM is enclosed inside a gas chromatography oven, so as to provide a stable environmental temperature for repeatable measurements [67, 17]. The inlet and outlet ports of the μTM is then connected to 1st and 2nd dimension capillary columns. The inlet of the ^{1}D and exit of the ^{2}D is connected to the injection device and the flame ionization detector respectively. The TEC, heaters and sensors are then connected to the data acquisition system and external power supplies for operation. First, the TEC is switched on and the temperature of the stage of the μTM is allowed to stabilize. Sharp voltage pulses of ~ 100 ms each are then applied to the heaters on the 1st and 2nd stage of the thermal modulator via the computer controller. These pulses are staggered with an interval of ~ 500 ms between the heat pulse applied on the 1st and 2nd stage. The period is known as the offset (O_s). For the same stage, the heat pulse is applied at an interval of approximately 6 seconds and is known as the modulation period (P).

The physics in this two-stage thermal modulator is governed by mass transfer and chemical kinetics. Consequently, we use gas chromatography equations first developed by van Deemter et al [102], and extend it to two-stage thermal modulators. To develop our model, we simplify our μTM and assume that the simulation domain consists of the two stages, three interconnects and the ^{2}D. The interconnects provide a continuous gas flow path between the ^{1}D to the 1st stage, between the 1st and the 2nd stage of the μTM, and between the 2nd stage of the μTM and the ^{2}D. For the purpose of our simulation, we restrict our study to two modulation periods, starting at the end of the heating pulse on the first stage. We assume prior knowledge of the incoming peak shape to the μTM inlet, and assume that a ^{2}D column is attached to the μTM.

The governing equation in the mobile and stationary phase in the domain of the μTM and the 2D column is given by:

$$V_1 \frac{\partial c_1}{\partial t} + V_2 \frac{\partial c_2}{\partial t} = V_1 \left(D_m \frac{\partial^2 c_1}{\partial x^2} - U \frac{\partial c_1}{\partial x} \right) \qquad 6.1$$

$$c_2 = K c_1 \qquad 6.2$$

Here V_1represents the volume of the stationary phase, V_2represents the volume of the mobile phase, $c_1$represents the concentration in the mobile phase, $c_2$represents the concentration in the stationary phase, $D_m$represents the diffusion coefficient of the species in the mobile phase, U is the velocity of flow of the carrier gas in the thermal modulator, and $K$is the partition coefficient in the stationary phase. Descriptions of V_1, V_2, D_m, K are provided in the aforementioned paper and are omitted here [110]. The partition coefficient K and the diffusion coefficient (D_m) are functions of the local temperature in the domain T.

Since the primary difference between the one-stage and the two-stage operation is that of the temperature pulse, we provide the temperature function below.

$$T_2(x,t) = T_{cold} * step_2(x) + T_1 * rect_1(x) + T_{cold} * rect_2(x) + T_2 * rect_3(x) + T_{cold} * rect_4(x) + T_{2D} * step_3(x) \quad 6.3$$

$$T_1(t) = T_{min_1} + T_{heat_1}(t + 0.5) + T_{heat_1}(t - 5.5) \quad 6.4$$

$$T_2(t) = T_{min_2} + T_{heat_2}(t) + T_{heat_2}(t - 6) \quad 6.5$$

$$T_{heat_1}(t) = \left(T_{max_1} - T_{min_1}\right) * \exp\left(-\frac{t - 0.7}{\tau_1}\right) * step_1(t + 5.5) \quad 6.6$$

$$T_{heat_2}(t) = \left(T_{max_2} - T_{min_2}\right) * \exp\left(-\frac{t - 0.7}{\tau_2}\right) * step_1(t + 5.5) \quad 6.7$$

Here T_{cold} represents the temperature of the cold interconnect; T_1 represents the temperature of the 1st stage; T_2 represents the temperature of the 2nd stage; T_{max_1} represents the maximum temperature of the 1st stage; $T_{\min_1}$represents the minimum temperature of the 1st stage; T_{max_2} represents the maximum temperature of the 2nd stage; T_{min_2} represents the minimum temperature of the 2nd stage; T_{heat_1}, T_{heat_2} represent intermediary temperature functions.

The above simulations enable us to obtain descriptions of the FWHH of the modulated peak. However the goal of our modeling is to improve the performance of the μTM operation in a two-dimensional gas chromatography system. The performance of comprehensive two-dimensional gas chromatography is represented by peak capacity, which can be thought of as the theoretical number of compounds that can be separated by the

system. While there has been a lot of work to show the efficacy of two-dimensional systems via experimental methods, there have been only a few theoretical studies which have shown the dependence of various operational parameters on the two-dimensional gas chromatography performance. Blumberg et al was one of the first ones to develop a theoretical relationship, which is presented below [111]:

$$G_{\{\frac{1}{2}\}} = \frac{n_{2D_1}}{n_{2D_2}} = \frac{\left\{\frac{2}{\pi}.\ {}^{1}n.\ {}^{2}n\right\}_1}{\left\{\frac{2}{\pi}.\ {}^{1}n.\ {}^{2}n\right\}_2} = \frac{\left\{\ {}^{1}U.\ {}^{1}n_o.\ {}^{2}U_S.\ {}^{2}n\right\}_1}{\left\{\ {}^{1}U.\ {}^{1}n_o.\ {}^{2}U_S.\ {}^{2}n\right\}_2} = \frac{\left\{\ {}^{2}U_S.\ {}^{2}n\right\}_1}{\left\{\ {}^{2}U_S.\ {}^{2}n\right\}_2} \quad (6.8)$$

$${}^{2}\mathrm{U_S} = \frac{{}^{2}\mathrm{s_c}}{{}^{2}\mathrm{s_{co}}} = \frac{1}{\ln \mathrm{X}} \ln \frac{\mathrm{X} + \sqrt{\mathrm{X}^2 + \mathrm{x}^2}}{1 + \sqrt{1 + \mathrm{x}^2}},\ \mathrm{X} = 2 + {}^{2}\mathrm{k_{end}},\ \mathrm{x} = \frac{{}^{2}\sigma_{\mathrm{i}}}{{}^{2}\sigma_{\mathrm{M0}}},\ {}^{2}\sigma_{\mathrm{M_0}} = \gamma_{\mathrm{gas}}\ {}^{2}\mathrm{L},\ {}^{2}\mathrm{L} = 0.4,\ \gamma_{\mathrm{gas}} = 7.3\ \mathrm{ms/m} \quad (6.9)$$

$$\ln \mathrm{k} = \frac{\mathrm{slope}}{\mathrm{T}} + \mathrm{intercept};\ \text{Slope} = 2781.8;\ \text{Intercept} = -9.752.\ \mathrm{T} = 273 + 33 = 306 \quad (6.10)$$

$${}^{2}n = 1 + \frac{\sqrt{N_{eff}}}{4} ln \frac{t_n}{t_1},\ t_n = P_M,\ t_1 = holdup\ \ time = \frac{{}^{2}L}{\frac{Flow}{Area}}, \quad (6.11)$$

$$\mathrm{N=H/L};\ \mathrm{N} = 5.54 \left(\frac{\mathrm{t_r}}{\mathrm{w_{\frac{1}{2}}}}\right)^2;\ \frac{\mathrm{H}}{\mathrm{L}} = 5.54 \left(\frac{\mathrm{t_r}}{\mathrm{FWHH}}\right)^2 = 5.54^2 \left(\frac{\mathrm{t_r}}{\sigma}\right)^2 \quad (6.12)$$

$$
\begin{aligned}
{}^{2}\sigma_{\text{broadening}} &= 5.54\, t_r \left(\frac{L}{H}\right)^{0.5}; H \\
&= \frac{2D_g}{\bar{v}_z} + \frac{(1 + 6k + 11k^2) d_c^2 \bar{v}_z}{96(1+k)^2 D_g}
\end{aligned}
\tag{6.13}
$$

$$
\begin{aligned}
{}^{2}\sigma_{\text{eff}} &= \left({}^{2}\sigma^2_{\text{broadening}} + {}^{2}\sigma_i^2 \right)^{0.5}, \; N_{\text{eff}} = 5.54^2 \left(\frac{t_r}{\sigma_{\text{eff}}}\right)^2, t_r \\
&= (1 + k_{\text{end}}) t_1
\end{aligned}
\tag{6.14}
$$

Here $G_{\{\frac{1}{2}\}}$ represents the fractional gain for the same two-dimensional system with a change in a design/operational parameter; ${}^{1}n$ represents the peak capacity of the ^{1}D, ${}^{2}n$ represents the peak capacity of the ^{2}D, ${}^{1}U$ represents the effect of discretization on the ^{1}D peak capacity, ${}^{2}U$ represents the effect of the less-than ideal FWHH of the peak injected into the ^{2}D. The definition for the rest of the parameters can be found elsewhere, and is omitted here for the sake of brevity [99, 87, 111]

6.3. Results

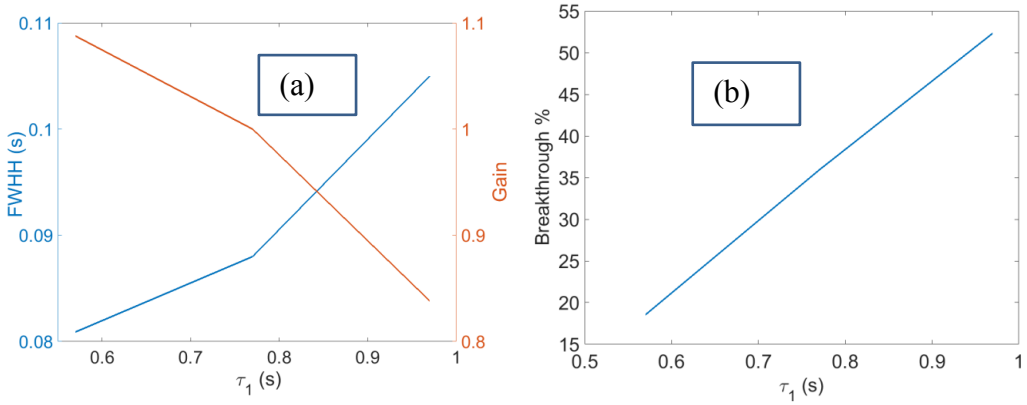

Figure 6.2 a) FWHH of modulated peak and Gain ($G_{\{\frac{1}{2}\}}$) as a function of τ_1 b) Breakthrough as a function τ_1

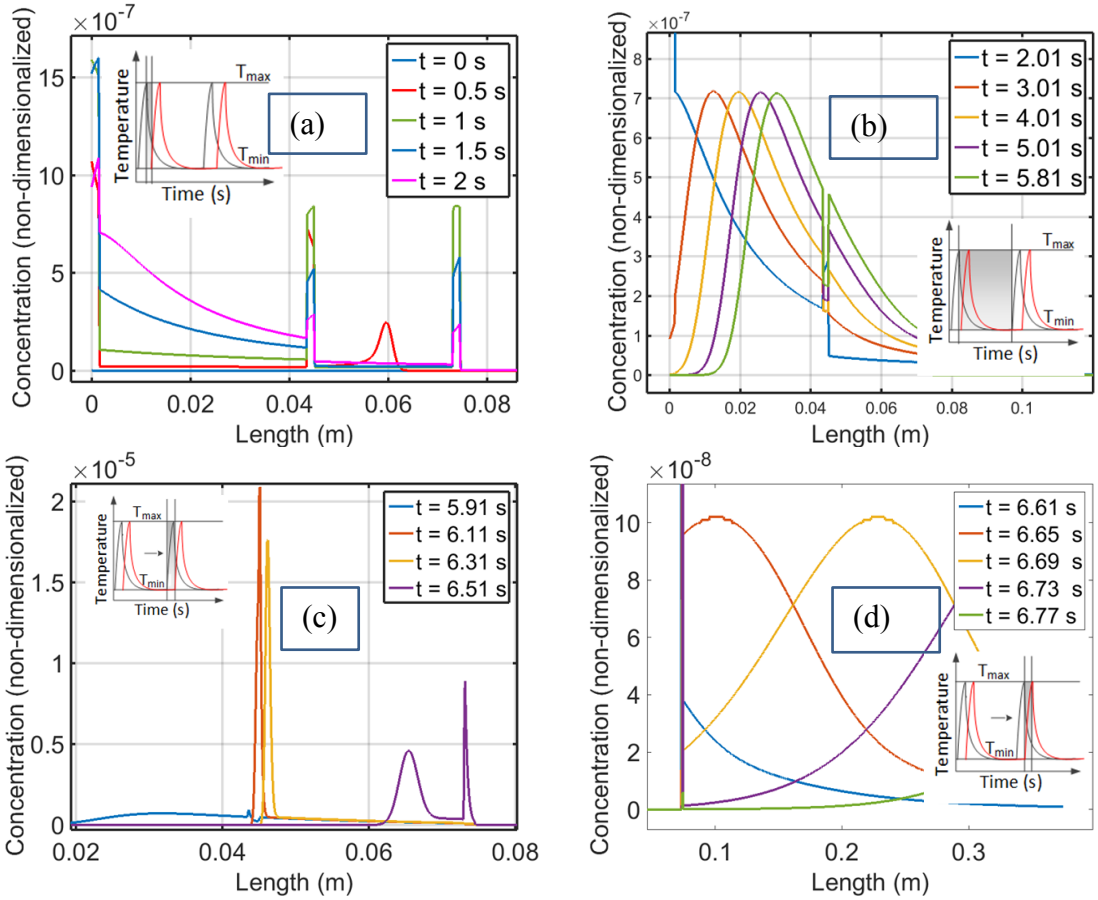

Figure 6.3. Total concentration in channel a) t=0 to 2 s, when concentration inside channel increases in magnitude b) t=2.01 s to 5.81 s, maximum concentration remains the same, peak moves towards exit c) t=5.91 s to 6.51 s. Heater on first stage is fired, species moves into second stage. Heater on second stage is fired, species moves into second stage d) t= 6.61 to 6.77 s, species moves out of second stage into 2nd dimension column and moves out.

As can be seen from Figure 6.2a the FWHH increases almost linearly with increase in the cooling time constant, while the gain decreases linearly with increase in cooling time constant. Further, breakthrough increases proportionately with time constant (Figure 6.2b). This is because small time constants result in a lower effective trapping temperature. Here effective trapping temperature is defined as the average temperature between two heating pulse. If the effective trapping temperature is lower, more amount of species is trapped within the stage and within a shorter region at the inlet of the first stage. This results in a smaller FWHH. Since the gain is inversely proportional to the FWHH of the modulated peak, Gain increases with decreasing time constant of the primary stage. Breakthrough on the other hand, increases linearly with increase in time constant. To understand these variations from the fundamental physics point of view, we plot Figure 6.3 and Figure 6.4.

Figure 6.3 plots the variation in the total concentration profile inside the thermal modulator and in the ^{2}D as a function of time. The entire process is broken up into 4 stages, based on the occurrence of the heating pulse. Figure 6.3a represents the temporal concentration profile from the start of the simulation to the application of the heat pulse to the second stage, Figure 6.3b represents the temporal concentration profile from the onset of the 1^{st} heat pulse to the 2^{nd} stage, to the application of the heat pulse to the 1^{st} stage, Figure 6.3c represents the temporal concentration profile from the onset of the 2^{nd} heat pulse to the 2^{nd} stage till the end of the simulation. At the beginning of the simulation, species accumulates at the inlet of the 1^{st} stage. Since the temperature of the coldspots are consistently low, it can be seen that the amount of species trapped is significantly higher than nearby regions. Because the temperature of the 2^{nd} stage is much lower than the first stage, at

the beginning of the cycle, there is almost no breakthrough. This can be observed in Figure 6.3b. When the heat pulse is switched on at t=2s, species are still be adsorbed into the stationary phase. Once the peak is mostly adsorbed, the temperature of the stationary phase remains approximately constant, thus leading to a constant partition coefficient. A constant but low partition coefficient means that the adsorbed species moves along with the mobile phase, but at a very slow speed. Further, the peak shape remains almost unaltered. Further, we observe that species does bleed through to the second stage to some extent. Because the temperature of the coldspots are higher than that of the surrounding stages, the total concentration is lower in the coldspots compared to the stages (during the cooling cycle). This is in sharp contrast to the conventional wisdom in thermal modulator operational understanding. It is typically assumed that all species get adsorbed in the first stage, and that the 2^{nd} stage acts only in a way to prevent breakthrough from happening, when the temperature of the first stage is too high to trap species. Further, it's usually assumed that the species remains trapped in the 1^{st} stage, and is immobile. Our simulations show that the trapped species are not really "trapped", but move at a small but significant speed, especially compared to the length of the first stage of the thermal modulator. On application of heat pulse to the first stage, species collected in the first stage rapidly elutes and accumulates at the 2^{nd} coldspot and at the entrance of the 2^{nd} stage. Because the species is already focused in the first stage, the peak adsorbed in the second stage is much sharper than in the first stage. On application of heat pulse to the 2^{nd} stage, the species trapped in the 2^{nd} stage elutes rapidly towards the third coldspot, as shown by t=6.51 s. Since the temperature of the coldspot hold constant, it elutes the trapped species slowly, resulting in the broad peak in the 2^{nd} stage as

seen in Figure 6.3c. As the peak moves through the 2nd stage, it encounters the 3rd coldspot, where it gets partially trapped again, and partially bleeds out to the 2nd dimension. Since the temperature of the 3rd coldspot is significantly lower, it bleeds the trapped species slowly, thus resulting in further broadening of the peak, as seen in Figure 6.3d. While, we cannot directly compare the peak width observed in Figure 6.3d to that in the preceding figures, we expect that without the presence of the coldspots, the FWHH of the peak would be much smaller.

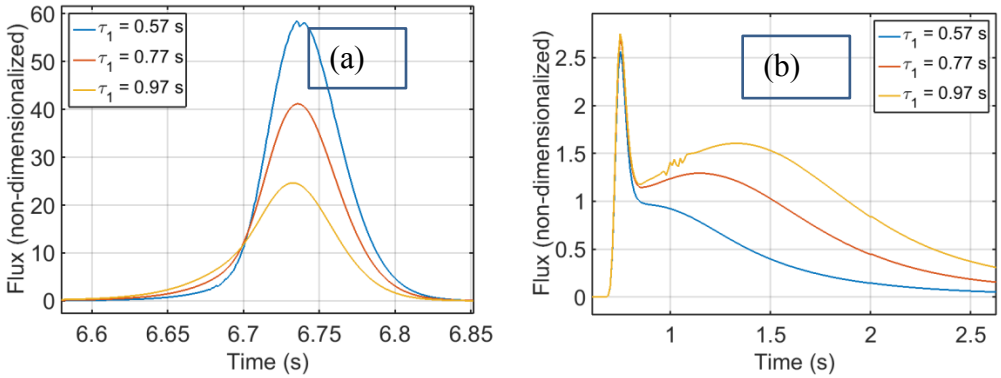

Figure 6.4 a) Flux as a function of time (s) for various τ_1 b) Break-through as a function time (s) for various τ_1

The peak width of the eluting species in Figure 6.3d, is directly related to the trapping length in Figure 6.3a-b, which in turn is directly related to the effective time constant of the first stage during the cooling phase. A lower time constant would result in a lower effective trapping temperature during the cooling phase, thus resulting in a smaller FWHH of the eluting peak, and thus a higher gain. Further, a lower effective trapping temperature, would result in lower breakthrough, thus more amount of species would elute with the primary peak. This can be observed in a, where the flux height for the lowest time constant is much lower than the flux peak height for the highest time constant. In Figure 6.4b, the first peak

height remains approximately the same regardless of the time constant. This is primarily because a change in the time constant doesn't change the effective temperature in the first part of the trapping phase significantly, and the temperature of the 2nd stage is the same. However, the effective temperature in the 2nd trapping phase is significantly different, with much lower effective trapping temperature obtained at higher values of time constant.

This is because at small amounts of time constant, the first stage goes to the minimum temperature very fast. As a result there is minimal breakthrough that happens in the first stage. Because of the sharp drop in temperature, only a small amount of species escapes to the second stage. This small amount of compound then comes out as the second peak during the breakthrough. At higher values of τ_1, more amount of species bleeds into the second stage, as a result the second peak is higher in magnitude. This can be observed by seeing plots Figure 6.3a and b. It can be observed that that most of the species gets trapped in the 1st stage, however some amount of species gets trapped in the second stage as well. Particularly at t=2 seconds we see the concentration peak containing species trapped in the second stage eluting from the 2nd stage and forming the peak in Figure 6.4b. After the 1st peak moves through the 2nd stage, the incoming peak keeps on moving in, and the full concentration peak is formed. This concentration peak then moves towards the exit. We can see that at the exit of the second stage, the total concentration is not exactly zero. This non-zero concentration means that species are flowing into the second dimension and ultimately form the secondary breakthrough peak.

It is also clearly visible that the flux concentration for lower τ_1 is higher than that at higher τ_1.(reword sentence) This is because more amount of species breakthrough into the

second dimension and ultimately to the FID during the trapping phase, at higher values of τ_1. Further a higher value of $\tau_1$means that the species are trapped over a longer length of the 1st stage. Thus when the species are eluted into the second stage, and the temperature pulse is applied, a broader peak is formed in the FID.

Since the peak capacity gain over and above the mean ($G_{\{\frac{1}{2}\}}$) is function of FWHH of the peak, the effective gain increases as the FWHH decreases.

6.4. Conclusion

In this paper we have shown the dependence of the gain in peak capacity, the FWHH and breakthrough with increase in the time constant of the first stage. We find that the FWHH increases, peak capacity decreases and breakthrough increases, with increase in the time constant of the first stage. One aspect not captured by our model is the non-ideality of the temperature profile. When the first stage fires, the temperature of the second stage increases. However this is not captured by our current model. This will slightly increase the FWHH of the modulated peak. Our systematic sensitivity analysis shows that the breakthrough can be decreased to as low as 3% from 30% by carefully choosing the correct parameters, while FWHH can be decreased and peak capacity improved by as much as 50% by reasonable modification of the design parameters. What do you plan to do in future.

Chapter 7. Conclusions and Future Work

7.1. Summary of Thesis

The research performed above demonstrates for the first time, a microscale comprehensive two-dimensional gas chromatography using a micro-scale thermal modulator. Further a fundamental physics based model for thermal modulation is presented in this thesis for the first time. A summary of these achievements are given in the following sections.

7.1.1 Demonstration of $\mu GC \times \mu GC$

The first goal of this thesis is to demonstrate micro-scale comprehensive two-dimensional gas chromatography. While the performance of our micro-thermal modulator (μTM) had been demonstrated before, it had not been used for separation of a complex mixture. This goal is achieved in two-steps.

First, the capability of our μTM in conjunction with conventional gas chromatography columns to perform comprehensive two-dimensional gas chromatography is demonstrated. The operational parameters are optimized for a set of compounds. These optimized operational parameters are then used to perform separation of 21 compound mixture within 3 min. Further, I demonstrated the capability of our system to generate structured chromatograms, which is a hall-mark of an efficient $GC \times GC$ system.

Second, our μTM is coupled with micro-fabricated columns to demonstrate comprehensive two-dimensional gas chromatography with all micro-fabricated components.. These micro-columns are coated with PDMS in the ^{1}D, and PTFPMS/RTIL in the ^{2}D. Coating was performed in house with techniques developed by our collaborator in the chemistry department. Optimized operational conditions were obtained from the previous demonstration. The use of RTIL can potentially extend the range of compounds that can be separated using our μTM. In this thesis, I showed the separation of a 18 compound mixture with a wide range of boiling point and polarity in <6 min with both RTIL and PTFMS coating in the ^{2}D. The capability of the $\mu GC \times \mu GC$ system to perform temperature programmed gas chromatography is also demonstrated. Temperature ramping enables us to improve peak capacity as well as orthogonality (utilization of separation space) in our separations.

7.1.2 Modeling of μTM as a single stage modulator

While thermal modulators have existed for around 20 years now, most efforts to improve the performance of the thermal modulator has focused on the mechanism of obtaining lower trapping temperature or more reliable modulators. However, the fundamental physical phenomena behind thermal modulators hasn't been modelled so far.. Thermal modulators were treated as a black box with a certain minimum and maximum temperature and a certain length of the capillary column. Further, most conventional thermal modulators used extremely high operational power to achieve trapping, or expensive cryogenic

consumables. Since our goal is to make a portable thermal modulator, our power budget is limited to ~ 20W of cooling using the TEC.

A FWHH of the modulated peak close to 10 ms maybe possible by optimizing the design of the μTM. To do so, we need a model for thermal modulators, however currently no such model exists. Hence, I developed a fundamental physics based model for our μTM. This model considers the diffusion and convection happening within the thermal modulator, as well as partitioning of species from the mobile phase to the stationary phase. It accounts for the Gaussian nature of the incoming peak as well as the phase difference between the peak of the incoming peak to the thermal modulator and the heat pulse applied to the modulator. We validated our model with experiments to within 10% error. This is the first time that such a model has been built, and this model can be extended to drastically improve the performance of current thermal modulators as well as propose completely new designs.

7.1.3 Effect of time constant on asynchronous modulation of μTM

While our previous model only considers a single stage modulator with both stages operating simultaneously, our μTM is a two-stage device. Hence we need to account for the asynchronous modulation as well as any non-idealities associated with this model. Towards this goal, we modified our original model to account for the temperature fluctuation as well as temperature coupling between the two –stages. We performed sensitivity studies and identified the most important design and operational parameters. In this thesis we show one such parameter, the time constant of the 1st stage. We show that with increase in time constant (τ_1) results in significant increase in the FWHH of the modulated peak and

breakthrough associated with modulation. Results not shown in this thesis also show that by optimizing each of these parameters, it's possible to reduce the FWHH of the modulated peak by atleast 50%, while increasing the breakthrough by 10 fold.

7.2. Future Research Direction

There are multiple directions that can be taken going forward. While we have shown optimum operating characteristics based on our model, our model does not take into consideration the interaction between the various independent parameters. To account for this, a 1D/3D thermal model should be built. Based on this model, we can then study whether the optimum design parameters . Some preliminary work based on simplified lumped system model and static heat transfer has already been performed, but since there is significant temperature fluctuation, a full 3D model needs to be developed and simulated. Based on this model, we can then figure our optimum design features for our thermal modulator. This modeling is necessary since fabrication of our thermal modulator is very expensive, and such simulations will reduce the amount of trial and error necessary very significantly. Based on this design, we will need to fabricate our modulator and perform experiments to show the improvement in performance of our modulator. Finally, the thermal modulator, columns, pre-concentrators, detection systems need to be assembled and integrated to form a portable two-dimensional gas chromatography system.

References

1] A. B. Littlewood, Gas Chromatography: Principles, Techniques, and Applications, New York: Academic, 1970.

2] A. V. Es, High-Speed Narrow Bore Capillary Gas Chromatography, Heidelberg, Germany: Huthig Buch Verlag, 1992.

3] G. Lambertus, A. Elstro, K. Sensenig, J. Potkay, M. Agah, S. Scheuering, K. Wise, F. Dorman and R. Sacks, "Design, fabrication, and evaluation of microfabricated columns for gas chromatography," *Analytical Chemistry,* vol. 76, pp. 2629-2637, 2004.

4] M. Adahchour, J. Beens and U. A. T. Brinkman, "Recent developments in the application of comprehensive two-dimensional gas chromatography," *Journal of Chromatography A,* vol. 1186, no. 1-2, pp. 67-108, 2008.

5] L. Ramos, Comprehensive Two Dimensional Gas Chromatography, Amsterdam, The Netherlands: Elsevier, 2009.

6] J. B. Phillips, R. B. Gaines, J. Blomberg, F. W. M. van der Wielen, J.-M. Dimandja, V. Green, J. Granger, D. Patterson, L. Racovalis, H.-J. de Geus, J. de Boer, P. Haglund, J. Lipsky, S. Veena and E. B. Ledfored Jr., "A Robust Thermal Modulator for Comprehensive Two-Dimensional Gas Chromatography," *Journal of High*

Resolution Chromatography, vol. 22, no. 1, pp. 3-10, 1999.

7] S. Reidy, G. Lambertus, J. Reece and R. Sacks, "High-Performance, Static-Coated Silicon Microfabricated Columns for Gas Chromatography," *Analytical Chemistry,* vol. 78, no. 8, pp. 2623-2630, 2006.

8] M. Agah, J. A. Potkay, G. Lambertus, R. Sacks and K. D. Wise, "High-Performance Temperature-Programmed Microfabricated Gas Chromatography Columns," *Journal of Microelectromechanical Systems,* vol. 14, no. 5, pp. 1039-1050, 2005.

9] G. Serrano, S. M. Reidy and E. T. Zellers, "Assessing the reliability of wall-coated microfabricated gas chromatographic separation columns," *Sensors and Actuators B: Chemical,* vol. 141, no. 1, pp. 217-226, 2009.

10] M. Pursch, K. Sun, B. Winniford, H. Cortes, A. Weber, T. McCabe and J. Luong, "Modulation techniques and applications in comprehensive two-dimensional gas chromatography (GC×GC)," *Analytical and Bioanalytical Chemistry,* vol. 373, no. 6, pp. 356-367, 2002.

11] J. Harynuk and T. Gorecki, "New liquid nitrogen cryogenic modulator for comprehensive two-dimensional gas chromatography," *Journal of Chromatography A,* vol. 1019, no. 1-2, pp. 53-63, 2003.

12] M. Libardoni, J. H. Waite and R. Sacks, "Electrically Heated, Air-Cooled Thermal Modulator and at-Column Heating for Comprehensive Two-Dimensional Gas Chromatography," *Analytical Chemistry,* vol. 77, no. 9, pp. 2786-2794, 2005.

P. J. Marriott and R. M. Kinghorn, "Longitudinally Modulated Cryogenic
13] System. A Generally Applicable Approach to Solute Trapping and Mobilization in Gas Chromatography," *Analytical Chemistry,* vol. 69, no. 13, pp. 2582-2588, 1997.

Z. Liu and J. B. Phillips, "Comprehensive Two-Dimensional Gas
14] Chromatography using an On-Column Thermal Modulator Interface," *Journal of Chromatography Science,* vol. 29, no. 6, pp. 227-231, 1991.

E. B. Ledford Jr. and C. . Billesbach, "Jet-Cooled Thermal Modulator for
15] Comprehensive Multidimensional Gas Chromatography," *Journal of High Resolution Chromatography,* vol. 23, no. 3, pp. 202-204, 2000.

M. Adahchour, J. Beens, R. J. J. Vreuls and U. A. T. Brinkman, "Recent
16] developments in comprehensive two-dimensional gas chromatography (GC × GC) ☆: II. Modulation and detection," *TrAC Trends in Analytical Chemistry,* vol. 25, no. 6, pp. 540-553, 2006.

S.-J. Kim, S. M. Reidy, B. Block, K. D. Wise, E. T. Zellers and K.
17] Kurabayashi, "Microfabricated thermal modulator for comprehensive two-dimensional micro gas chromatography: design, thermal modeling, and preliminary testing," *Lab on Chip,* vol. 10, pp. 1647-1654, 2010.

S.-J. Kim, G. Serrano, K. D. Wise, K. Kurabayashi and E. T. Zellers,
18] "Evaluation of a Microfabricated Thermal Modulator for Comprehensive Two-Dimensional Microscale Gas Chromatography," *Analytical Chemistry,* vol. 83, no. 14, pp. 5556-5562, 2011.

S.-J. Kim and K. Kurabayashi, "Uniform-temperature, microscale thermal
19] modulator with area-adjusted air-gap isolation for comprehensive two-dimensional gas chromatography," *Sensors and Actuators B: Chemical,* vol. 181, pp. 518-522, 2013.

I. Gracia, P. Ivanov, F. Blanco, N. Sabate, X. Vilanova, X. Correig, L. Fonseca,
20] E. Figueras, J. Santander and C. Cane, "Sub-ppm gas sensor detection via spiral jipreconcentrator," *Sensors and Actuators B,* vol. 132, pp. 149-154, 2008.

W. -C. Tian, S. W. Pang, C.-J. Lu and E. T. Zellers, "Microfabricated
21] preconcentrator-focuser for a microscale gas chromatograph," *Journal of Microelectromechanical Systems,* vol. 12, pp. 264-272, 2003.

W.-C. Tian, H. K. L. Chan, C.-J. Lu, S. W. Pang and E. Zellers, "Multiple-stage
22] microfabricated preconcentrator-focuser for micro gas chromatography system," *Journal of Microelectromechanical Systems,* vol. 14, pp. 498-507, 2005.

A. M. Ruiz, I. Cracia, N. Sabate, P. Ivanov, A. Sanchez, M. Duch, M. Gerboles,
23] A. Moreno and C. Cane, "Membrane-suspended microgrid as a gas preconcentrator for chromatographic applications," *Sensors and Actuators A,* vol. 135, pp. 192-196, 2007.

H.-S. Noh, P. J. Hesketh and G. C. Frye-Mason, "Parylene gas chromatographic
24] column for rapid thermal cycling," *Journal of Microelectromechanical Systems,* vol. 11, pp. 718-725, 2002.

J. A. Dziuban, J. Mroz, M. Szczygielska, M. Malachowski, A. Gorecka-
25] Drzazga, R. Walczak, W. Bula, D. Zalewski, L. Nieradko, J. Lysko, J. Koszur and P. Kowalski, "Portable gas chromatograph with integrated components," *Sensors and*

Actuators A, vol. 115, pp. 318-330, 2004.

26] H. Kim, W. H. Steinecker, S. M. Reidy, G. R. Lambertus, A. Astle, K. Najafi, E. T. Zellers, L. P. Bernal, P. Washabaug and K. D. Wise, "A Micropump-driven highspeed MEMS gas chromatography system," in *IEEE International Conference on Solid-State Sensors and Actuators (Transducers)* , Lyon, France, 2007.

27] Q.-Y. Cai and E. T. Zellers, "Dual-chemiresistor GC detector employing monolayer-protected metal nanocluster interfaces," *Analytical Chemistry,* vol. 74, pp. 3533-3539, 2002.

28] C.-J. Lu, J. Whiting, R. D. Sacks and E. T. Zellers, "Portable gas chromatograph with tunable retention and sensor array detection for determination of complex vapor mixtures," *Analytical Chemistry,* vol. 74, pp. 1400-1409, 2003.

29] M.-D. Hsieh and E. T. Zellers, "Limits of recognition for simple vapor mixtures determined with a microsensor array," *Analytical Chemistry,* vol. 76, pp. 1885-1895, 2004.

30] G. R. Lambertus, C. S. Fix, S. M. Reidy, R. A. Miller and D. Wheeler, "Silicon microfabricated column with microfabricated differential mobility spectrometer for GC analysis of volatile organic compounds," *Anlaytical Chemistry,* vol. 77, pp. 7563-7571, 2005.

31] S. K. Kim, H. Chang and E. T. Zellers, "Prototype micro gas chromatograph for breath biomarkers of respiratory disease," in *Denver, CO*, 2009, IEEE International Conference on Solid-State Sensors and Actuators (Transducers).

G. Serrano, H. Chang and E. T. Zellers, "A micro gas chromatograph for
32] highspeed determinations of explosive vapors," in *IEEE International Conference on Solid-State Sensors and Actuators (Transducers)*, Denver, CO, 2009.

C.-J. Lu, W. H. Steinecker, W.-C. Tian, M. C. Oborny, J. M. Nichols, M. Agar,
33] J. A. Potkay, H. K. L. Chan, J. Driscoll, R. D. Sacks, K. F. Wise, S. W. Pang and E. T. Zellers, "First-generation hybrid MEMS gas chromatograph," *Lab on a Chip,* vol. 141, pp. 1123-1131, 2005.

S. Zampolli, I. Elmi, F. Mancerella, P. Betti, E. Dalcanale, G. C. Cardinali and
34] M. Sveri, "Real-time monitoring of sub-ppb concentrations of aromatic volatiles with a MEMS-enabled miniaturized gas-chromatograph," *Sensors and Actuators B,* vol. 141, pp. 322-328, 2009.

P. R. Lewis, R. P. Manginell, D. R. Adkins, R. J. Kottenstette, D. R. Wheeler,
35] S. S. Sokolowski, D. E. Trudell, J. E. Byrnes, M. . Okandan, J. M. Bauer, R. G. Manley and G. C. Frye-Mason, "Recent Advancements in the gas-phase MicroChemlab," *IEEE Sensors Journal,* vol. 6, pp. 784-795, 2006.

E. T. Zellers, G. . Serrano, H. Chang and L. K. Amos, "A micro gas
36] chromatograph for rapid determinations of explosive marker compounds," in *IEEE International Conference on Solid-State Sensors and Actuators (Transducers)*, Beijing, China, 2011.

S. C. Terry, J. H. Jerman and J. B. Angell, "A gas chromatographic air analyzer
37] fabricated on a silicon wafer," *IEEE Transactions on Electron Devices,* vol. 26, pp.

1880-1886, 1979.

R. R. Reston and E. S. Kolesar, "Silicon-micromachined gas chromatography
38] system used to separate and detect ammonia and nitrogen dioxide-Part I: design fabrication, and integration of the gas chromatography system," *Journal of Microelectromechanical Systems,* vol. 3, pp. 134-146, 1994.

E. S. Kolesar and R. R. Reston, "Silicon-micromachined gas chromatography
39] system used to separate and detect ammonia and nitrogen dioxide-Part II: evaluation, analysis, and theoretical modeling of the gas chromatography system," *Journal of Microelectromechanical Systems,* vol. 3, pp. 147-154, 1994.

R. P. Manginell, J. M. Bauer, M. W. Moorman, L. J. Sanchez, J. M. Anderson,
40] J. J. Whiting, D. A. Porter, D. Copie and K. E. Achyuthan, "A monolithicallyintegrated flGC chemical sensor system," *Sensors,* vol. 11, pp. 6517-6532, 2011.

R. P. Manginell, D. R. Adkins, M. W. Moorman, R. Hadizadeh, D. Copic, D.
41] A. Porter, J. M. Anderson, V. M. Hietala, J. R. Bryan, D. R. Wheeler, K. B. Pfeifer and A. Rumpf, "Mass-sensitive microfabricated chemical preconcentrator,"," *Journal of Microelectromechanical Systems,* vol. 1407, p. 1396, 2008.

S. K. Kim, H. Chang and E. T. Zellers, "Microfabricated gas chromatograph for
42] the selective determination of trichloroethlyene vapor at sub-parts-per-billion concentrations in complex mixtures," *Analytical Chemistry,* vol. 83, pp. 7198-7206, 2011.

J. H. Wahl, D. M. Riechers, M. E. Vucelick and B. W. Wright, "A portable

43] multi-dimensional gas chromatographic system for field applications," *Journal of Separation Science,* vol. 26, pp. 1083-1090, 2003.

A. E. Sinha, B. J. Prazen, C. G. Fraga and R. E. Synovec, "Valve-based
44] comprehensive two-dimensional gas chromatography with time-of-flight mass spectrometric detection: instrumentation and figures-of-merit," *Journal of Chromatography A,* vol. 1019, no. 1-2, pp. 79-87, 2003.

R. E. Mohler, B. J. Prazen and R. E. Synovec, "Total-transfer, valve-based
45] comprehensive two-dimensional gas chromatography," *Analytica Chimica Acta,* vol. 555, no. 1, pp. 68-74, 2006.

J. Liu, J. H. Seo, Y. Li, D. Chen, K. Kurabayashi and X. Fan, "Smart multi-
46] channel two-dimensional micro-gas chromatography for rapid workplace hazardous volatile organic compounds measurement," *Lab on Chip,* vol. 13, pp. 818-825, 2013.

G. Serrano, D. Paul, S.-J. Kim, K. Kurabayashi and E. T. Zellers,
47] "Comprehensive Two-Dimensional Gas Chromatographic Separations with a Microfabricated Thermal Modulator," *Analytical Chemistry,* vol. 84, no. 16, pp. 6973-6980, 2012.

W. R. Collin, A. Bondy, D. Paul, K. Kurabayashi and E. T. Zellers, "μGC ×
48] μGC: Comprehensive Two-Dimensional Gas Chromatographic Separations with Microfabricated Components," *Analytical Chemistry,* vol. 87, no. 3, pp. 1630-1637, 2015.

B. Alfeeli, D. Cho, M. Ashraf-Khorassani, L. T. Taylor and M. Agah, "MEMS-

49] based multi-inlet/outlet preconcentrator coated by inkjet printing of polymer adsorbents," *Sensors and Actuators B: Chemical,* vol. 133, no. 1, pp. 24-32, 2008.

50] A. D. Radadia, R. I. Masel, M. A. Shannon, J. P. Jerrel and K. R. Cadwallader, "Micromachined GC Columns for Fast Separation of Organophosphonate and Organosulfur Compounds," *Analytical Chemistry,* vol. 80, no. 11, pp. 4087-4094, 2008.

51] M. A. Zareian-Jahromi, M. Ashraf-Khorassani, L. T. Taylor and M. Agah, "Design, Modeling, and Fabrication of MEMS-Based Multicapillary Gas Chromatographic Columns," *Journal of Micromechanical Systems,* vol. 18, no. 1, pp. 28-37, 2009.

52] R.-S. Jian and R.-X. Huang, "A micro GC detector array based on chemiresistors employing various surface functionalized monolayer-protected gold nanoparticles," *Talanta,* vol. 88, pp. 160-167, 2012.

53] M. Li, E. B. Myers, H. X. Tang, S. J. Aldridge, H. C. McCaig, J. J. Whiting, R. J. Simonson, N. S. Lewis and M. L. Roukes, "Nanoelectromechanical Resonator Arrays for Ultrafast, Gas-Phase Chromatographic Chemical Analysis," *Nano Letters,* vol. 10, no. 10, pp. 3899-3903, 2010.

54] K. Reddy, Y. Guo, J. Liu, W. Lee, M. K. K. Oo and X. Fan, "On-chip Fabry–Pérot interferometric sensors for micro-gas chromatography detection," *Sensors and Actuators B: Chemical,* vol. 159, no. 1, pp. 60-65, 2011.

D. Cruz, J. P. Chang, S. K. Showalter, F. Gelbard, R. P. Manginell and M. G.

55] Blain, "Microfabricated thermal conductivity detector for the micro-ChemLab™," *Sensors and Actuators B: Chemical,* vol. 121, pp. 414-422, 2007.

56] P. Galambos, J. Lantz, M. S. Baker, J. McClain, G. R. Bogart and R. J. Simonson, "Active MEMS Valves for Flow Control in a High-Pressure Micro-Gas-Analyzer," *Journal of Microelectromechanical Systems,* vol. 20, no. 5, pp. 1150-1162, 2011.

57] "Canary-3 Chemical Detector," Defiant Technologies, [Online]. Available: http://www.defiant-tech.com/canarythree.php. [Accessed 4 8 2015].

58] S. K. Kim, D. R. Burris, H. Chang, J. Bryant-Genevier and E. T. Zellers, "Microfabricated Gas Chromatograph for On-Site Determination of Trichloroethylene in Indoor Air Arising from Vapor Intrusion. 1. Field Evaluation," *Environmental Science and Technology,* vol. 46, no. 11, pp. 6065-6072, 2012.

59] S. K. Kim, D. R. Burris, J. Bryant-Genevier, K. A. Gorder, E. M. Dettenmaier and E. T. Zellers, "Microfabricated Gas Chromatograph for On-Site Determinations of TCE in Indoor Air Arising from Vapor Intrusion. 2. Spatial/Temporal Monitoring," *Environmental Science and Technology,* vol. 46, no. 11, pp. 6073-6080, 2012.

60] V. R. Reid and R. E. Synovec, "High-speed gas chromatography: The importance of instrumentation optimization and the elimination of extra-column band broadening," *Talanta,* vol. 76, no. 4, pp. 703-717, 2008.

61] J. Dalluge, J. Beens and U. A. T. Brinkman, "Comprehensive two-dimensional gas chromatography: a powerful and versatile analytical tool," *Journal of*

Chromatography A, vol. 1000, no. 1-2, pp. 69-108, 2003.

62] J. V. Seeley, N. J. Micyus, S. V. Bandurski, S. K. Seeley and J. D. McCurry, "Microfluidic Deans Switch for Comprehensive Two-Dimensional Gas Chromatography," *Analytical Chemistry,* vol. 79, no. 5, pp. 1840-1847, 2007.

63] M. Adahchour, J. Beens and U. A. T. Brinkman, "Single-jet, single-stage cryogenic modulator for comprehensive two-dimensional gas chromatography (GC × GC)," *Analyst,* vol. 128, pp. 213-216, 2003.

64] O. Panic, T. Gorecki, C. McNeish, A. H. Goldstein, B. J. Williams, D. R. Worton, S. V. Hering and N. M. Kreisberg, "Development of a new consumable-free thermal modulator for comprehensive two-dimensional gas chromatography," *Journal of Chromatography A,* vol. 1218, no. 20, pp. 3070-3079, 2011.

65] F. Begnaud, C. Debonneville, J.-P. Probst, A. Chaintreau, P. D. Morrison, J. L. Adcock and P. J. Marriott, "Effects of variation in modulator temperature during cryogenic modulation in comprehensive two-dimensional gas chromatography," *Journal of Separation Science,* vol. 32, no. 18, pp. 3144-3151, 2009.

66] M. Libardoni, C. Fix, J. H. Waite and R. Sacks, "Design and performance evaluation of a two-stage resistively-heated thermal modulator for GC × GC," *Analytical Methods,* vol. 2, pp. 936-943, 2010.

67] D. Paul, G. Serrano, E. T. Zellers and K. Kurabayashi, "Comprehensive Two-dimensional Gas Chromatography Using a MEMS Thermal Modulator," in *(MEMS) IEEE International Conference on Micro Electro Mechanical Systems*, Paris, France,

2012.

W. Khummueng, J. Harynuk and P. J. Marriott, "Modulation Ratio in
68] Comprehensive Two-dimensional Gas Chromatography," *Analytical Chemistry,* vol. 78, no. 13, pp. 4578-4587, 2006.

R. L. Grob and E. F. Barry, Modern Practice of Gas Chromatography, 3rd
69] Edition, Chapter 3, New York: Wiley-Interscience, 2005.

R. A. Sheillie, L.-L. Xie and P. J. Marriott, "Retention time reproducibility in
70] comprehensive two-dimensional gas chromatography using cryogenic modulation: An intralaboratory study," *Journal of Chromatography A,* vol. 968, no. 1-2, pp. 161-170, 2002.

E. Gallego, Air Quality in the 21st Century, Hauppage, NY: Nova Science
71] Publishers, 2010.

G. de Gennaro, L. de Gennaro, A. Mazzone, F. Porcelli and M. Tutino, "Indoor
72] air quality in hair salons: Screening of volatile organic compounds and indicators based on health risk assessment," *Atmospheric Environment,* vol. 83, pp. 119-126, 2014.

T. Petry, D. Vitale, F. J. Joachim, B. Smith, L. Cruse, R. Mascarenhas, S.
73] Schneider and M. Singal, "Human health risk evaluation of selected VOC, SVOC and particulate emissions from scented candles," *Regulatory Toxicology and Pharmacology,* vol. 69, no. 1, pp. 55-70, 2014.

O. Terzic, I. Swahn, G. Cretu, M. Palit and G. Mallard, "Gas chromatography–
74] full scan mass spectrometry determination of traces of chemical warfare agents and

their impurities in air samples by inlet based thermal desorption of sorbent tubes," *Journal of Chromatography A,* vol. 1225, pp. 182-192, 2012.

C.-Y. Peng and S. Batterman, "Performance evaluation of a sorbent tube
75] sampling method using short path thermal desorption for volatile organic compounds," *Journal of Environmental Monitoring,* vol. 2, pp. 313-324, 2000.

"Welcome to Torion.com," Torion Technologies, [Online]. Available:
76] http://torion.com/home.html. [Accessed 31 7 2015].

"HAPSITE ER Chemical Identification System," INFICON, [Online].
77] Available: http://products.inficon.com/en-us/nav-products/Product/Detail/HAPSITE-ER-Identification-System?path=Products%2Fpg-ChemicalDetection%2F. [Accessed 31 7 2015].

"Chemical Detector," Defiant Technologies, [Online]. Available:
78] http://www.defiant-tech.com/. [Accessed 31 7 2015].

"Apix Analytics," APIX Analytics, [Online]. Available:
79] http://www.apixanalytics.com/. [Accessed 31 7 2015].

W. R. Collin, G. Serrano, L. K. Wright, H. Chang, N. Nunovero and E. T.
80] Zellers, "Microfabricated Gas Chromatograph for Rapid, Trace-Level Determinations of Gas-Phase Explosive Marker Compounds," *Analytical Chemistry,* vol. 86, no. 1, pp. 655-663, 2014.

R.-S. Jian, Y.-S. Huang, S.-L. Lai, L.-Y. Sung and C.-J. Lu, "Compact
81] instrumentation of a μ-GC for real time analysis of sub-ppb VOC mixtures,"

Microchemical Journal, vol. 108, pp. 161-167, 2013.

82] H. Shakeel and M. Agah, "Self-Patterned Gold-Electroplated Multicapillary Gas Separation Columns With MPG Stationary Phases," *Journal of Microelectromechanical Systems,* vol. 22, no. 1, pp. 62-70, 2013.

83] K. Reddy, J. Liu, M. K. K. Oo and X. Fan, "Integrated Separation Columns and Fabry-Perot Sensors for Microgas Chromatography Systems," *Journal of Microelectromechanical Systems,* vol. 22, no. 5, pp. 1174-1179, 2013.

84] Y. Qin and Y. B. Gianchandani, "A facile, standardized fabrication approach and scalable architecture for a micro gas chromatography system with integrated pump," in *Transducer* , Barcelona, Spain, 2013.

85] R. C. Y. Ong and P. J. Marriott, "A Review of Basic Concepts in Comprehensive Two-Dimensional Gas Chromatography," *Journal of Chromatographic Science,* vol. 65, no. 1, pp. 25-42, 2014.

86] M. Edwards, A. Mostafa and T. Gorecki, "Modulation in comprehensive two-dimensional gas chromatography: 20 years of innovation," *Analytical and Bioanalytical Chemistry,* vol. 401, no. 8, pp. 2335-2349, 2011.

87] L. M. Blumberg, F. David, M. S. Klee and P. Sandra, "Comparison of one-dimensional and comprehensive two-dimensional separations by gas chromatography," *Journal of Chromatography A,* vol. 1188, no. 1, pp. 2-16, 2008.

88] J. J. Whiting, C. S. Fix, J. M. Anderson, A. W. Staton, R. P. Manginell, D. R. Wheeler, E. B. Myers, M. L. Roukes and R. J. Simonson, "High-speed two-

dimensional gas chromatography using microfabricated GC columns combined with nanoelectromechanical mass sensors," in *Solid-State Sensors and Actuators*, Denver, Co, 2009.

89] A. C. Lewis, J. F. Hamilton, C. N. Rhodes, J. Halliday, K. D. Bartle, P. Homewood, R. J. P. Grenfell, B. Goody, A. M. Harling, P. Brewer, G. Vargha and M. J. T. Milton, "Microfabricated planar glass gas chromatography with photoionization detection," *Journal of Chromatography A,* vol. 1217, no. 5, pp. 768-774, 2010.

90] M. D. Joshi and J. L. Anderson, "Recent advances of ionic liquids in separation science and mass spectrometry," *Rsc Advances,* vol. 2, pp. 5470-5484, 2012.

91] J. L. Anderson and D. W. Armstrong, "Immobilized Ionic Liquids as High-Selectivity/High-Temperature/High-Stability Gas Chromatograp," *Analytical Chemistry,* vol. 77, no. 19, pp. 6453-6462, 2005.

92] T. Payagala, Y. Zhang, E. Wanigasekara, K. Huang, Z. S. Breitbach, P. S. Sharma, L. M. Sidisky and D. W. Armstrong, "Trigonal Tricationic Ionic Liquids: A Generation of Gas Chromatographic Stationary Phases," *Analytical Chemistry,* vol. 81, no. 1, pp. 160-173, 2009.

93] R. C. M. de Nijs, G. A. F. M. Rutten, J. J. Franken, R. P. M. Dooper and J. A. Rijks, "A new surface roughening method for glass capillary columns. Sodium chloride deposition from suspension," *Journal of High Resolution Chromatography,* vol. 2, no. 7, pp. 447-455, 1979.

K. Grob, Making and manipulating capillary columns for gas chromatography,

94] 1986.

J. B. Phillips and J. Beens, "Comprehensive two-dimensional gas
95] chromatography: a hyphenated method with strong coupling between the two dimensions," *Journal of Chromatography A,* vol. 856, no. 1-2, pp. 331-347, 1999.

P. Haglund, M. Harju, R. Ong and P. Marriott, "Shape selectivity: A key factor
96] in comprehensive two-dimensional gas chromatographic analysis of toxic PCBs," *Journal of Microcolumn Separations,* vol. 13, no. 7, pp. 306-311, 2001.

S. Zhu, "Effect of column combinations on two-dimensional separation in
97] comprehensive two-dimensional gas chromatography: Estimation of orthogonality and exploring of mechanism," *Journal of Chromatography A,* vol. 1216, no. 15, pp. 3312-3317, 2009.

D. Ryan, P. Morrison and P. Marriott, "Orthogonality considerations in
98] comprehensive two-dimensional gas chromatography," *Journal of Chromatography A,* vol. 1071, no. 1-2, pp. 47-53, 2005.

L. M. Blumberg, "Comprehensive two-dimensional gas chromatography:
99] metrics, potentials, limits," *Journal of Chromatography A,* vol. 985, no. 1-2, pp. 29-38, 2003.

R. M. Kinghorn, P. J. Marriott and P. A. Dawes, "Design and Implementation
100] of Comprehensive Gas Chromatography with Cryogenic Modulation," *Journal of Separation Science,* vol. 23, no. 3, pp. 245-252, 2000.

L. Lapidus and N. R. Amundson, "Mathematics of Adsorption in Beds. VI. The

101] Effect of Longitudinal Diffusion in Ion Exchange and Chromatographic Columns," *Journal of Physical Chemistry,* vol. 56, no. 8, pp. 984-988, 1952.

J. J. van Deemter, F. J. Zuiderweg and A. Klinkenberg, "Longitudinal diffusion
102] and resistance to mass transfer as causes of nonideality in chromatography," *Chemical Engineering Science,* vol. 5, no. 6, pp. 271-289, 1956.

A. J. P. Martin and R. L. M. Synge, "A new form of chromatogram employing
103] two liquid phases: A theory of chromatography. 2. Application to the micro-determination of the higher monoamino-acids in proteins," *Biochemical Journal,* vol. 35, no. 12, pp. 1358-1368, 1941.

J. C. Giddings, Dynamics of Chromatography, New York: Marcel Dekker,
104] 1965.

T. C. Greene and X. J. Rong, "Evaluation of Techniques for Slice Sensitivity
105] Profile Measurement and Analysis," *Journal of Applied Clinical Medical Physics,* vol. 15, pp. 281-294, 2014.

L. S. Ettre and , Open Tubular Columns in Gas Chromatography, New York:
106] Plenum Press, 1965.

L. M. F. Barreira, J. Parshintsev, N. Karkkainen, K. Hartonen, M. Jussila, M.
107] Kajos, M. Kulmala and M.-L. Riekkola, "Field measurements of biogenic volatile organic compounds in the atmosphere by dynamic solid-phase microextraction and portable gas chromatography-mass spectrometry," *Atmospheric Environment,* vol. 115, pp. 214-222, 2015.

J. Ji, C. Deng, W. Shen and X. Zhang, "Field analysis of benzene, toluene,
108] ethylbenzene and xylene in water by portable gas chromatography–microflame ionization detector combined with headspace solid-phase microextraction," *Talanta,* pp. 894-899, 2006.

M. Jia, J. Koziel and J. Pawliszyn, "Fast Field Sampling/Sample Preparation
109] and Quantification of Volatile Organic Compounds in Indoor Air by Solid-Phase Microextraction and Portable Gas Chromatography," *Field Analytical Chemistry and Technology,* pp. 73-84, 2000.

D. . Paul and K. Kurabayashi, "First-principle modeling and characterization of
110] thermal modulation in comprehensive two-dimensional gas chromatography using a microfabricated device," *Sensors and Actuators B,* p. (under review), 2015.

M. S. Klee, J. Cochran, M. Merrick and L. M. Blumberg, "Evaluation of
111] conditions of comprehensive two-dimensional gas chromatography that yield a near-theoretical maximum in peak capacity gain," *Journal of Chromatography A,* vol. 1383, pp. 151-159, 2015.

B. J. Williams, J. T. Jayne, A. T. Lambe, T. Hohaus, J. R. Kimmel, D. Sueper,
112] W. Brooks, L. R. Williams, A. M. Trimborn, R. E. Martinez, P. L. Hayes, J. L. Jimenez, N. M. Kreisberg, S. V. Hering, D. R. Worton, A. H. Goldstein and D. R. Worsnop, "The First Combined Thermal Desorption Aerosol Gas Chromatograph—Aerosol Mass Spectrometer (TAG-AMS)," *Aerosol Science and Technology,* vol. 48, no. 4, pp. 358-370, 2013.